

FINITE ELEMENT SIMULATION OF TUNNEL  
EXCAVATIONS IN CREEPING ROCK

FINITE ELEMENT SIMULATION OF TUNNEL  
EXCAVATIONS IN CREEPING ROCK

by

EZZAT A. HANAFY, B.Sc. (CIVIL ENGINEERING)

A Thesis

Submitted to the School of Graduate Studies  
in Partial Fulfilment of the Requirements

for the Degree

Master of Engineering

McMaster University

March, 1976

MASTER OF ENGINEERING (1976)  
(Civil Engineering)

McMASTER UNIVERSITY  
Hamilton, Ontario.

TITLE: Finite Element Simulation of Tunnel  
Excavations in Creeping Rock

AUTHOR: Ezzat A. Hanafy, B.Sc. Cairo University,  
Egypt.

SUPERVISOR: Dr. John J. Emery

NUMBER OF PAGES: xii, 131

SCOPE AND CONTENTS:

A procedure based on the finite element method was developed for simulating the excavation of underground openings in rock for the actual initial state of stress in the field for various K conditions. This procedure can also incorporate orthotropic behaviour due to rock bedding, and other directional variations in the elastic properties of rock. This excavation simulation was then coupled into the time-dependent analysis of underground openings to study the influence of rock squeezing using the incremental initial strain method. Appropriate stress-strain-time relationships and strain accumulation methods are readily incorporated into this finite element program. (A survey of time-dependent constitutive relationships for rock is given to guide in the selection of appropriate creep laws.) The excavation and creep simulation aspects were then extended to model underground linings and lining placement strategies. This includes the ability to consider the lining and the rock as two different materials with rough or jointed interfaces between them. Further, this simulation allows for creep of the rock before lining installation, and creep

of the rock and concrete lining after its construction for appropriate rock and concrete constitutive relationships. The full simulation procedure (excavation, creep and lining) was used to study an actual tunnel constructed in squeezing rock. There is reasonable agreement between the predicted performance and measured performance to date, and this comparison with monitored field information is continuing.

## ACKNOWLEDGEMENTS

I am most thankful to Dr. John J. Emery, my research supervisor, for his continued encouragement and guidance at every stage of the study. It has been a privilege and a pleasure to work under his supervision.

I also take this opportunity to thank the following:

- i) The National Research Council of Canada for financial support during this study.
- ii) McMaster University for providing the excellent computing facilities that made much of the work possible.
- iii) Franklin Trow Associates Limited Rock Engineering Consultants for providing the field measurements.
- iv) Miss BettyAnne Bedell for her assistance in typing this thesis.
- v) And finally, and personally most important, my parents, for their understanding and continued encouragement.

To my wife ENASS

## TABLE OF CONTENTS

		Page
CHAPTER 1	INTRODUCTION	1
1.1	Outline of the Problem	2
1.2	Scope of this Investigation	4
CHAPTER 2	REVIEW OF LITERATURE	6
2.1	Introduction	6
2.2	Creep of Rock	7
2.2.1	Available Creep Relationships	7
2.2.2	Limitations	14
2.3	Finite Element Method	14
CHAPTER 3	EXCAVATION ANALYSIS	17
3.1	Introduction	17
3.2	Excavation Procedure	17
3.2.1	Initial Stress Condition	18
3.2.2	Perturbation Stresses and Stiffness Matrix	23
3.2.3	Incorporation of Orthotropic Rock Properties	25
3.3	Brief Description of Initial Strain Method	28
3.4	General Program Description	29
3.5	Example Problem	32
CHAPTER 4	TUNNEL SUPPORT SYSTEMS	42
4.1	Introduction	42
4.2	Creep of Concrete Linings	42
4.3	Modelling of Joints	44

4.4	Modelling of Concrete Linings	47
CHAPTER 5	SIMULATION OF TYPICAL FIELD PROBLEM	52
5.1	Introduction	52
5.2	Idealization	55
5.2.1	Mesh Configuration and Boundary Locations	55
5.2.2	Excavation	57
5.3	Discussion of Elastic Solutions	58
5.4	Creep	73
5.5	Discussion of Creep Solutions	73
5.6	Concrete Lining	89
CHAPTER 6	SUMMARY AND CONCLUSIONS	116
BIBLIOGRAPHY		119
APPENDIX A	FINITE ELEMENT METHOD	122
APPENDIX B	GENERAL INCREMENTAL APPROACH FOR NONLINEAR ELASTIC CREEP PROBLEMS	125
APPENDIX C	EQUATIONS REQUIRED FOR THE DETERMINATION OF THE TIME INCREMENTS AND THE COMPONENTS OF THE CREEP STRAIN INCREMENT	130



## LIST OF FIGURES

FIGURE	TITLE	PAGE
2.1	Typical creep behaviour under different compressive stresses.	9
2.2	Strain rate in constant stress creep test.	9
3.1	Excavation simulation.	19
3.2	In situ stress field	20
3.3	The equivalent nodal forces from the element stresses.	24
3.4	Isotropic and orthotropic (transversely isotropic) elastic rock.	27
3.5	Simplified flow chart for initial stress determination using the finite element method.	30
3.6	Simplified flow chart for excavation procedure using the finite element method.	31
3.7	Simplified flow chart for incremental creep analysis using the finite element method.	33
3.8	Idealization of the thick-walled cylinder for direct analysis.	34
3.9	Idealization of solid cylinder for "excavation" procedure.	35
3.10	Radial elastic deformation of the thick-walled cylinder.	37
3.11	Radial stress distribution in the thick-walled cylinder.	38
3.12	Axial stress distribution in the thick-walled cylinder.	39
3.13	Circumferential stress distribution in the thick-walled cylinder.	40
3.14	Inside and outside creep deformation of the thick-walled cylinder.	41
4.1	Joint element with its local coordinate system (Goodman et al., 1968).	45

4.2	Data from direct shear test on a rock joint (Goodman et al., 1968).	45
4.3	Concrete lining without joint elements (no separation between the rock and concrete-rough interface).	48
4.4	Simulation of concrete lining-rock interface with joint elements.	49
4.5	Simplified flow chart for lining simulation and creep analysis.	51
5.1	Finite element idealization of the tunnel.	56
5.2	Computed movements after excavation for isotropic elastic rock, $K = 1, 4$ .	59
5.3	Computed movements after excavation for isotropic elastic rock, $K = 7, 9$ .	60
5.4	Computed movements after excavation for orthotropic elastic rock, $K = 1, 4$ .	61
5.5	Stress concentration along vertical and horizontal sections, isotropic, $K = 1$ .	64
5.6	Stress concentration along vertical and horizontal sections, isotropic, $K = 4$ .	65
5.7	Stress concentration along vertical and horizontal sections, isotropic, $K = 7$ .	66
5.8	Stress concentration along vertical and horizontal sections, isotropic, $K = 9$ .	67
5.9	Stress concentration along vertical and horizontal sections, orthotropic, $K = 1$ .	68
5.10	Stress concentration along vertical and horizontal sections, orthotropic, $K = 4$ .	69
5.11	Computed (finite element) and measured horizontal normal stresses perpendicular to tunnel axis.	71
5.12	Shear stress distributions around the tunnel.	72
5.13	Radial displacement with time for $K = 1$ .	74
5.14	Radial displacement with time for $K = 4$ .	75
5.15	Radial displacement with time for $K = 7$ .	76

5.16	Radial displacement with time for $K = 9$ .	77
5.17	Computed movements around the tunnel with time for $K = 1$ .	79
5.18	Computed movements around the tunnel with time for $K = 4$ .	80
5.19	Comparison of measured creep displacements with those computed by finite element method.	83
5.20	Stress concentration along vertical and horizontal sections, creep, $K = 1$ .	85
5.21	Stress concentration along vertical and horizontal sections, creep, $K = 4$ .	86
5.22	Finite element idealization of the tunnel lining, rough interface.	90
5.23	Finite element idealization of the tunnel lining, jointed interface.	91
5.24	Radial displacements for the concrete lining with time for $K = 1$ .	95
5.25	Effect of the lining on the radial displacements for the rock with time for $K = 1$ .	97
5.26	Radial displacements for the concrete lining with time, with and without joints, for $K = 1$ .	98
5.27	Radial displacements for the rock after lining with time for $K = 4$ .	100
5.28	Radial stresses at the crown of the tunnel with time for $K = 1$ .	101
5.29	Tangential stresses at the crown of the tunnel with time for $K = 1$ .	102
5.30	Radial stresses at the crown of the tunnel with time for the rough and jointed interfaces, $K = 1$ .	104
5.31	Tangential stresses at the crown of the tunnel with time for the rough and jointed interfaces, $K = 1$ .	105
5.32	Radial stresses at the crown and spring points with time for $K = 4$ .	107
5.33	Tangential stresses at the crown and spring points with time for $K = 4$ .	108

5.34	Location of rock and concrete points.	109
5.35	Finite element representation of the concrete lining.	115

## LIST OF TABLES

TABLE	TITLE	PAGE
2.1	Summary of creep equations and limitations.	15
3.1	Review of published horizontal ground stress measurements.	22
5.1	Rock properties measured experimentally [FTA, 1975].	53
5.2	Summary of isotropic material properties.	54
5.3	Summary of orthotropic material properties.	54
5.4	Horizontal and vertical convergence values after excavation.	63
5.5	Summary of computed (finite element) convergence values and creep rates.	81
5.6	Comparison of measured convergence values with those computed by finite element method.	82
5.7	Radial and tangential compressive stresses around the tunnel for $K = 1$ .	87
5.8	Radial and tangential compressive stresses around the tunnel for $K = 4$ .	88
5.9	Summary of concrete properties for the lining.	93
5.10	Summary of linear element (joint) properties for the interface between the rock and the concrete lining (friction joint).	93
5.11	Stresses in the joints between the rock and the concrete lining constructed 2 months after excavation, $K = 1$ .	106
5.12	Long term stresses, rock, $K = 1$ .	110
5.13	Long term stresses, rock, $K = 4$ .	111
5.14	Long term stresses, concrete, $K = 1$ .	112
5.15	Long term stresses, concrete, $K = 4$ .	113

CHAPTER 1  
INTRODUCTION

Interest in the creep behaviour of rock has gained impetus in the last few years, particularly since "squeezing" has resulted in several recent failures (Jaeger, 1972). Examples of such failures would include: the El-Colegio Tunnel in Columbia; Kamui Tunnel in Japan; and North Tauern Tunnel in Austria (Lane, 1975). The linings for these tunnels had been placed before movement of the ground had ceased. Even in "good" rock (granite), creep deformations have been found in the quarries on Vinalhaven Island in Maine (Feld, 1966). In the Niagara formations, rock movements have been reported during the construction of tunnels and open trenches for the Ontario Hydro Adam Beck development (Lo and Morton, 1975) following completion of the Thorold Tunnel under the Welland Canal in 1973 and the Redhill Creek Culvert near Hamilton in 1975. The Thorold Tunnel and Redhill Creek Culvert movements caused significant damage to the linings and remedial work was required.

Terzaghi (1946) refers to this condition as "squeezing ground" and states that the loading on the tunnel support is likely to increase for weeks or even months after construction to a value which is many times higher than the initial one. This creep behaviour of rock under loading is observed in

both the laboratory and the field for a wide range of rock types. Generally speaking, current engineering practice is to ignore or approximate this time-dependency in the analysis of rock problems. The extent of the errors introduced by such approximations depends on the particular rock and problem being considered. It may also depend on whether the concern is for the stresses or for the displacements. In a situation involving nonhomogeneous media, such as a lined tunnel, peak stresses in the rock may actually increase with time. Also, there are occasions when knowledge of the entire displacement history may be of value. A displacement history which enables predicting the useful life of an underground opening or a slope allows the engineer to take remedial measures if necessary and possible. Also, underground excavation in rock is one of the most expensive forms of engineering construction. In practice, the ground support usually represents 30 to 50 percent of tunnelling costs, and its placement often controls the rate of progress. Thus, there is a pressing need for a systematic method for predicting both the severity of squeezing ground conditions (creep response) and for designing tunnel support systems and placement strategies compatible with the potential creep response.

### 1.1 Outline of the Problem

A major consideration in the design of excavations in rock is the evaluation of the structural stability of

the opening. The essential step in this evaluation is the determination of the deformations (strains) and stresses in the surrounding rock, and the excavation's behaviour with time. It would appear that the dependence of rock creep on stress level is nonlinear, so that incremental solution procedures are generally required to realistically analyze rock mechanics problems involving creep. Due to the complexity of material properties and boundary conditions, such problems are difficult to idealize, and cannot generally be solved analytically. Thus, the finite element method has been widely adopted for the solution of problems in rock mechanics.

The objective of this study is to simulate the excavation in rock for an underground opening, considering the initial state of stress and the bedding of the rock in order to realistically represent the actual field conditions. It is also important to predict the behaviour of the opening with time and to evaluate the time-dependent deformations and any stress concentrations that may build-up around the tunnel. Finally, it is necessary to evaluate the support system required for the tunnel, to predict any stress concentrations that can develop in the lining (tensile stresses), and the lining's influence on any creep. This is critical, as the lining can be crushed over a short period as a result of rock creep if adequate design precautions are not taken before the lining is placed.



## 1.2 Scope of this Investigation

The finite element method of stress analysis was used to simulate the excavation and creep response of a tunnel in squeezing rock. The initial state of stress representing the in situ stresses for various  $K$  conditions\* was adopted as the starting point for each simulation. For many rocks and tectonic histories, high values of  $K$  (range of 1 to 10) may be involved. A computer program for simulating the excavation procedure was developed, and the elastic displacements and stresses can be determined during a single step excavation simulation. Linear displacement triangular elements were adopted for this plane strain situation. Anisotropic properties can also be included in the analysis to more adequately represent rock bedding in the field. The incremental, initial strain method developed by Emery (1971) was then used to incorporate creep simulation into the analysis.

A thick-walled cylinder was used as a simple example application to verify the procedure adopted for the excavation and creep analyses.

A computer program was then developed to simulate placing the concrete lining after excavation, and to allow creep before and after the lining placement. This program can also incorporate joint elements placed between the concrete lining and the surrounding rock.

A typical field problem involving a large intake tunnel to be constructed in shale near Toronto was then

---

$K$  is the ratio between the horizontal stress and the vertical stress.

analyzed. The tunnel opening is 13 feet (4 meters) in diameter and at a depth of 200 feet (61 meters), in soft rock that has been classified as shale. Rock properties such as elastic modulus, unit weight and Poisson's ratio were assumed from initial test data (provided by Franklin Trow Associates Limited) and a careful examination of the properties of shale published in the literature. The initial stress state for various K conditions was determined before excavation and the deformations (strains) and the stresses after excavation of this underground opening were obtained for both isotropic and orthotropic rock properties. Creep solutions for the tunnel with, and without, a concrete lining in place, and for various placement strategies, are presented. The results from the finite element simulation and the field measurements during and after construction are then compared.

The conclusions and some possible extensions of the work are presented in the summary.

CHAPTER 2  
REVIEW OF LITERATURE

2.1 Introduction

Previous studies of time-dependent behaviour in rock mechanics have been primarily conducted in the laboratory. It has been observed that most rock exhibits significant time-dependency, at least at high stress levels and/or high temperatures (Winkle, 1970). Most of the laboratory investigations (Robertson, 1963; Hobbs, 1970; Winkle, 1970; and Afrouz and Harvey, 1974), and the corresponding stress-strain-time relations developed have been uniaxial in nature. A few tests have been conducted (United States Army Corps of Engineers, 1963; Semple, Hendron, and Mersi, 1973) to evaluate creep behaviour in triaxial tests. Some attempts have been made to gain insight into time-dependent problems by utilizing rheological models (Winkle, 1970; Emery, 1971). Numerical techniques utilizing computers have been used to study fairly complicated problems for realistic constitutive relationships. The finite element technique has been successfully applied to some problems in nonlinear creep analysis for different materials (Boresi and Deere, 1963; Greenbaum, 1966; Winkle, 1970). However, only a small amount of work concerning creep of rock has been published, and that work has been limited to specific types of rocks.

## 2.2 Creep of Rock

Creep can generally be described as inelastic deformation under constant stress, usually below the yield stress, and at any low strain rate. This expresses the dependence of strain rate on the stress history. It has been observed that all materials deform with time under sustained load. Metals, plastics, concrete, soils, and rock have very different structures, but all exhibit creep. The simplest assumption to make is that one fundamental mechanism causing creep is common to all, which immediately implies that the mechanism exists at a very small or fundamental level of structure (Winkle, 1970). In soils, the mechanism causes the gradual displacement of an inter-particle contact location until it can no longer be maintained (Semple et al., 1973). Failure of such contacts results in a rearrangement of particles with new contacts being formed and the process continuing. Creep may eventually lead to rupture. Such creep rupture is usually defined as failure of the material under a stress condition that is less than the applicable strength measured in standard laboratory tests. Without methods for the analysis of creep and creep rupture, design methods for structures must be based on high safety factors or the experience gained from previous failures.

### 2.2.1 Available Creep Relationships

The empirical approach appears to have the widest acceptance for representing the creep of rock (Robertson, 1963). In this empirical approach, various parameters such

as strain and strain rate are measured experimentally as a function of time, stress, and temperature under controlled conditions. From the parameters selected to represent the experimental data, creep equations are developed to describe the material behaviour. The creep of metals has been studied extensively (Lubahn et al., 1961; Penny et al., 1971) and the general behaviour of rocks has been found to be very similar. The typical behaviour of many metals and rocks is shown in Figures (2.1) and (2.2) which represent strain-time curves and the strain rate with time curve under uniaxial compression respectively. The total strain (elastic plus creep)  $\epsilon$  shown in Figure (2.1) for a fixed stress level (say  $\sigma_3$ ) may be represented by the following general equation:

$$\epsilon = \epsilon_0 + \epsilon_p(t) + At + \epsilon_T(t) \quad (2.1)$$

where:  $\epsilon_0$  is the instantaneous elastic strain;  $\epsilon_p(t)$  is the primary creep;  $At$  is the steady-state creep; and  $\epsilon_T(t)$  is the tertiary creep.

Creep Equation (2.1) is only one of the equations for rock given in the literature. However, only a limited amount of experimental work has been carried out on the inelastic (time-dependent) properties of rock. Some of the work published prior to 1964 has been summarized in review papers by Robertson (1963), and Murrell and Misra (1962). Other papers have been published by Boresi and Deere (1963), United States Army Corps of Engineers (1963), and Hobbs (1970). More

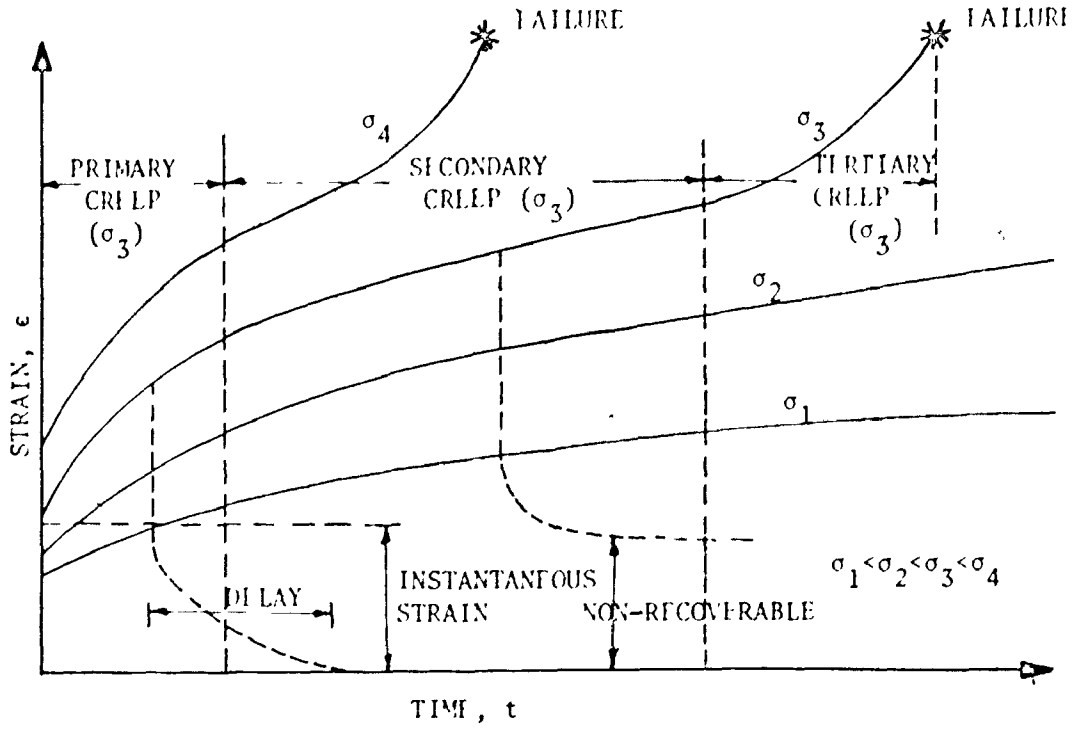


FIGURE 2.1 TYPICAL CREEP BEHAVIOUR UNDER DIFFERENT COMPRESSIVE STRESSES

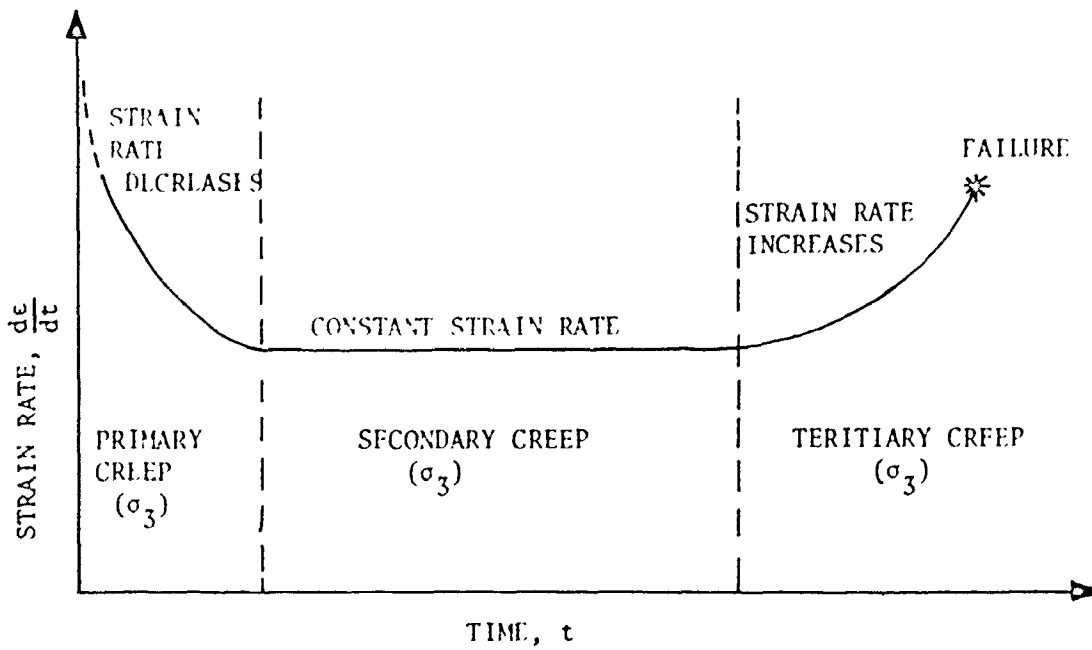


FIGURE 2.2 STRAIN RATE IN CONSTANT STRESS CREEP TEST

recently, papers have been published by Winkle (1970), Cruden (1971), Semple, Hendron, and Mersi (1973), and Afrouz and Harvey (1974).

There are several strain-time equations for rocks published in Obert and Duvall (1967), Farmer (1968), and Jaeger (1972), but these equations do not give the strain as a function of the stress level as well as the time. These equations are not generally of use in predicting the creep behaviour of rock masses, since it is clear that the creep behaviour of most rock is dependent on the stress level.

Boresi and Deere (1963) suggested a creep law for rock of the form:

$$\epsilon = k \sigma^n t^m \quad (2.2)$$

where:  $\epsilon$  is the creep strain;  $t$  is the time;  $\sigma$  is the stress; and  $k$ ,  $n$ , and  $m$  are constants. Tests have been conducted by the United States Army Corps of Engineers (1963) on rock salt to evaluate the constants  $k$ ,  $n$ , and  $m$  for Equation (2.2). They used triaxial extension tests where the confining pressure ranged from 1000 psi to 3850 psi. Equation (2.2), for the particular rock salt tested, becomes:

$$\epsilon = 1.87 \times 10^{-13} \sigma^{2.98} t^{0.36} \quad (2.3)$$

where:  $\sigma$  is in psi and  $t$  is in hours. This equation has been used by some investigators (Boresi and Deere, 1963; U.S. Army Corps of Engineers, 1963; Winkle, 1970; Nair et al., 1973) to study openings in rock salt. However, it is generally

agreed that this form of equation is really only applicable for evaporites.

An empirical exponential equation commonly used in rock mechanics creep problems is:

$$\dot{\epsilon} = A \sigma^n \quad (2.4)$$

where:  $\dot{\epsilon}$  is the strain rate;  $\sigma$  is the stress; and  $A$  and  $n$  are constants. The value of  $n$  for a number of rock types from uniaxial creep testing at room temperature is given in Robertson (1963), and Obert and Juvall (1967). This equation may not be valid for all ranges of strain or for creep occurring in the steady-state phase (Obert and Duvall, 1967).

Farmer (1968) gives the following creep law for different rocks:

$$\epsilon = \left(\frac{\sigma}{E}\right)^n \ln t \quad (2.5)$$

where:  $\epsilon$  is the strain;  $\sigma$  is the stress;  $E$  is the modulus of elasticity;  $t$  is the time; and  $n$  is a constant depending primarily on the stress magnitude. In this reference  $E$  and  $n$  are given for various types of rocks tested. This equation does not cover the secondary creep range.

Singh and Mitchell (1968) suggested a one-dimensional stress-strain-time function for soils. This equation is very useful in studying soil creep, and its application to the creep behaviour of fault gouge and the prediction of tunnel support requirement in squeezing ground conditions (Semple et al.,



1973) is now being developed.

Hobbs (1970) made attempts to fit a number of empirical equations to longitudinal strain-time results for a range of rock types. These experiments were carried out using uniaxial compression tests at room temperature. Uniaxial compressive stresses ranging from  $26.4 \text{ MN/m}^2$  (3800 psi) to  $41.4 \text{ MN/m}^2$  (6000 psi) for periods from a few minutes to more than a year were used in the experiments. Hobbs' equation may be applicable for the bulk of sedimentary rock types (siltstone, sandstone, shale, and limestone). The stress-strain-time equation developed by Hobbs is given by:

$$\epsilon = \epsilon_0 + g\sigma^f t + K_2 \sigma \log (t+1) \quad (2.6)$$

where:  $\epsilon_0$  is the instantaneous elastic strain;  $\sigma$  is the stress;  $t$  is the time; and  $g$ ,  $f$ , and  $K_2$  are constants for each type of rock. Hobbs tested four types of rock: siltstone; sandstone; shale; and limestone. The constants for each rock type were determined by Hobbs (1970). He found that the strain rates predicted by Equation (2.6) when  $t$  is small are less than the experimentally observed strain rates, but that at longer times (up to a year) the strain rate predictions were reasonable. It is considered by the writer, based on the literature review, that this is a most reasonable creep law for shale if the one year base is recognized.

Afrouz and Harvey (1974) completed their experiments at room temperature on dry and saturated rocks exhibiting

uniaxial creep compressive stresses within the soft to medium strength range such as air-dried and saturated coal, underclay, limestone, and sandstone. The compressive stresses were in the range between  $6.6 \text{ Kg/cm}^2$  (94 psi) and  $58.5 \text{ Kg/cm}^2$  (830 psi). They obtained best fits for the experimental results by a computer analysis for the rocks tested. They also compared the experimental results with measurements of time-dependent deformation of underclay along the floor or mine roadway and close similarity was achieved. They found that the creep relationship depended on general rock type as follows:

- a) Air-dried soft to medium strength rocks behave in an elastic-viscous manner that can be described by the Burgers Body model expressed in the general form:

$$\epsilon = A + Bt^C + D [1 - \exp(-Et)] \quad (2.7)$$

- b) Saturated soft rocks exhibit nonlinear creep behaviour expressed by:

$$\epsilon = A + Bt^C + Dt^E \quad (2.8)$$

where:  $\epsilon$  is the strain;  $t$  is the time; and  $A$ ,  $B$ ,  $C$ ,  $D$ , and  $E$  are constants depending on the rock type and its conditions. These equations, in which the strain is only a function of time, need laboratory tests at appropriate stress levels to determine the constants applicable for use in predicting field creep behaviour.

### 2.2.2 Limitations

A number of creep relationships for rock have been presented. These are summarized in Table (2.1) with the limitations clearly indicated for each. In addition to the limited applicability of the laws, there are limitations related to the testing.

Winkle (1970) studied the time-dependent deformation occurring in mine openings in potash ore. He concluded that uniaxial unconfined tests are not sufficient to obtain a complete description of the material response. Multiaxial loading and unloading tests are required.

A comparison of the steady state creep rates for uniaxial compression and triaxial extension tests was done by the United States Army Corps of Engineers (1963) and the results are given in Stagg and Zienkiewicz (1968). This comparison shows that the rates of creep in triaxial extension are less than those at the same stress level in uniaxial compression. Thus, the uniaxial creep test is too severe for use in predicting time-dependent displacements around underground openings. This is obviously an area that requires further testing and research.

### 2.3 Finite Element Method

To handle the complicated geometries, boundary conditions, and loadings involving nonlinear, time-dependent behaviour of rock, the finite element method (Zienkiewicz and Holister, 1965; Desai and Abel, 1972) of stress analysis

TABLE 2.1 SUMMARY OF CREEP EQUATIONS AND LIMITATIONS

ROCK CREEP EQUATION	ROCK TYPES	LIMITATIONS
$\epsilon = K \sigma^n t^m$ (Boresi and Deere, 1963)	Rock Salt	The constants (K,n,m) are given only for rock salt and for stresses ranging between 1000 psi and 3850 psi
$\dot{\epsilon} = A \sigma^n$ (Robertson, 1963)	Most rocks	Values of n calculated from primary creep data are given in Robertson (1963). This equation may not be valid for all ranges of strains, i.e. does not cover the steady state creep and the tertiary creep. Also, it requires experiments to define the constant A for the rock type used.
$\epsilon = \left(\frac{\sigma}{E}\right)^n \ln t$ (Farmer, 1968)		This equation does not include the secondary creep. The values of n are dependent on the stress magnitude and the elastic modulus.
$\epsilon = \epsilon_0 + g\sigma^f t + K_2\sigma \log(t+1)$ (Hobbs, 1970)	Siltstone, sandstone, shale, and limestone.	The constants (g,f,K <sub>2</sub> ) are given for the four rock types for stresses ranging between 3800 psi and 6000 psi. The equation does not cover tertiary creep.
$\epsilon = A + Bt^C + D[1-\exp(-Et)]$ (Afrouz and Harvey, 1974)	Air-dried soft (coal, underclay) to medium (sandstone, limestone) rocks	The constants (A,B,C,D,E) are given for stresses ranging between 6.6 kg/cm <sup>2</sup> (94.0 psi) to 58.5 kg/cm <sup>2</sup> (830 psi) In these equations the strain is only a function of time. The constants for the rock type tested should be determined experimentally for the stress level anticipated.
$\epsilon = A + Bt^C + Dt^E$ (Afrouz and Harvey, 1974)	Saturated soft (coal, underclay) rocks	

is used in conjunction with appropriate creep relationships. Closed form solutions become very difficult, if not impossible, to formulate for many practical problems. In rock mechanics, problems such as: the stability of rock slopes (Desai, 1971); the design of underground structures (Zienkiewicz, 1971); the prediction of displacements and stresses during and after excavation (Meek, 1973; Kulhawy, 1974, 1975); initiation of cracks (Desai, 1971); and elastic, elasto-plastic, linear and nonlinear material behaviour (Greenbaum, 1966; Desai, 1971; Meek, 1973) can be studied by finite element techniques. The finite element method also has the capability of being used to: model joints (Goodman et al., 1968) and other forms of discontinuities that exist in rock masses; incorporate no-tension solutions to redistribute the stresses; and propagate joints or cracked zones. Also, in earthquake and dynamic analysis, the method has found application in soil-structure interaction problems. A summary of various applications of the finite element method in geotechnical engineering and rock mechanics are found in Zienkiewicz et al. (1965), Zienkiewicz (1971), Desai (1971), and Desai et al. (1972). A brief description of the method is given in Appendix A.

CHAPTER 3  
EXCAVATION ANALYSIS

3.1 Introduction

Time effects play an important role in determining the deformations and stress distributions associated with underground openings, particularly when long-term behaviour is of interest. Also, the in situ stresses before construction of an underground opening will affect the behaviour of the rock after excavation. A procedure, and a computer program, were developed for modelling the excavation of underground openings using the finite element technique. This procedure is based on the criteria for modelling underground tunnels established recently by Meek (1973) and Kulhawy (1974). The finite element stress analysis for a thick-walled cylinder is used to check the accuracy of the techniques, and the results obtained are in good agreement with the closed-form solution (Greenbaum, 1966).

3.2 Excavation Procedure

Goodman and Brown (Desai et al., 1972) developed the general numerical procedures for simulating embankment construction and excavation problems in geotechnical engineering. The procedure adopted in this study to simulate excavation is based on this method, and is similar to the analysis used in the theory of plates to obtain the stresses in a plate with a hole,

subjected to in plane forces. This procedure was also used by Meek (1973) for excavation simulation.

Figure (3.1) illustrates the main steps of the excavation analysis performed here, assuming that the entire construction takes place in a single operation. It represents the actual site of the tunnel and the boundaries which are assumed to be far enough away to have small influence on the opening. The final stresses,  $\sigma_1$ , around the tunnel after excavation can be considered to be the sum of two cases. The first case is the initial stress field,  $\sigma_0$ , due to the actual field conditions before excavation. The second case is the perturbation stresses,  $\Delta\sigma_1$ , due to the release forces acting around the opening.

### 3.2.1 Initial Stress Condition

Existence of a nonzero state of stress prior to loading of a geological medium can significantly affect its subsequent deformation behaviour. For most problems in geotechnical engineering, the initial stress condition depends on the consolidation and subsequent loading history of the particular deposit. These stresses, for a deposit with a horizontal surface, are given by  $\sigma_v$  and  $\sigma_h$ . The vertical state of stress,  $\sigma_v$ , at a point is computed as the overburden pressure due to gravity as shown in Figure(3.2). The horizontal stresses,  $\sigma_h$ , is calculated from the condition of zero lateral strain. Thus, the in situ stresses are given by:

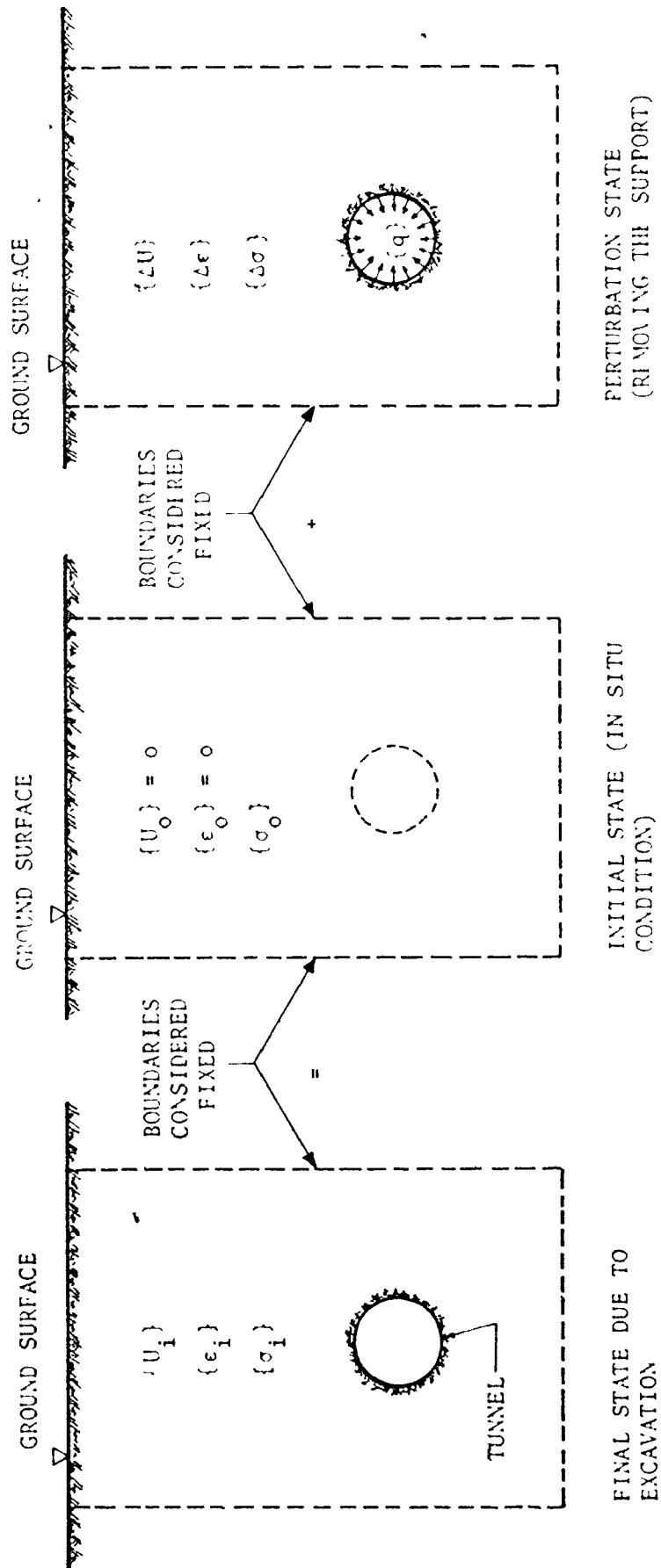


FIGURE 3.1 EXCAVATION SIMULATION



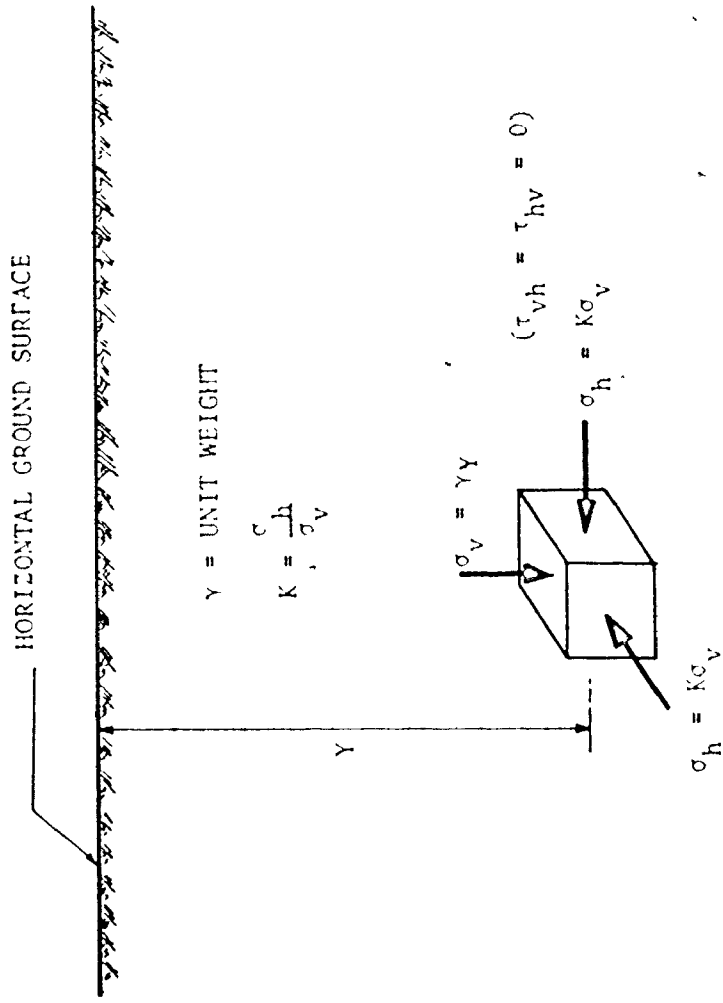


FIGURE 3.2 IN SITU STRESS FIELD

$$\sigma_v = \gamma Y \quad (3.1)$$

$$\sigma_h = K \sigma_v \quad (3.2)$$

$$\tau_{vh} = \tau_{hv} = 0 \quad (3.3)$$

where:  $\gamma$  is the unit weight;  $Y$  is the depth;  $\tau$  is the shear stress; and  $K$  is the ratio between the horizontal stress and the vertical stress.  $K$  is often evaluated from the theory of elasticity which is not usually realistic for rock with large lateral pressures:

$$K = \nu / (1 - \nu) \quad (3.4)$$

where  $\nu$  is Poisson's ratio. The value of  $K$  in rock depends upon many factors such as overconsolidation, the stress history, faults, folds and other tectonic effects (Desai, 1971). The only reliable way of estimating the value of  $K$  is by means of field measurements (Jaeger, 1972).

A review of ground stress measurements for Western Ontario shown in Table (3.1) indicates that the horizontal stresses are higher than those acting vertically computed on the basis of the gravitational loading due to overburden. From a detailed examination of this data, a  $K$  value range of from 1 to 10 is considered more likely to apply for much of the rock in Southern Ontario of interest to this study. (Those values shown with a question mark appear extremely high from the literature.)

TABLE 3.1 REVIEW OF PUBLISHED HORIZONTAL GROUND STRESS MEASUREMENTS

LOCATION	ROCK TYPE	DEPTH (FEET)	PRINCIPAL VERTICAL STRESS (psi) <sup>1</sup>	PRINCIPAL HORIZONTAL STRESS (psi) <sup>1</sup>		$k = \frac{h}{v}$
				MAJOR	MINOR	
Thorold, Ontario	Dolomite & Limestone	~ 42 to 81	43.7 to 84.4	959 to 2130	756 to 1750	$20^2$ to $23^2$
Mississauga, Ontario	Dundas Shale	24 to 40 <sup>3</sup>	25.0 to 41.7	up to 1200	—	29 <sup>2</sup>
Fickering, Ontario	Collingwood Shale	50 to 80	52.1 to 83.3	-285 to 1080	-111 to 956	12 <sup>2</sup>
Wesleyville, Ontario	Limestone	< 150	156.3	1200 to 1900	870 to 1540	11 <sup>2</sup>
Niagara Falls, Ontario	Dolomite & Shale	< 200	208.3	200 to 2800	-200 to 900	1 to 9 <sup>2</sup>
Niagara Falls, New York	Dolomite	~ 15 ~ 10	15.6 10.4	1000 <sup>1</sup> 870 <sup>1</sup>	-10 <sup>1</sup> -330 <sup>1</sup>	26 <sup>2,2</sup>
North Bay, Ontario	—	< 50	52.1	~ 1100 <sup>2</sup>	—	21 <sup>2</sup>
Ottawa, Ontario	—	< 50	52.1	~ 330 <sup>2</sup>	—	6
Illiot Lake, Ontario	Diabase	840	875.0	~ 3100 <sup>1</sup>	—	3.5

1. Average of several measurements
2. Average of major and minor principal stresses
3. Below the bedrock surface
4. Positive values indicate compressive stresses
5. Unit weight assumed to be 150 pcf

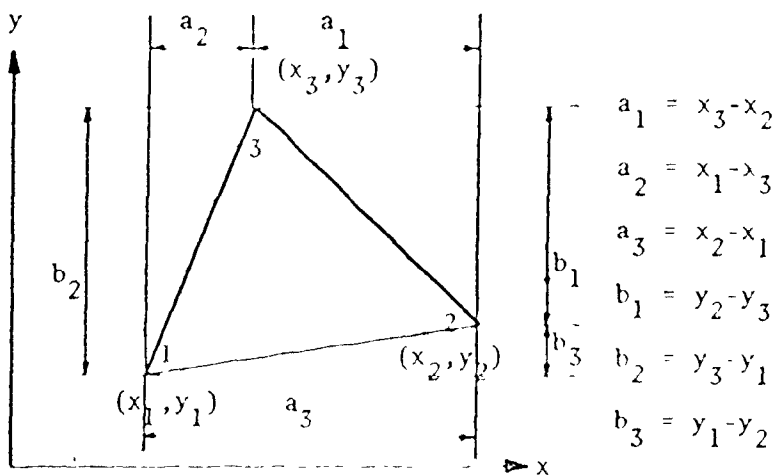
### 3.2.2 Perturbation Stresses and Stiffness Matrix

The perturbation stresses are developed when equivalent forces are applied at the nodes on the excavated surface to represent the excavation process as shown in Figure (3.1). These equivalent forces are those necessary to give a stress free boundary at the excavated surface (Meek, 1973). The equivalent nodal forces are determined from the stresses within the elements removed to simulate the excavation process. Figure (3.3) shows the stress distribution within an element, and the equivalent forces at midsides between two adjacent nodes (Desai and Abel, 1972). Equation (3.5) gives the relationship between the nodal force vector prior to excavation, and the stresses within an element:

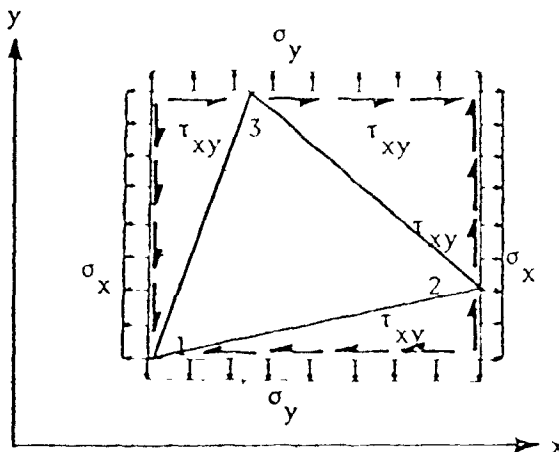
$$\{q\} = \begin{bmatrix} P_{u1} \\ P_{u2} \\ P_{u3} \\ P_{v1} \\ P_{v2} \\ P_{v3} \end{bmatrix} = -\frac{h}{2} \begin{bmatrix} b_3 + b_2 & 0 & a_3 + a_2 \\ b_1 + b_3 & 0 & a_1 + a_3 \\ b_2 + b_1 & 0 & a_2 + a_1 \\ 0 & a_3 + a_2 & b_3 + b_2 \\ 0 & a_1 + a_3 & b_1 + b_3 \\ 0 & a_2 + a_1 & b_2 + b_1 \end{bmatrix} \begin{bmatrix} \sigma_x \\ \sigma_y \\ \tau_{xy} \end{bmatrix} \quad (3.5)$$

where  $h$  is the thickness of the triangle in the  $Z$  direction. These forces, with opposite sign, then represent the equivalent nodal load vector for the removed elements and are applied at the nodes on the excavated surface.

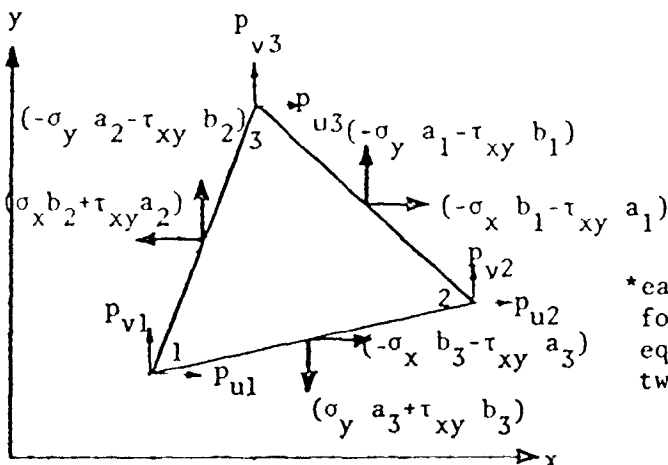
A) NOTATION



B) CONSTANT STRESS-DISTRIBUTION



C) STATICALLY EQUIVALENT FORCES AT MID SIDES (PER UNIT THICKNESS)



\*each of the midside forces is divided equally between the two adjacent nodes

FIGURE 3.3 THE EQUIVALENT NODAL FORCES FROM THE ELEMENT STRESSES

The main stiffness matrix is used when determining the nodal displacements for the complete mesh. After excavation, a new stiffness matrix is developed with due consideration of the removed elements. The coefficients of the stiffness matrix of the elements within the opening are reduced to negligible values. Kulhawy (1974) found that the modulus of the excavated elements must be reduced to at least  $10^{-6}$  times their value prior to excavation. If they are reduced by substantially lesser amounts, the values computed for the remaining elements are not reasonable (Kulhawy, 1974). The stiffness matrix of the new mesh is obtained, and displacements  $\{\delta U\}$ , strains  $\{\Delta \epsilon\}$  and stresses  $\{\Delta \sigma\}$  can also be determined.

The final displacements, strains and stresses after excavation are determined from the following equations:

$$\{U\} = \{U_0\} + \{\Delta U\} \quad (3.6)$$

$$\{\epsilon\} = \{\epsilon_0\} + \{\Delta \epsilon\} \quad (3.7)$$

$$\{\sigma\} = \{\sigma_0\} + \{\Delta \sigma\} \quad (3.8)$$

For excavation problems in soils and rocks, the displacements and the strain due to gravity loads before construction are not taken into consideration. Only the stresses before excavation are relevant.

### 3.2.3 Incorporation of Orthotropic Rock Properties

The conditions of homogeneity and isotropy generally assumed in theoretical stress analysis are seldom realized in

materials such as rock (Jaeger, 1972). Rock layers that show obvious differences in composition, grain size or shape, porosity, cementation, and other characteristics can be expected to have distinctive strength and deformational properties. But, even where compositional and other characteristics are sufficiently uniform for a rock sequence to be considered reasonably homogeneous, the presence of bedding surfaces can have pronounced effects on these properties.

The directional variations in the elastic properties of rock effects the stress distribution in rock surrounding an underground excavation (Obert and Duvall, 1967). For stratified or transversely isotropic material (in which a rotational symmetry of properties exists) five independent elastic constants are required for a full description of the rock.  $E_1$  and  $\nu_1$  are the elastic modulus and Poisson's ratio in the plane of the strata and  $E_2$ ,  $\nu_2$  and  $G_2$  are the elastic modulus, Poisson's ratio and shear modulus in the plane perpendicular to the strata. Figure (3.4) shows the directions and moduli involved.

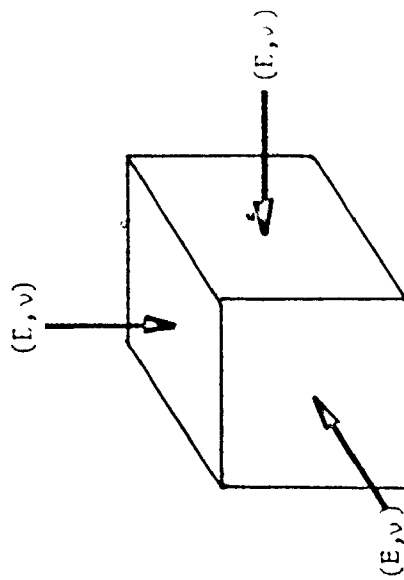
The general stress-strain relationship is given by Equation (3.9).

$$\{\sigma\} = [D] \{\epsilon\} \quad (3.9)$$

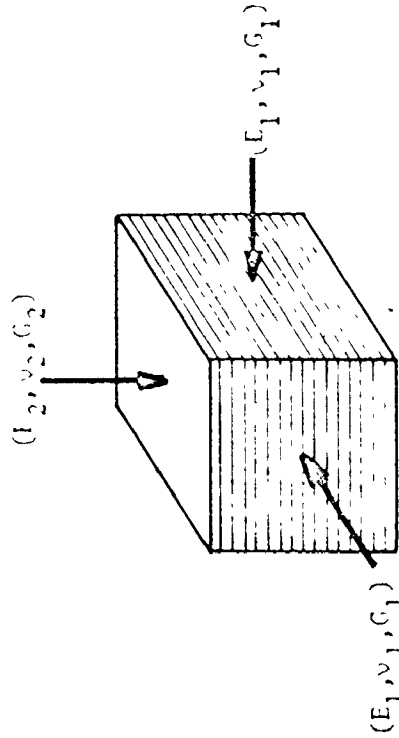
where  $[D]$  is the constitutive matrix. For isotropic material and the plane strain idealization ( $\epsilon_z = 0$ ), Equation (3.9) becomes:

$E_1$  = ELASTIC MODULUS IN THE PLANE OF THE STRATA  
 $E_2$  = ELASTIC MODULUS NORMAL TO THE PLANE OF THE STRATA  
 $\nu_1$  = POISSON'S RATIO IN THE PLANE OF THE STRATA  
 $\nu_2$  = POISSON'S RATIO NORMAL TO THE PLANE OF THE STRATA  
 $G_1$  = SHEAR MODULUS IN THE PLANE OF THE STRATA  
 $G_2$  = SHEAR MODULUS NORMAL TO THE PLANE OF THE STRATA

$E$  = ELASTIC MODULUS  
 $\nu$  = POISSON'S RATIO



(A) ISOTROPIC MATERIAL



(B) ORTHOTROPIC MATERIAL

FIGURE 3.4 ISOTROPIC AND ORTHOTROPIC (TRANSVERSELY ISOTROPIC) ELASTIC ROCK



$$\begin{bmatrix} \sigma_x \\ \sigma_y \\ \tau_{xy} \end{bmatrix} = \frac{E}{(1+\nu)(1-2\nu)} \begin{bmatrix} (1-\nu) & \nu & 0 \\ \nu & (1-\nu) & 0 \\ 0 & 0 & \frac{(1-2\nu)}{2} \end{bmatrix} \begin{bmatrix} \epsilon_x \\ \epsilon_y \\ \gamma_{xy} \end{bmatrix} \quad (3.10)$$

For a transversely isotropic medium and the plane strain idealization Equation (3.9) becomes:

$$\begin{bmatrix} \sigma_x \\ \sigma_y \\ \tau_{xy} \end{bmatrix} = \frac{E_2}{(1+\nu_1)(1-\nu_1-2n\nu_2^2)} \begin{bmatrix} n(1-n\nu_2^2) & n\nu_2(1+\nu_1) & 0 \\ n\nu_2(1+\nu_1) & (1-\nu_1^2) & 0 \\ 0 & 0 & m(1+\nu_1)(1-\nu_1-2n\nu_2^2) \end{bmatrix} \begin{bmatrix} \epsilon_x \\ \epsilon_y \\ \gamma_{xy} \end{bmatrix} \quad (3.11)$$

where:  $n = E_1/E_2$ ; and  $m = G_2/E_2$ . The stress in the Z direction,  $\sigma_z$ , is calculated from:

$$\sigma_z = \nu_1 \sigma_x + n \nu_2 \sigma_y \quad (3.12)$$

To obtain the elastic solution for an underground opening taking into consideration the stratified rock conditions, it is only necessary to specify the five elastic constants for the rock in the computer program. The new stiffness matrix [K] for the model can then be generated since [D] for each element is known.

### 3.3 Brief Description of Initial Strain Method

The initial strain method is based on the general incremental approach that is often used for nonlinear analysis,

in which the solution is developed by considering a series of linear problems (i.e., multi-linear). This procedure begins with the elastic solution and the incremental creep strains for an appropriately small time interval and the selected creep law are computed by the methods given in Appendices B and C. The creep strains are regarded as initial strains and equivalent creep nodal forces are introduced into the solution to evaluate the incremental nodal displacements. Element strains and stresses are then determined (incremental, total, creep and elastic) for the end of the interval and used for the next creep increment. This creep solution then proceeds to the final desired time (Greenbaum, 1966; Emery, 1971). In this study the incremental, initial strain method developed by Emery (1971) was adopted and is given in more detail in Appendix B.

### 3.4 General Program Description

To study the aspects of tunnel behaviour of interest, a plane strain, linear displacement, triangular element, finite element computer program was developed that:

- a) determines the initial state of stress in the field;
- b) simulates excavation of the tunnel;
- c) allows for creep of the tunnel; and,
- d) incorporates various tunnel linings and lining strategies.

Simplified flow charts describing the program steps for determination of the initial stresses and simulating excavation procedure are shown in Figures (3.5) and (3.6) respectively. The

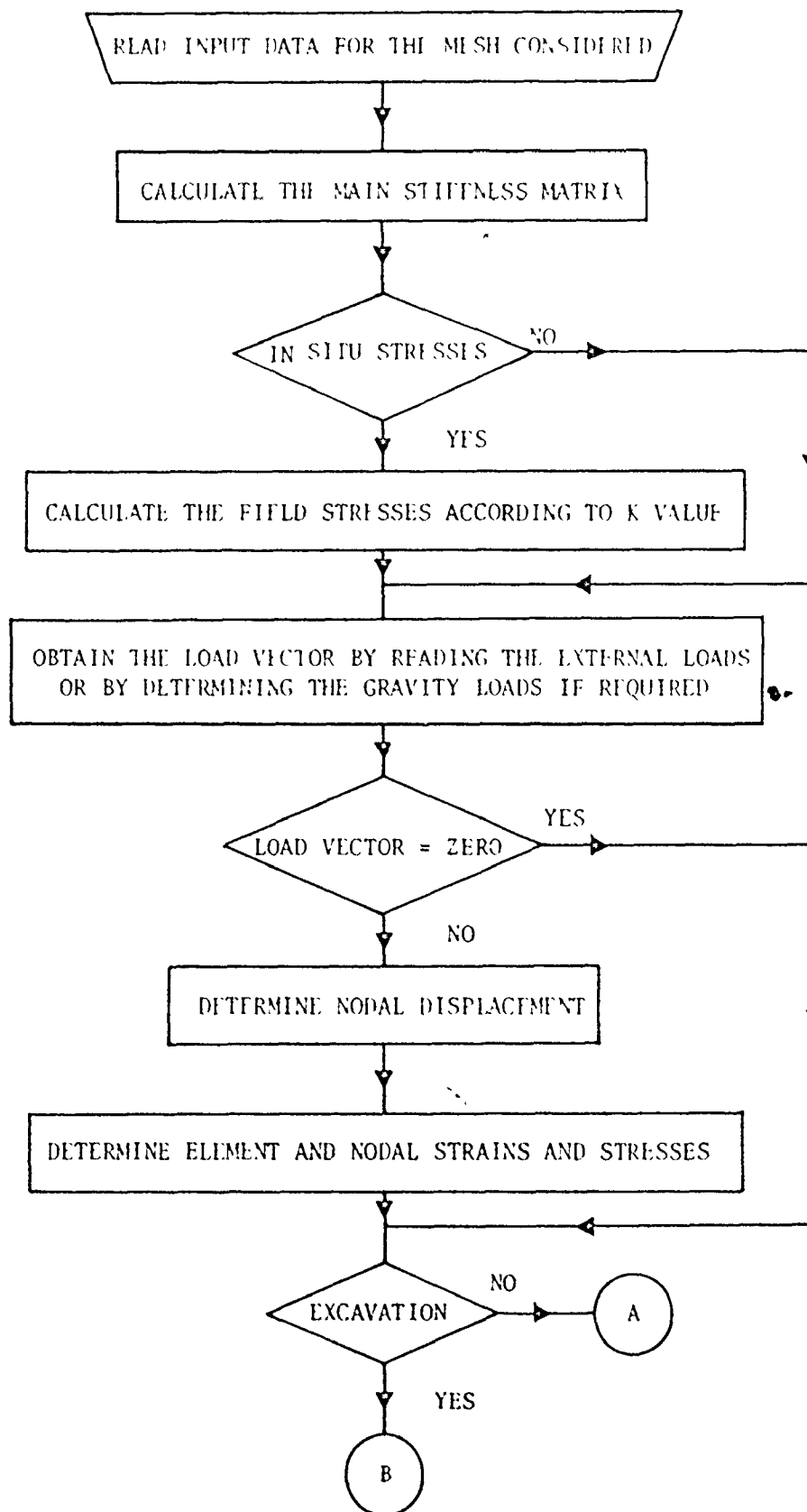


FIGURE 3.5 SIMPLIFIED FLOW CHART FOR INITIAL STRESS DETERMINATION USING THE FINITE ELEMENT METHOD

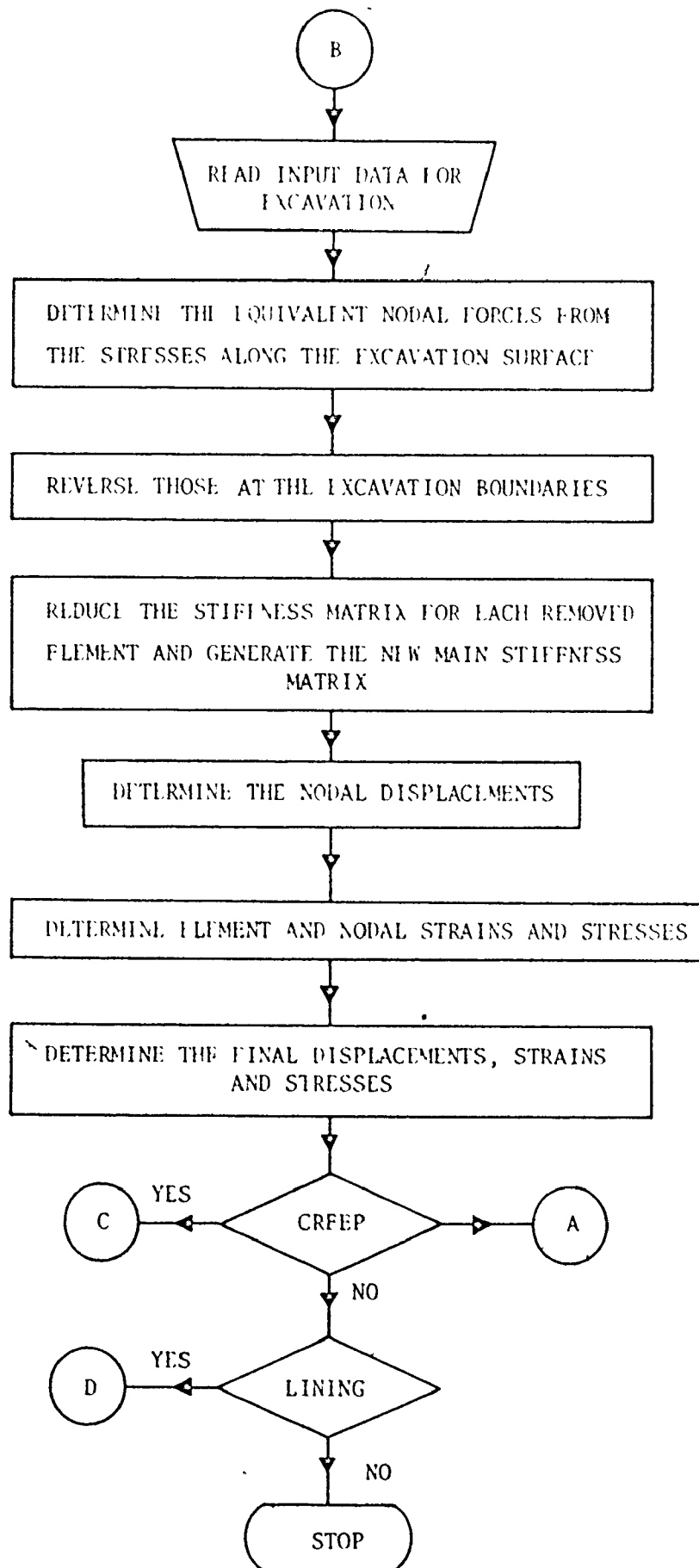


FIGURE 3.6 SIMPLIFIED FLOW CHART FOR EXCAVATION PROCEDURE USING THE FINITE ELEMENT METHOD

creep aspects of the computer program were developed from the programs provided by Lmery (1971). The simplified flow chart for the creep steps of the program is given in Figure (3.7). The lining aspects of the program are discussed in Chapter 4. The program can also be used for problems involving different materials and a wide variety of creep laws.

### 3.5 Example Problem

A thick-walled cylinder was used to check the accuracy of the techniques adopted as analytical solutions are available for this problem (Greenbaum, 1966). The radial deformations and stress distributions in the cylinder due to an internal pressure of 365 psi were determined by two finite element methods. The first finite element method used was a direct solution. Figure (3.8) gives the finite element idealization of the cylinder used for this solution. Because of the method used to handle boundary conditions, it was necessary to analyze a quadrant of the cross-section and equivalent nodal forces were specified to represent the internal pressure. The second method is the full "excavation" finite element procedure explained before. A solid cylinder was considered with the same outside radius and same properties as for the first method. The internal pressure was replaced by equivalent nodal forces acting at an imaginary boundary (nodes a to o in Figure 3.9) represented by the inside radius of the opening. After obtaining the element stresses, equivalent nodal forces were calculated for the material removed from inside the opening. These forces, with reversed sign, were then applied to the mesh at nodes a to o after reducing the

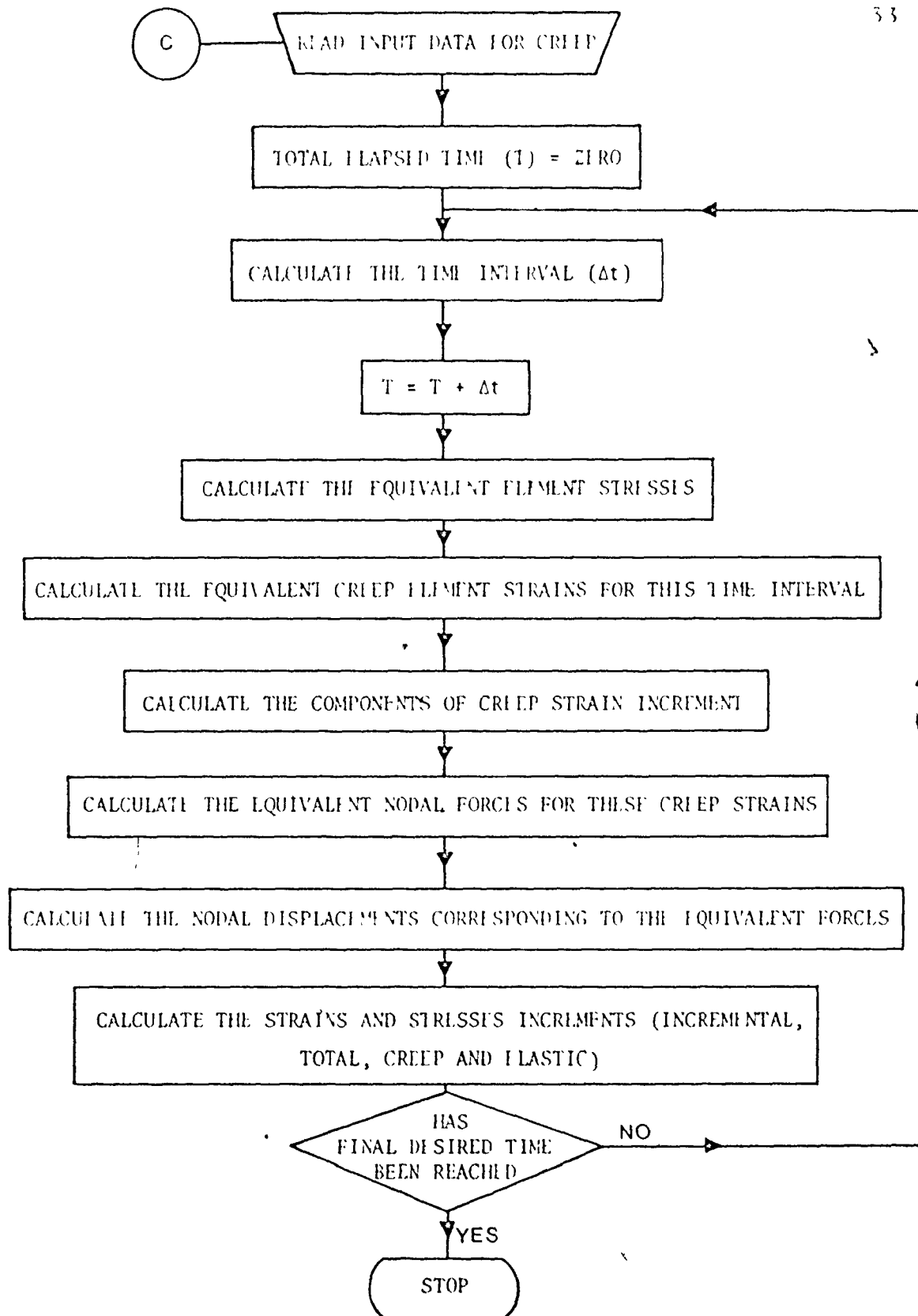


FIGURE 3.7 SIMPLIFIED FLOW CHART FOR INCREMENTAL CREEP ANALYSIS USING THE FINITE ELEMENT METHOD

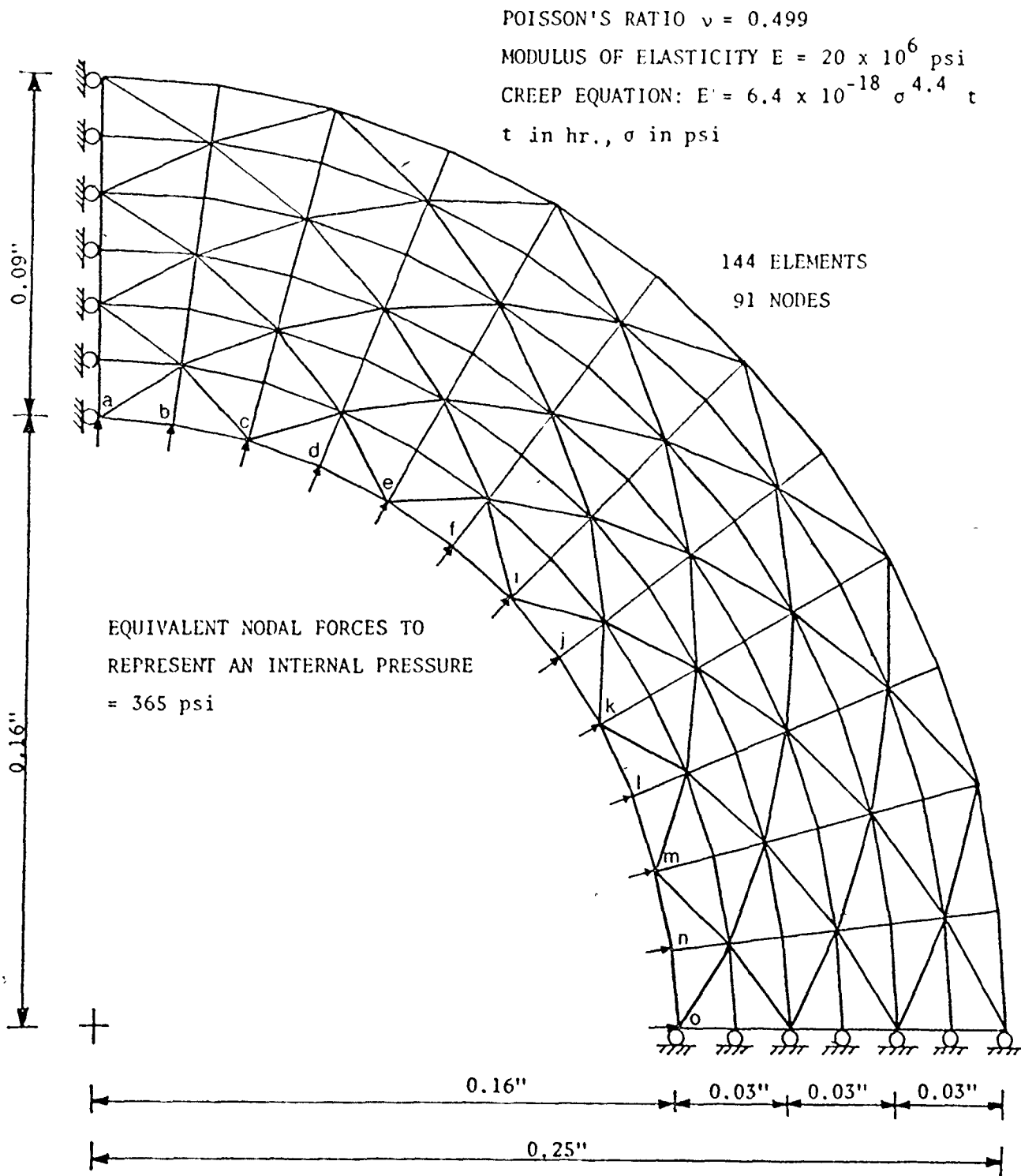


FIGURE 3.8 IDEALIZATION OF THE THICK-WALLED CYLINDER FOR DIRECT ANALYSIS

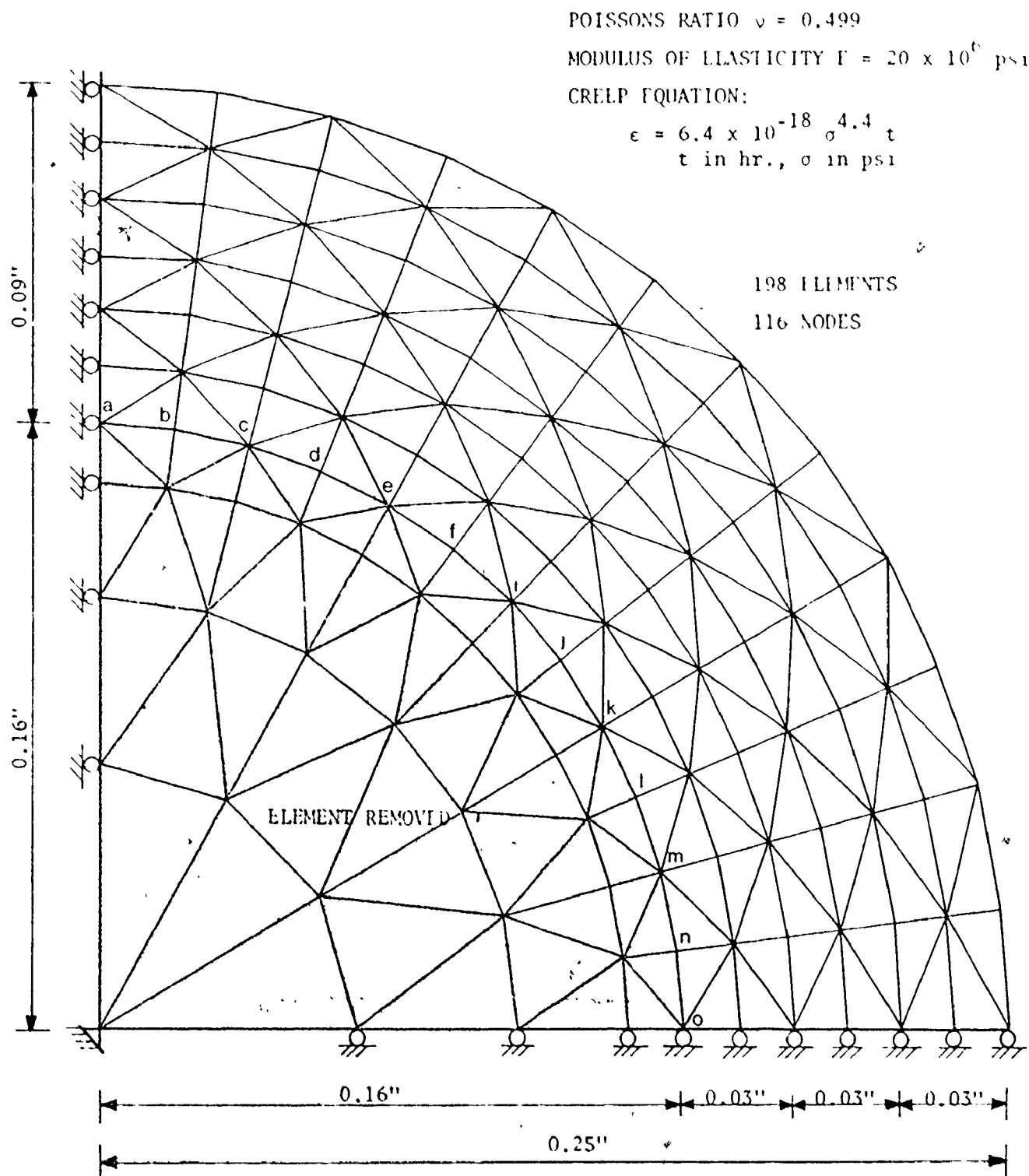


FIGURE 3.9 IDEALIZATION OF SOLID CYLINDER FOR "EXCAVATION"  
 PROCEDURE



modulus of any removed elements. The perturbation stresses were then obtained, and using these and the initial stresses, the final stress distribution was determined. In both methods, creep was then initiated from the elastic stress state.

The creep relationship used to check the program is given by:

$$\epsilon = 6.4 \times 10^{-18} \sigma^{4.4} t \quad (3.14)$$

where:  $\epsilon$  is the creep strain;  $\sigma$  is the stress in psi; and  $t$  is the time in minutes.

For the two finite element methods, the results were identical. Figure (3.10) represents the radial deformations and Figures (3.11) to (3.13) give the radial, circumferential and axial stress distributions in the cylinder respectively. The elastic stresses, steady state creep stresses (about two hours after creep) and radial deformations were then compared with the plane strain closed-form solution for this problem (Greenbaum, 1966). Figures (3.11) to (3.14) show these comparisons. It can be seen that there is close agreement with the closed-form solutions.

The finite element excavation procedure is used in Chapter 5 when the actual tunnel is considered.

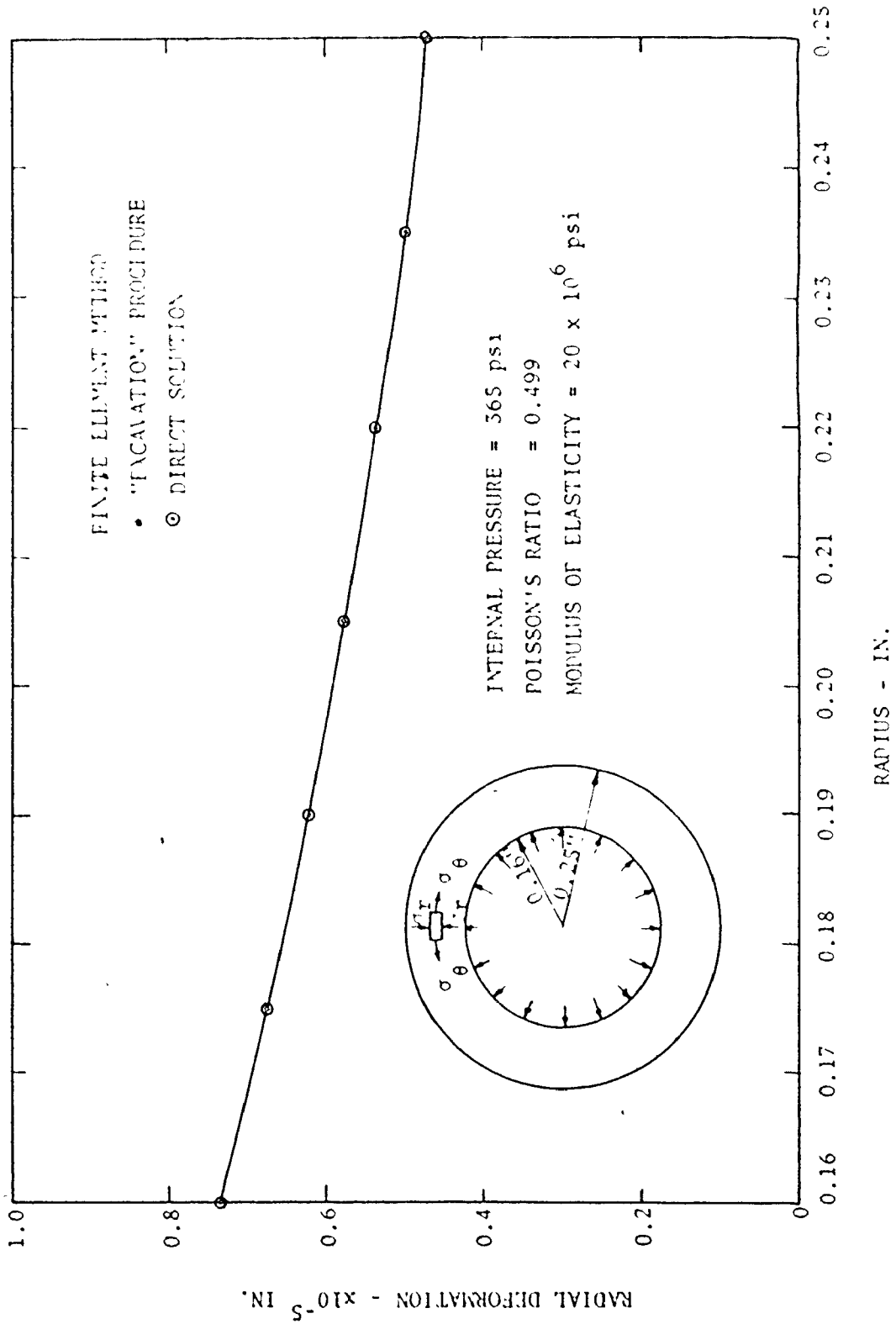


FIGURE 3.10 RADIAL ELASTIC DEFORMATION OF THE THICK-WALLED CYLINDER

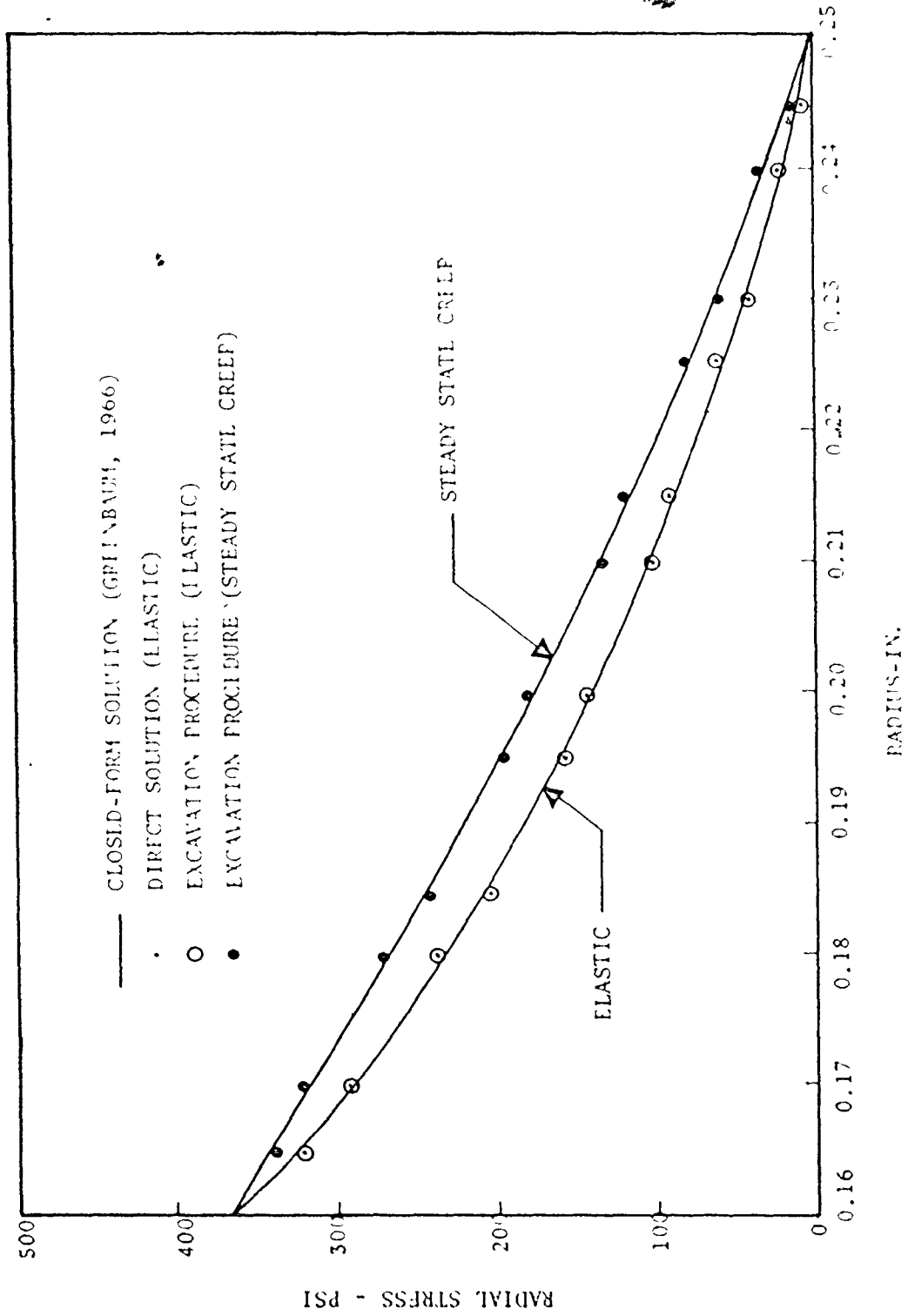


FIGURE 3.11 RADIAL STRESS DISTRIBUTION IN THE THICK-WALLED CYLINDER

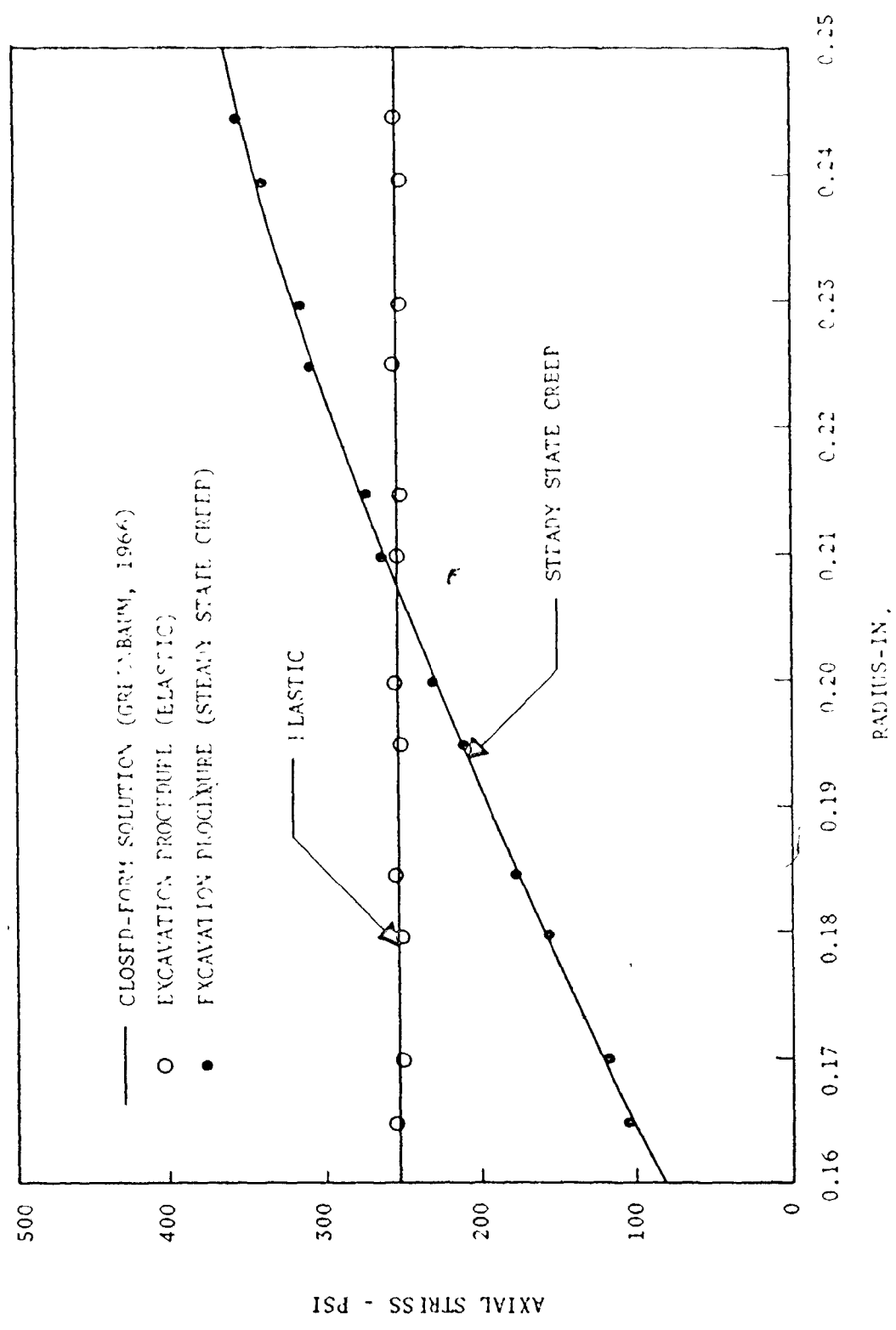


FIGURE 3.12 AXIAL STRESS DISTRIBUTION IN THE THICK-WALLED CYLINDER

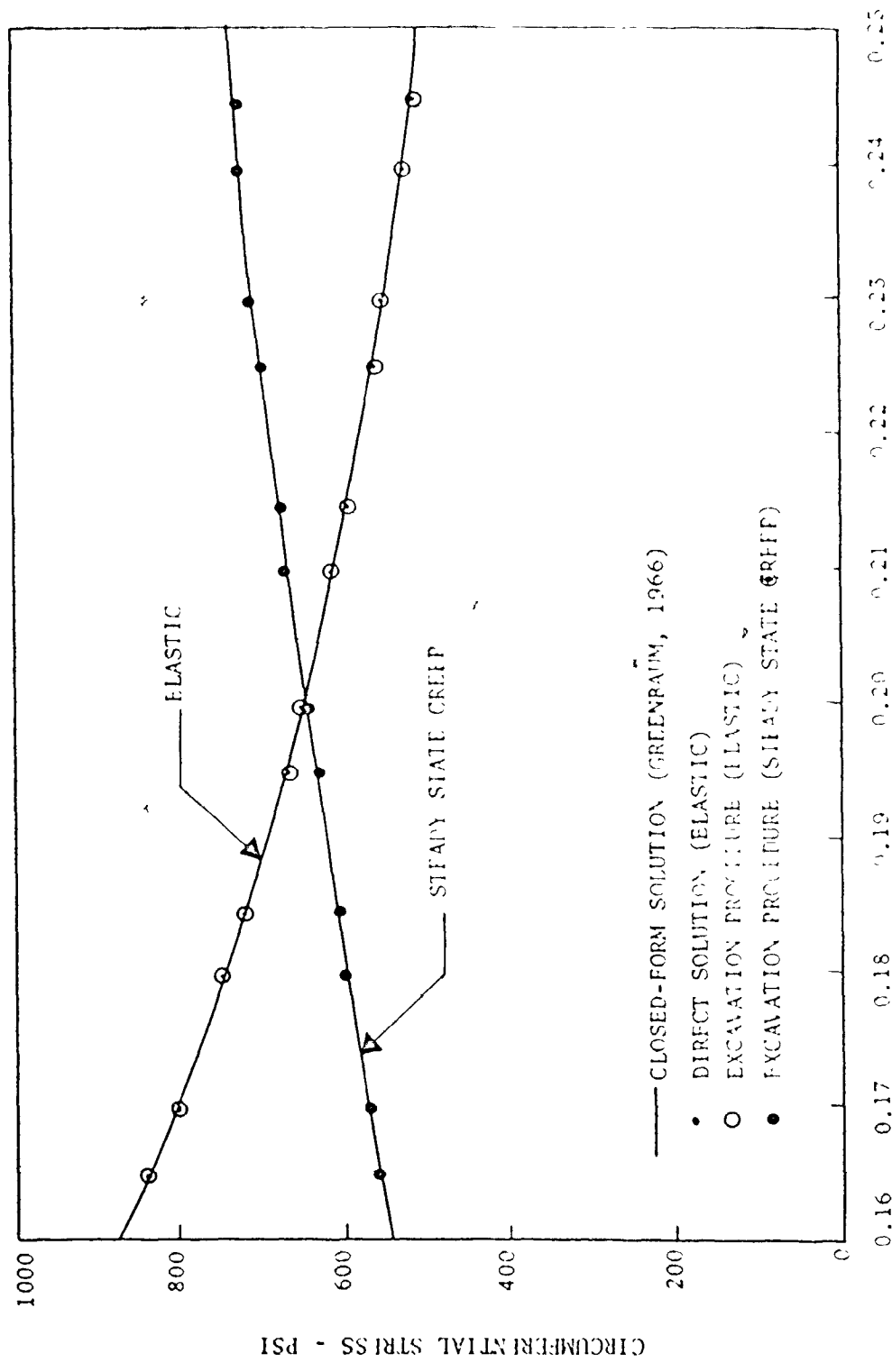


FIGURE 3.13 CIRCUMFERENTIAL STRESS DISTRIBUTION IN THE THICK-WALLED CYLINDER

FIGURE 3.13 CIRCUMFERENTIAL STRESS DISTRIBUTION IN THE THICK-WALLED CYLINDER

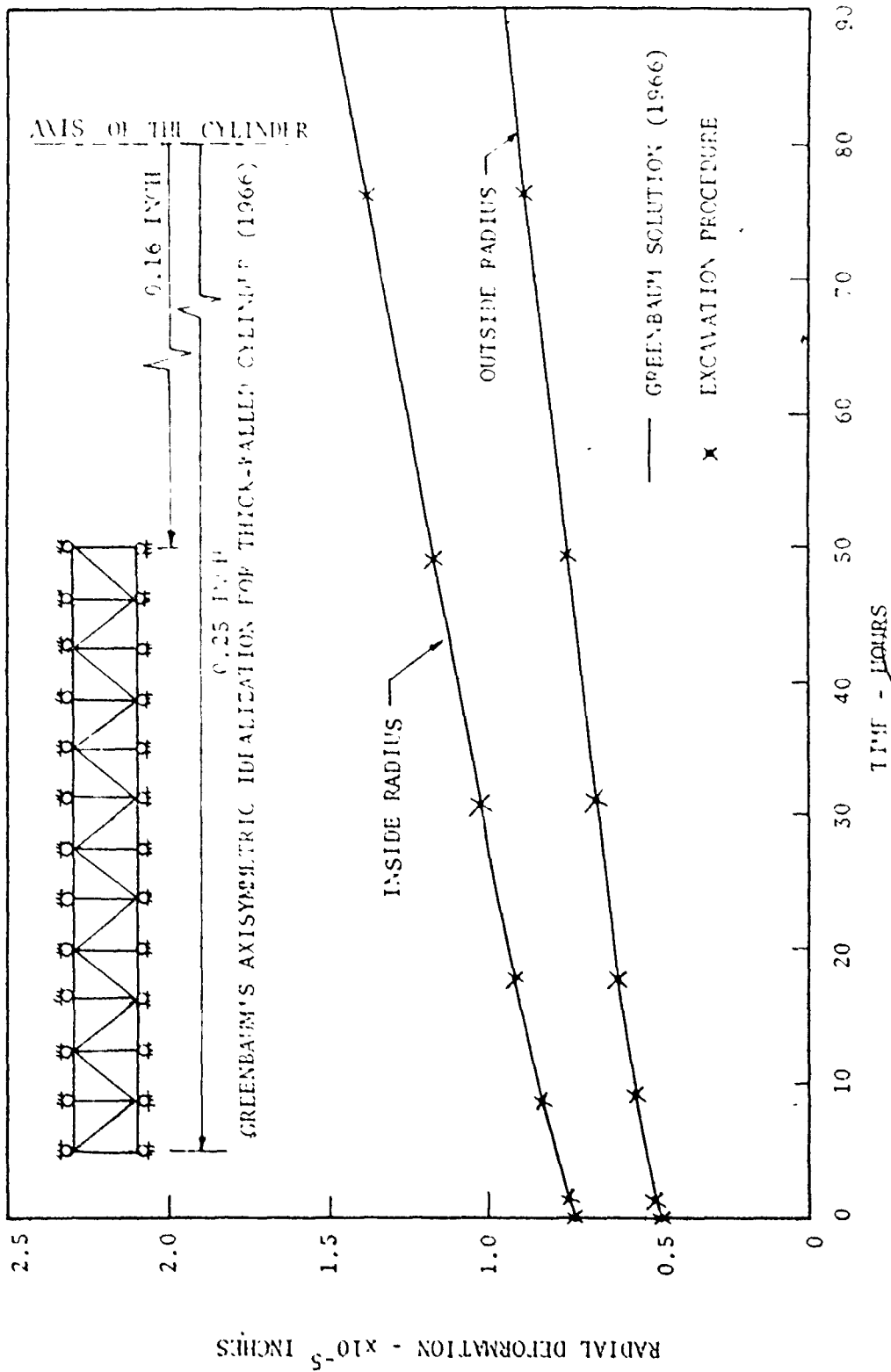


FIGURE 3.14 INSIDE AND OUTSIDE CREEP DEFORMATION OF THE THICK-WALLED CYLINDER

CHAPTER 4  
TUNNEL SUPPORT SYSTEMS

4.1 Introduction

The main functions of the tunnel support system are: a) to stiffen the underground structure; b) to reduce or prevent any swelling (expansion of rock due to water absorption); and c) to prevent failures due to ground squeezing. For openings in rock, support design is still a highly empirical practice and the Terzaghi design system is often adopted in which a zone of failure over the arch is prevented from collapsing (Terzaghi, 1946). Theoretical approaches (using shell theory, or considering the tunnel support as a fixed arch or a circular ring) are being used, but none are widely used or have been adequately validated in the field (Lane, 1975). There is a great need to model such problems with a realistic representation of squeezing ground in order to develop rational approaches for the design of underground supports.

4.2 Creep of Concrete Linings

After construction, the concrete lining may be subjected to additional stresses due to loading from the squeezing rock (concrete itself has time-dependent properties) and the lining creeps under these additional stresses (Neville, 1970).

Thus, in order to adequately simulate the behaviour of a concrete lining, this time-dependency must also be included.

Attempts have been made to express the creep behaviour of concrete observed in laboratory tests in the form of simple creep laws that can be used for predicting long-term responses in the field (Straub, 1930; Neville, 1970; Spooner, 1971; Illston and Jordaan, 1972; Dhir and Sangha, 1972). These creep relationships contain a varying number of constants, some of which have direct physical interpretation, but most of which require tests for their determination. The most important expressions for creep of concrete have been reviewed by Neville (1970) and will not be given in detail here.

Straub (1930) studied the creep behaviour of concrete and suggested the following creep equation:

$$\epsilon = K \sigma^n t^m \quad (4.1)$$

where:  $\epsilon$  is the creep strain;  $\sigma$  is the stress;  $t$  is the time; and  $K$ ,  $n$  and  $m$  are constants depending on the properties of concrete. Equation (4.1) has often been adopted to study the time-dependent deformations of concrete (Neville, 1970). Straub (1930) developed the constants ( $K$ ,  $n$  and  $m$ ) for Equation (4.1) from experimental work for a study of the creep behaviour of an unreinforced concrete arch subjected to uniformly distributed loads. Straub's problem was similar to the study presented here, consequently Equation (4.1) is the most appropriate and realistic stress-strain-time relationship available. Equation (4.1) will be used in the following form:



$$\epsilon = 56.7 \times 10^{-10} \sigma^{1.3} t^{0.4} \quad (4.2)$$

where:  $\sigma$  is in psi and  $t$  is in days.

#### 4.3 Modelling of Joints

In this study, joints between the lining and the surrounding rock were considered. The computer program for joints developed by Nguyen (1976) to study ice slope problems was incorporated into the tunnel creep program. The Goodman et al. (1968) theory for rock joints used is summarized in Figures (4.1) and (4.2). The main assumptions made to model the interfaces between the rock and the concrete lining as linear elements were: a) these elements can not sustain any tensile stresses; b) the width of the elements equals zero; and c) the linear elements represent rock-concrete interfaces and have no time-dependent properties.

The joint parameters  $K_n$ ,  $K_s$  and  $K_{sr}$  are required input data, where  $K_n$  and  $K_s$  are the joint stiffnesses per unit length of the joint in the normal and tangential directions with respect to the linear element, respectively.  $K_{sr}$  is the residual joint stiffness per unit length of the joint in the tangential direction. For this study, appropriate  $K_n$ ,  $K_s$  and  $K_{sr}$  values were obtained from tests made by Goodman et al. (1968) on rock joints. Since jointing between rock and concrete is a recent research area, detailed information on these values was not available. This area needs further experimental research work.

The stiffness matrix of each linear element was

$\tau$  TANGENTIAL STRESS  
 $\sigma_n$  NORMAL STRESS  
 $W$  WIDTH = 0

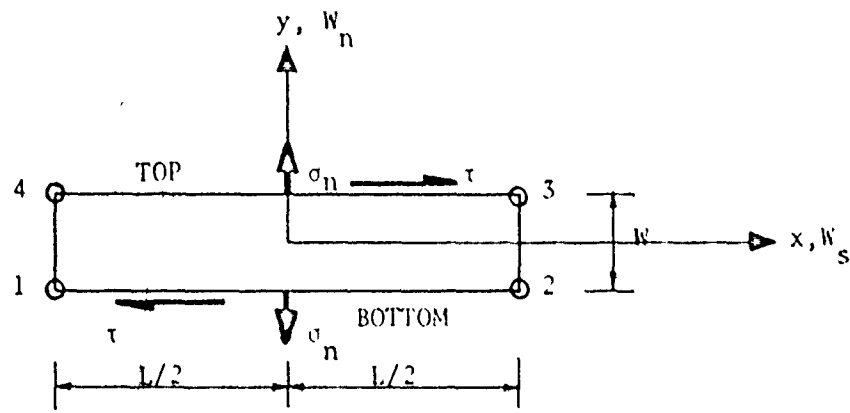


FIGURE 4.1 JOINT ELEMENT WITH ITS LOCAL COORDINATE SYSTEM (GOODMAN et al., 1968)

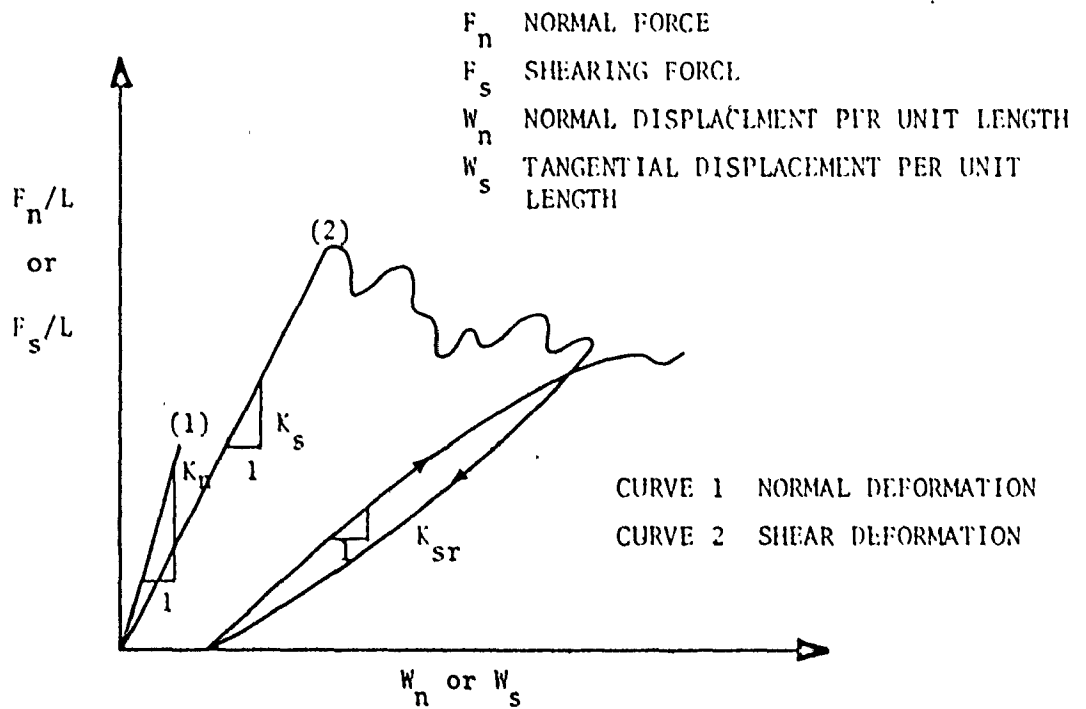


FIGURE 4.2 DATA FROM DIRECT SHEAR TEST ON A ROCK JOINT (GOODMAN et al., 1968)

obtained from:

$$[K] = \frac{1}{6} \begin{bmatrix} 2K_s & 0 & K_s & 0 & -K_s & 0 & -2K_s & 0 \\ 0 & 2K_n & 0 & K_n & 0 & -K_n & 0 & -2K_n \\ K_s & 0 & 2K_s & 0 & -2K_s & 0 & -K_s & 0 \\ 0 & K_n & 0 & 2K_n & 0 & -2K_n & 0 & -K_n \\ -K_s & 0 & -2K_s & 0 & 2K_s & 0 & K_s & 0 \\ 0 & -K_n & 0 & -2K_n & 0 & 2K_n & 0 & K_n \\ -2K_s & 0 & -K_s & 0 & K_s & 0 & 2K_s & 0 \\ 0 & -2K_n & 0 & -K_n & 0 & K_n & 0 & 2K_n \end{bmatrix} \quad (4.3)$$

These joint element stiffnesses were incorporated into the main stiffness matrix. After each stress determination, a check on the joint stresses is necessary to generate the appropriate main stiffness matrix for the next iteration. If a joint "fails" due to the joint shear stress exceeding the joint shear strength, the coefficient  $K_{sT}$  will be used in Equation (4.3) instead of the coefficient  $K_s$  and  $K_n$  remains unchanged. If the joint failure is due to tensile stresses perpendicular to a joint, the computer removes the influence of this "debonded" joint from the main stiffness matrix. This procedure is repeated for a number of cycles until a stable configuration is obtained. More detail on the linear joint elements is given in the literature (Goodman et al., 1968; Nguyen, 1976).

#### 4.4 Modelling of Concrete Linings

There are several important factors that must not be neglected during the design of a lining. These factors are: the rock structure and its properties; the state of stress before constructing the lining; the creep behaviour of the surrounding rock; the stiffness of the lining itself; and the creep behaviour of the concrete lining due to any ground squeezing. In the simulation developed here, all these factors are considered, based on the assumptions that the concrete lining is homogeneous and isotropic. The elastic modulus of the concrete was assumed to be constant with time. This assumption is reasonably accurate as long as the concrete lining does not take any significant loads before gaining full strength.

In this study, to compare the general interaction between the lining and the surrounding rock, cases representative of the two possible extreme conditions were considered. In the first, a rough interface was assumed, i.e., no separation between the elements representing the concrete lining and surrounding rock. Figure (4.3) shows this simulation (two different materials connected by the same nodal points) for the underground opening with its concrete lining. In the second case, linear joint elements between the rock and the concrete lining were used to allow for slip or actual openings between the materials. These linear elements have strength parameters dependent on the contact and friction between the rock and the concrete lining. Figure (4.4) shows the simulation

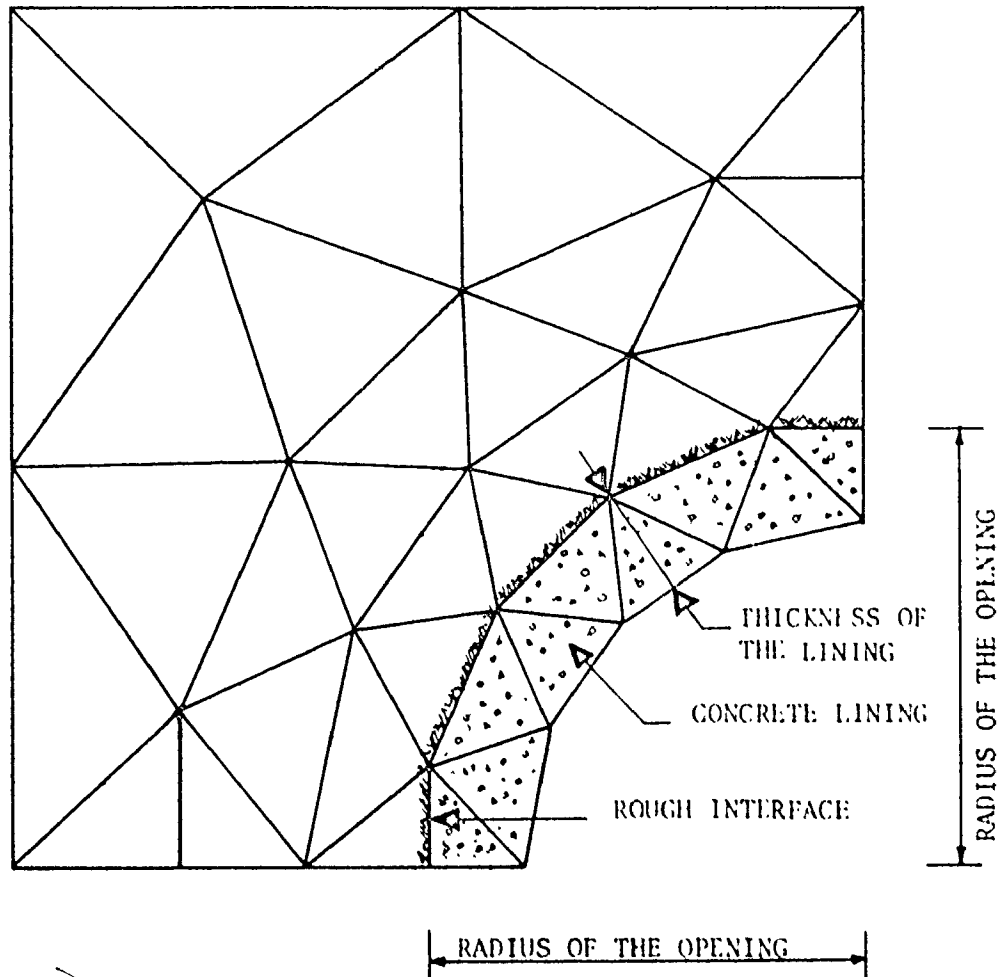


FIGURE 4.3 CONCRETE LINING WITHOUT JOINT ELEMENTS  
(NO SEPARATION BETWEEN THE ROCK AND  
CONCRETE-ROUGH INTERFACE)

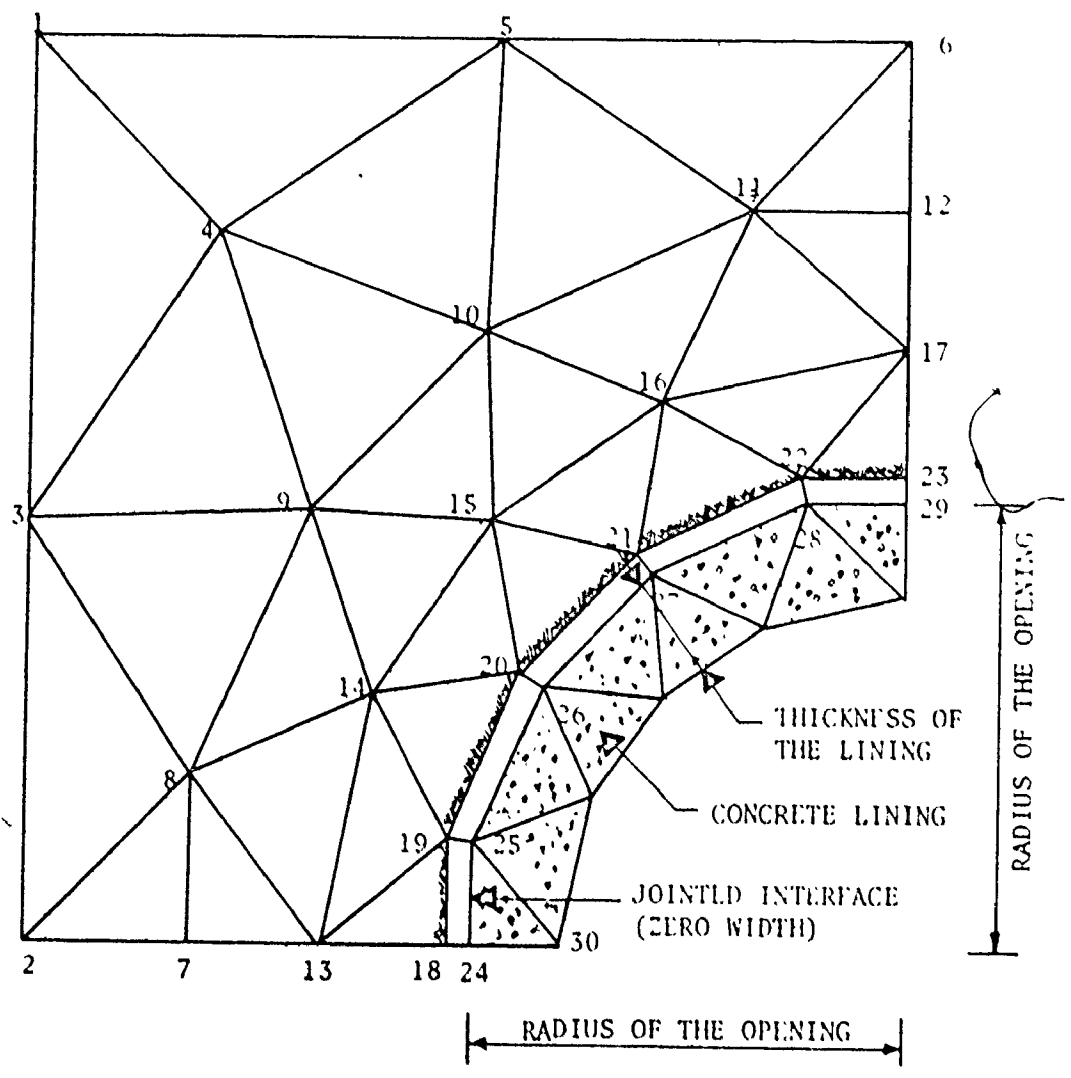


FIGURE 4.4 SIMULATION OF CONCRETE LINING-ROCK INTERFACE WITH JOINT ELEMENTS

for the lining with joints.

A simplified flow chart for the finite element computer program for lining simulation and creep analysis is shown in Figure (4.5). To save computer storage and time, there is one restriction on numbering the nodes for the rock interface if a lining is to be placed. The nodes at the excavated surface should be numbered last as shown in Figure (4.4) for minimum increase in band width when the lining elements are incorporated. The concrete elements are incorporated in a stress free state. Therefore, for the first creep increment after placing the lining, only the rock undergoes creep deformations. The creep forces then cause displacement of all the nodes including the lining nodal points, and hence internal strains and stresses start to develop in the lining. Creep then continues for both materials according to their creep laws. This will be shown in detail where specific examples are given in the next chapter.

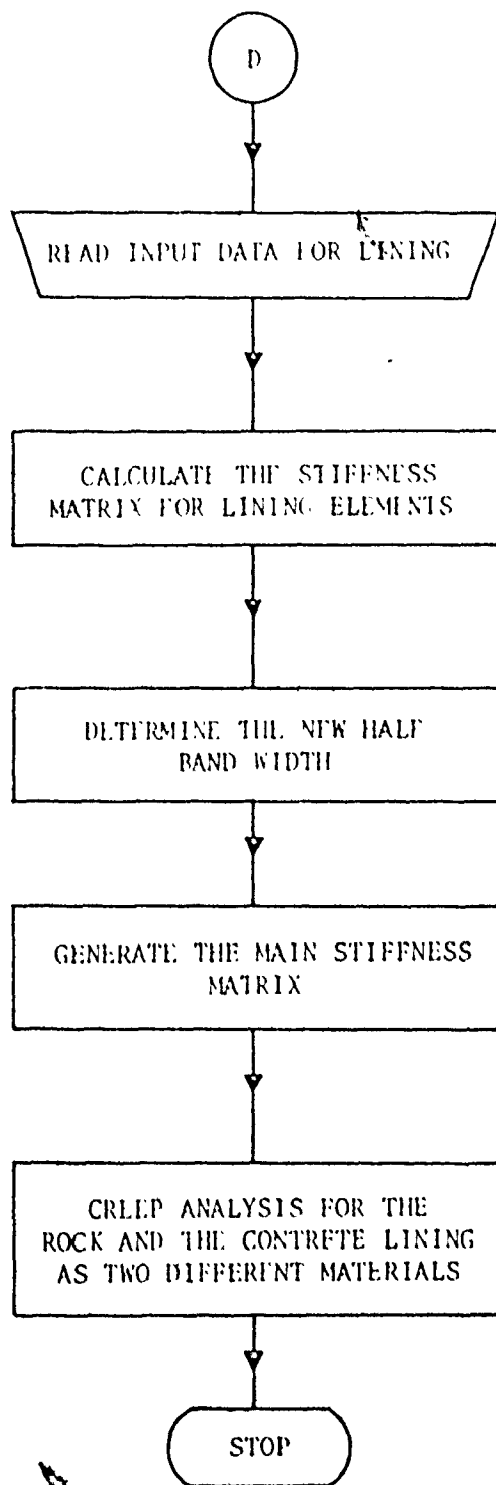


FIGURE 4.5 SIMPLIFIED FLOW CHART FOR LINING SIMULATION AND CREEP ANALYSIS



CHAPTER 5  
SIMULATION OF A TYPICAL  
FIELD PROBLEM

5.1 Introduction

The finite element method presented in the previous chapters was used to simulate the creep behaviour of an underground intake tunnel for a large filtration plant near Toronto. This tunnel is a circular opening of 13 feet (4 meters) diameter at a depth of 200 feet (61 meters). Previous Geological Survey of Canada (Map No. 1263 A) work indicated that the tunnel is located in Collingwood shale. The general trend of the bedding dip in this part of Ontario is south-westerly with a magnitude of 0.2 degrees, i.e., the bedding is nearly horizontal. Table (5.1) shows the rock properties at the site of the tunnel as measured experimentally by Franklin Trow Associates Limited, who have cooperated in the field aspects of this tunnel simulation study. These values were not all available at the time of the study, so that the set of representative values shown in Tables (5.2) and (5.3) were assumed from initial test data and a careful examination of the properties of shale published in the literature (Farmer, 1968; Jaeger, 1972; Bollinger, 1974). It can be seen from Tables (5.1) to (5.3) that the assumed values are very close to the final measured values.

TABLE 5.1 ROCK PROPERTIES MEASURED EXPERIMENTALLY  
[FTA, 1975]

ROCK PROPERTY	MEASURED VALUES	
	RANGE	AVERAGE
UNIAXIAL STRENGTH PERPENDICULAR TO THE BEDDING (psi)	1870 - 2860	2555
BULK UNIT WEIGHT (pcf)	140 - 152	146
ELASTIC MODULUS PARALLEL TO THE BEDDING (psi) x 10 <sup>6</sup>	0.7 - 2.7	1.46
ELASTIC MODULUS PERPENDICULAR TO THE BEDDING (psi) x 10 <sup>6</sup>	0.16 - 0.47	0.30
WATER CONTENT (%)	1.88 - 3.35	2.74
POISSON'S RATIO PARALLEL TO THE BEDDING	---	0.25
POISSON'S RATIO PERPENDICULAR TO THE BEDDING	---	0.17

TABLE 5.2 SUMMARY OF ISOTROPIC MATERIAL PROPERTIES

MATERIAL	ELASTIC MODULUS -E x 10 <sup>6</sup> psi	POISSON'S RATIO -ν	UNIT WEIGHT -γ pcf	AVERAGE	
				E x 10 <sup>6</sup> psi	ν
SHALE	0.2 - 1.1	0.22 - 0.40	140 - 160	0.65	0.31
					150

TABLE 5.3 SUMMARY OF ORTHOTROPIC MATERIAL PROPERTIES

MATERIAL	ELASTIC MODULUS IN X-DIRECTION E <sub>x</sub> * x 10 <sup>6</sup> psi	ELASTIC MODULUS IN Y-DIRECTION E <sub>y</sub> * x 10 <sup>6</sup> psi	POISSON'S RATIO X-Y DIRECTION ν <sub>xy</sub>	POISSON'S RATIO X-Z DIRECTION ν <sub>xz</sub> **	SHEAR MODULUS X-Y DIRECTION G <sub>xy</sub> x 10 <sup>6</sup> psi

\* X AND Z ARE PARALLEL TO THE BEDDING PLANES, FIGURE 3.4

\*\* Y IS PERPENDICULAR TO THE BEDDING PLANES, FIGURE 3.4

In this chapter, a complete finite element simulation of the problem is presented, including: elastic solutions for isotropic and orthotropic rock properties for various initial states of stress; and a complete time-dependent analysis, with and without a concrete lining. A comparison of the rock movements as measured at the site of the tunnel and those predicted by the finite element simulation is also given.

## 5.2 Idealization

The plane strain, linear displacement, triangular element, finite element idealization for the opening is shown in Figure (5.1). Because of the symmetry of the tunnel with respect to its vertical axis (geometric and loading), it was only necessary to analyze one half of the cross section. (Due to gravity loading considerations, there is no horizontal symmetry). For the opening itself, it was adequate to represent the rock removed from the opening during excavation by a single row of elements (24 elements for the half cross section). This row of elements is shaded in Figure (5.1).

### 5.2.1 Mesh Configuration and Boundary Locations

The finite element mesh was carefully selected to ensure that the results obtained were not significantly influenced by:

- a) the mesh not being fine enough; or
- b) the boundaries not being far enough away from the opening.

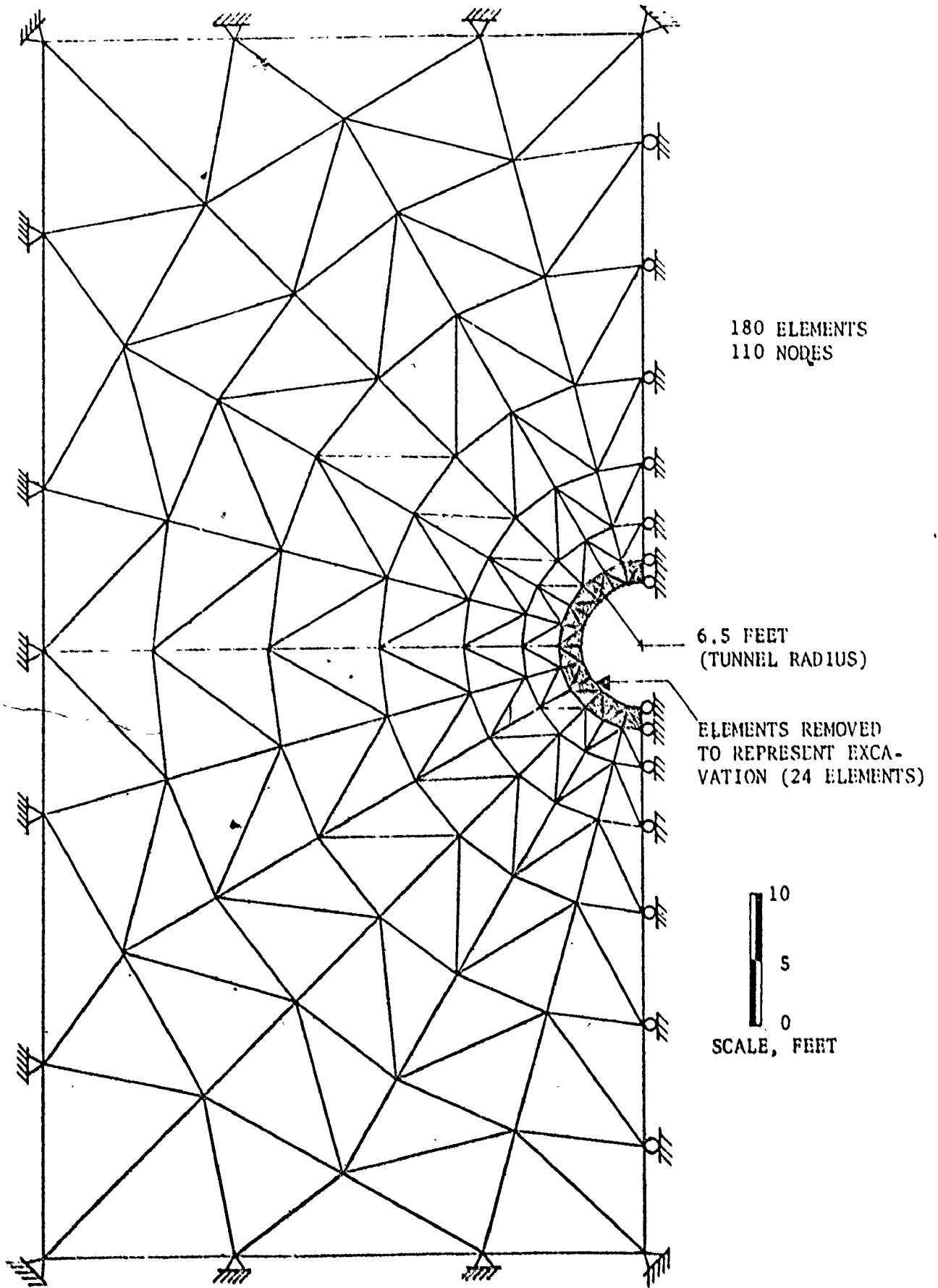


FIGURE 5.1 FINITE ELEMENT IDEALIZATION OF THE TUNNEL

Kulhawy (1974) found that a reasonable criterion for meshes would be a minimum of 125-150 elements for typical plane strain finite element simulations of structures in homogeneous rock where there is a plane of symmetry as in Figure (5.1). Kulhawy (1974) also found that to have a "perfect" comparison with the closed-form theoretical solution, the boundaries of the finite element mesh would have to be at "infinity". Obviously, this perfect comparison is impossible to achieve and Kulhawy indicated that the mesh would be adequate if the largest difference between any of the computed and theoretical stresses or displacements, on or near the opening, is less than 10 percent. He found that this 10 percent criterion is readily satisfied with a boundary located 6 times the radius away from the centre of the opening. Therefore, to be conservative, boundaries 7 times the radius away from the centre of the opening and 180 elements were adopted in the mesh used to study the tunnel.

### 5.2.2 Excavation

The solution in each case was started by obtaining the appropriate initial stresses for various representative  $K$  conditions. For excavation simulations in isotropic elastic rock,  $K$  values of 1, 4, 7 and 9 were considered with the larger values representing higher initial horizontal stresses. For excavation simulations in orthotropic elastic rock,  $K$  values of 1 and 4 were considered. Then, the first row of the elements (shaded elements) of the finite element

mesh shown in Figure (5.1) was removed to simulate excavation of the tunnel opening. The elastic displacements, strains and perturbation stresses due to excavation of the opening were then computed. These displacements, strains and perturbations stresses plus the initial stresses, Figure (3.1), then represented the elastic (instantaneous) displacements, strains and stresses in the rock due to the construction of the underground opening.

### 5.3 Discussion of Elastic Solutions

#### a) Displacements

For the isotropic elastic rock, the instantaneous displacements around the tunnel due to excavation were uniform for the  $K$  equal to 1 condition as shown in Figure (5.2). This is as expected since the  $K$  equal to 1 condition is similar to a hydrostatic loading condition. When high initial horizontal stresses were modelled for the tunnel site as indicated by  $K$  equal to 4, 7 and 9, the horizontal displacements increased as shown in Figures (5.2) and (5.3). However, the inward displacements for the crown point "A" and the floor point "E" decreased, and for  $K$  equal to 7 and 9, points "A" and "E" actually moved outwards. This divergence under high lateral stresses is expected from field evidence of arch failures in some tunnels where high lateral stresses were known to exist.

For the orthotropic elastic rock (bedded) and  $K$  equal to 1, it can be seen from Figure (5.4) that the vertical

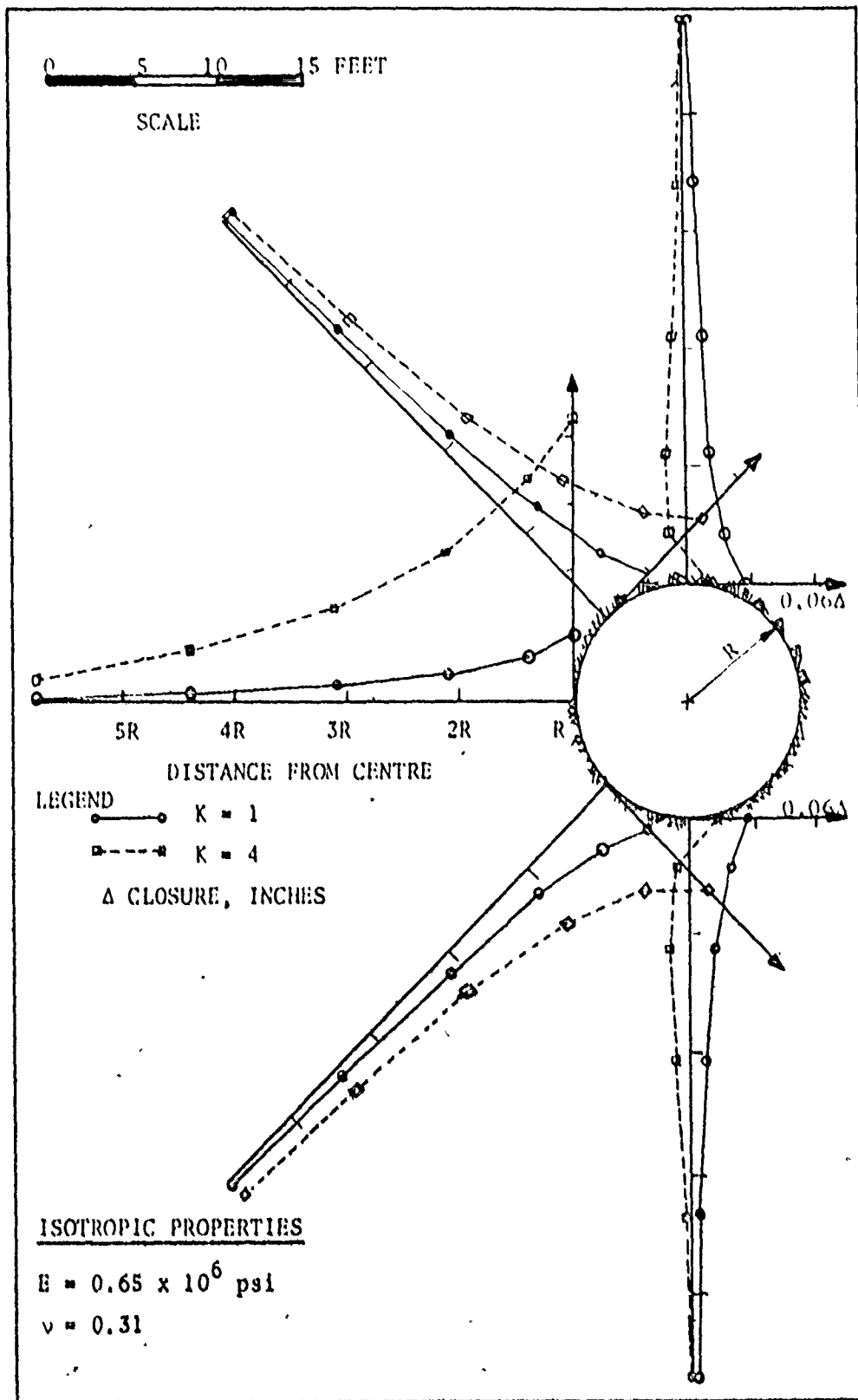


FIGURE 5.2 COMPUTED MOVEMENTS AFTER EXCAVATION FOR ISOTROPIC ELASTIC ROCK,  $K = 1, 4$  (POSITIVE DISPLACEMENT MAGNITUDES CORRESPOND TO INWARDS MOVEMENT).



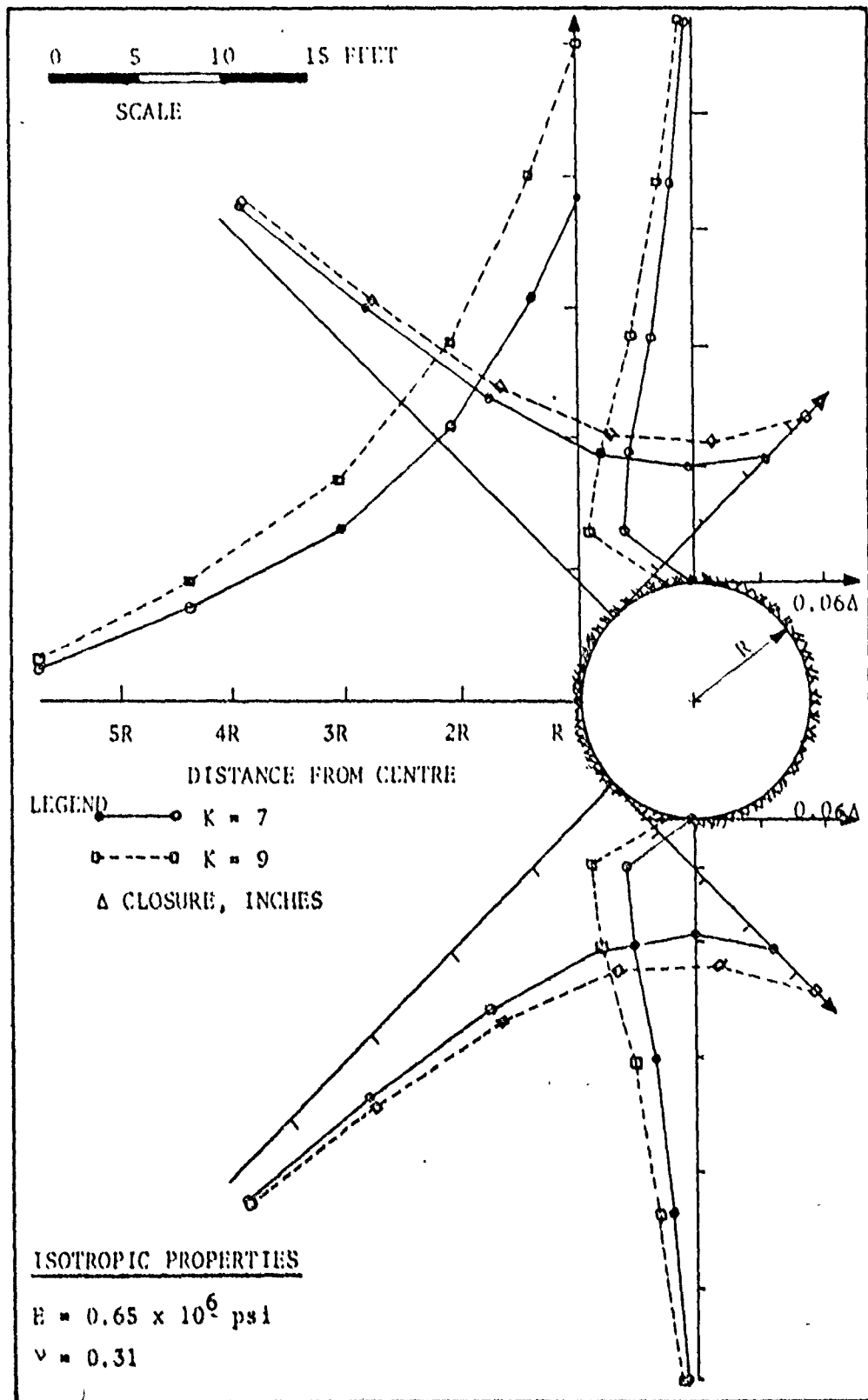


FIGURE 5.3 COMPUTED MOVEMENTS AFTER EXCAVATION FOR ISOTROPIC ELASTIC ROCK,  $K = 7, 9$  (POSITIVE DISPLACEMENT MAGNITUDES CORRESPOND TO INWARDS MOVEMENT).

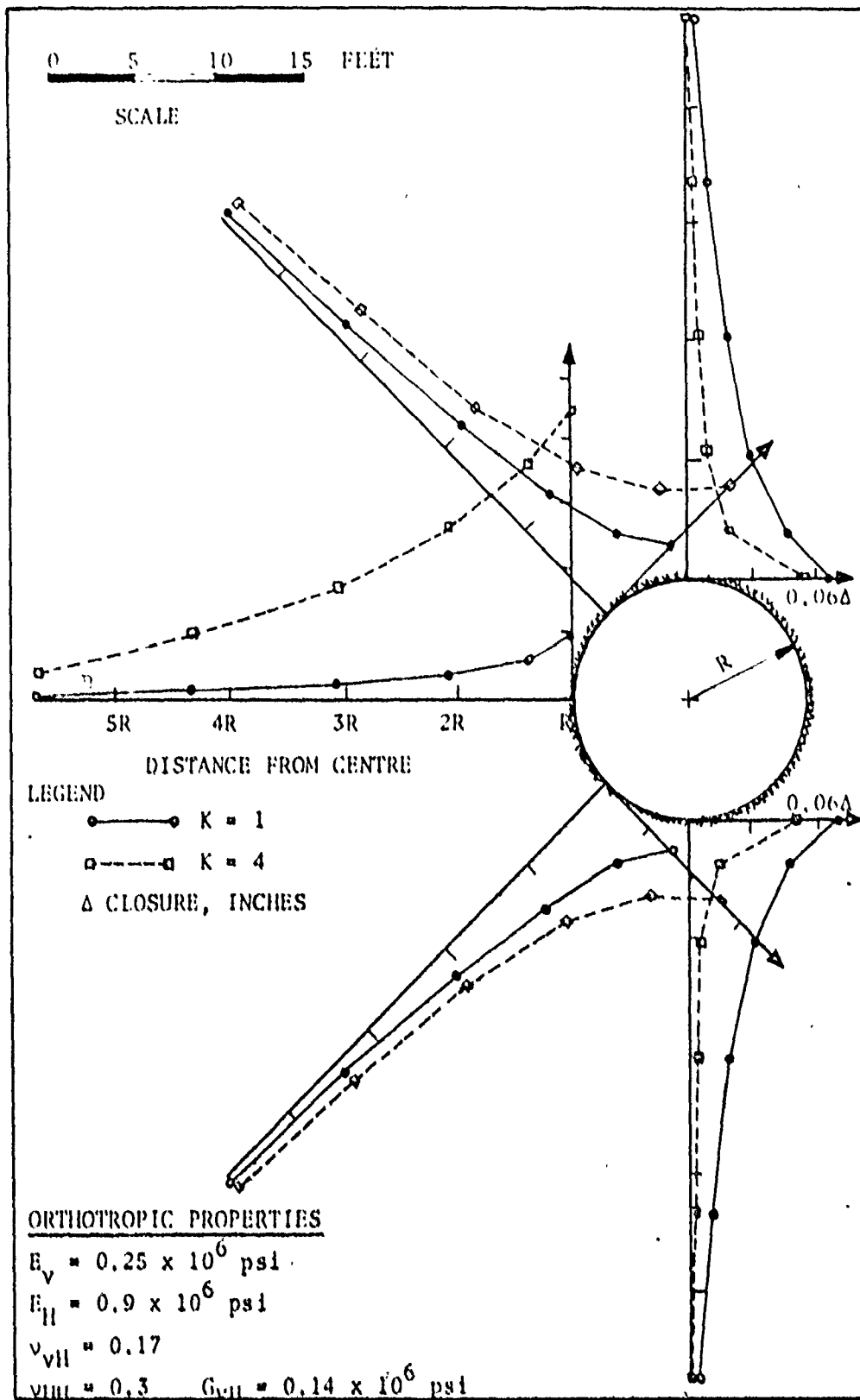


FIGURE 5.4 COMPUTED MOVEMENTS AFTER EXCAVATION FOR ORTHOTROPIC ELASTIC ROCK,  $K = 1, 4$  (POSITIVE DISPLACEMENTS MAGNITUDES CORRESPOND TO INWARDS MOVEMENT).

convergence is greater than the horizontal convergence due to bedding influences represented by the orthotropic condition. With  $K$  increased to 4, the horizontal convergence value increased and the vertical convergence value decreased. Table (5.4) summarizes the horizontal and vertical convergence values for both isotropic and orthotropic elastic rock and various  $K$  values. It can be seen that the horizontal convergence values for both isotropic and orthotropic cases are nearly the same, but the vertical convergence for the orthotropic case is greater than for the isotropic case.

b) Stress Concentrations

Figures (5.5) to (5.8) show the stress concentrations for isotropic elastic rock for  $K$  equal to 1, 4, 7 and 9, respectively. Figures (5.9) and (5.10) show the stress concentrations for orthotropic elastic rock for  $K$  equal to 1 and 4. It should be pointed out that the nodal stresses at the surface are actually the average of the stresses in the adjacent elements and will not generally be equal to the actual surface values. Generally, due to excavation the radial stresses decreased while the tangential stresses increased near the opening. With increasing distance away from the opening, the various stresses converged to their values before excavation, i.e., stress concentrations became unity as anticipated. At the springline, the radial compressive stresses increased with increasing  $K$  value (high initial horizontal stresses), while the tangential

TABLE 5.4 HORIZONTAL AND VERTICAL CONVERGENCE VALUES AFTER EXCAVATION

INITIAL STRESS CONDITION	ELASTIC ISOTROPIC		ELASTIC ORTHOTROPIC	
	HORIZONTAL CONVERGENCE inch	VERTICAL CONVERGENCE inch	HORIZONTAL CONVERGENCE inch	VERTICAL CONVERGENCE inch
K = 1	0.057	0.057	0.058	0.138
K = 4	0.262	0.024	0.264	0.106
K = 7	0.467	-0.008*	---	---
K = 9	0.604	-0.030*	---	---

\* NEGATIVE VALUES CORRESPOND TO OUTWARDS MOVEMENT

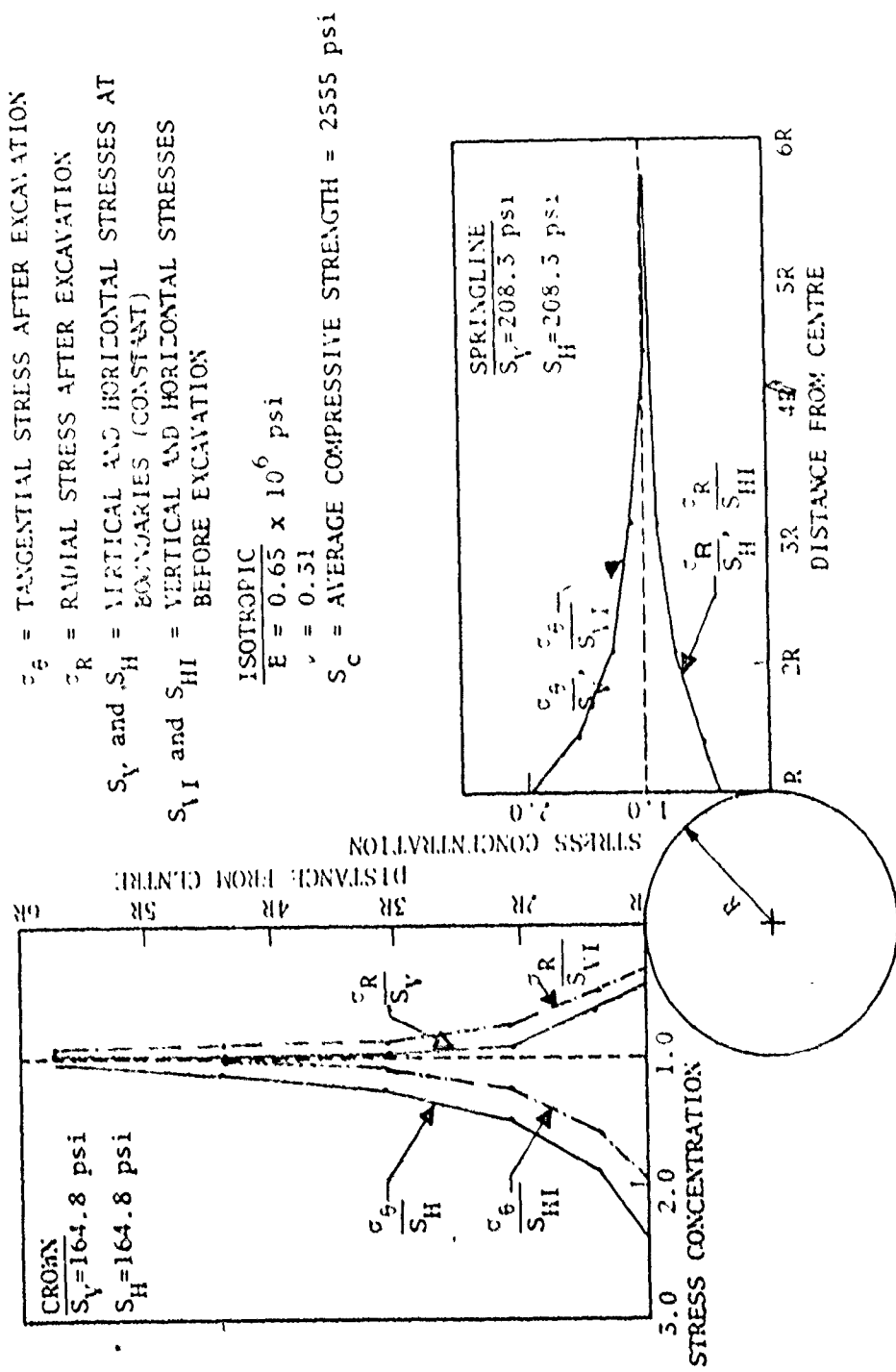


FIGURE 5.5 STRESS CONCENTRATION ALONG VERTICAL AND HORIZONTAL SECTIONS, ISOTROPIC,  $K = 1$

$\sigma_{\theta}$  = TANGENTIAL STRESS AFTER EXCAVATION  
 $\sigma_r$  = RADIAL STRESS AFTER EXCAVATION  
 $S_V$  and  $S_H$  = VERTICAL AND HORIZONTAL STRESSES AT BOUNDARIES (CONSTANT)  
 $S_{VI}$  AND  $S_{HI}$  = VERTICAL AND HORIZONTAL STRESSES BEFORE EXCAVATION

ISOTROPIC

$E = 0.65 \times 10^6$  psi  
 $\nu = 0.31$

$S_c$  = AVERAGE COMPRESSIVE STRENGTH  
 $= 2555$  psi

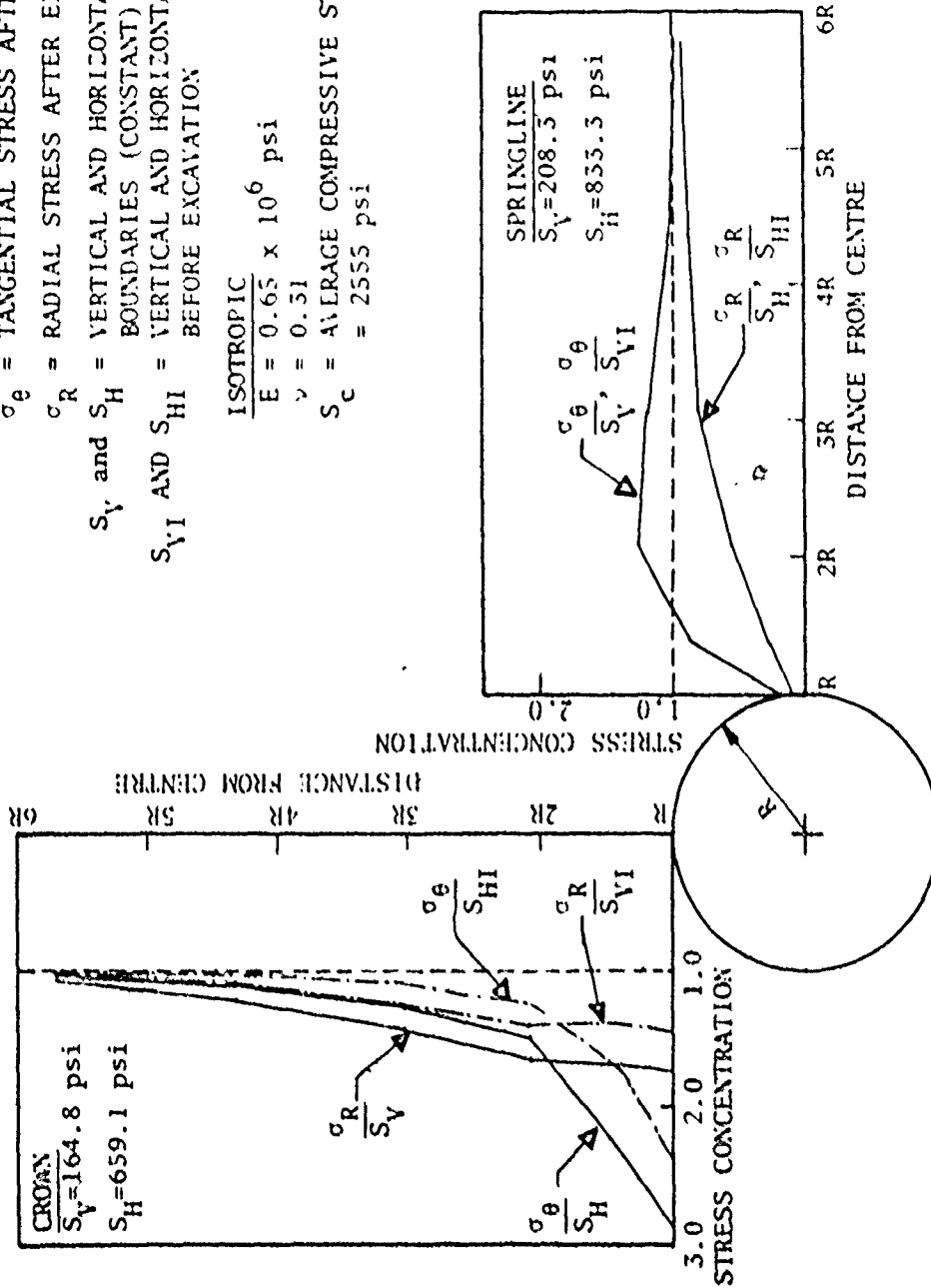


FIGURE 5.6 STRESS CONCENTRATION ALONG VERTICAL AND HORIZONTAL SECTIONS, ISOTROPIC,  $K = 4$

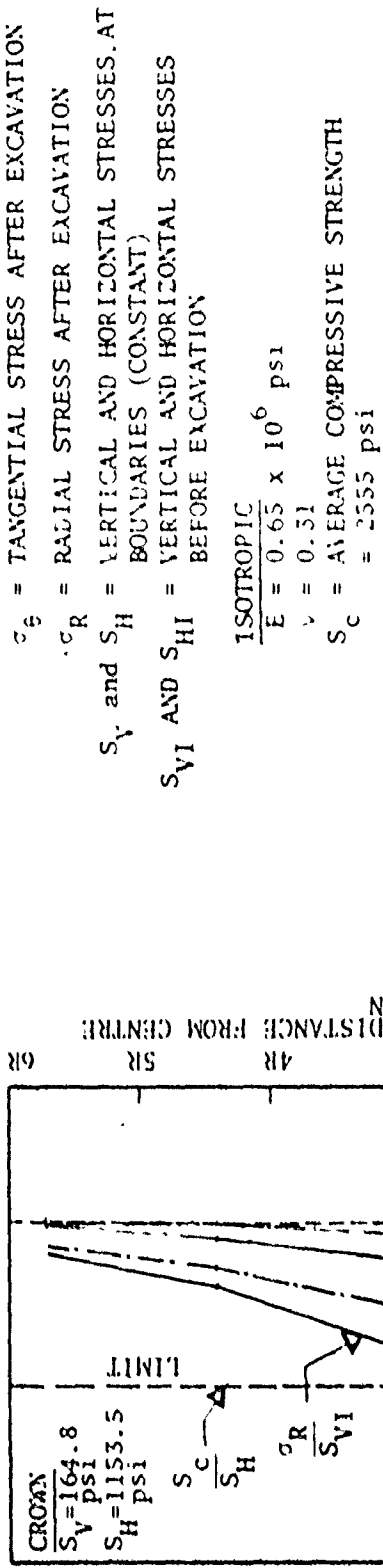


FIGURE 5.7 STRESS CONCENTRATION ALONG VERTICAL AND HORIZONTAL SECTIONS, ISOTROPIC, K = 7

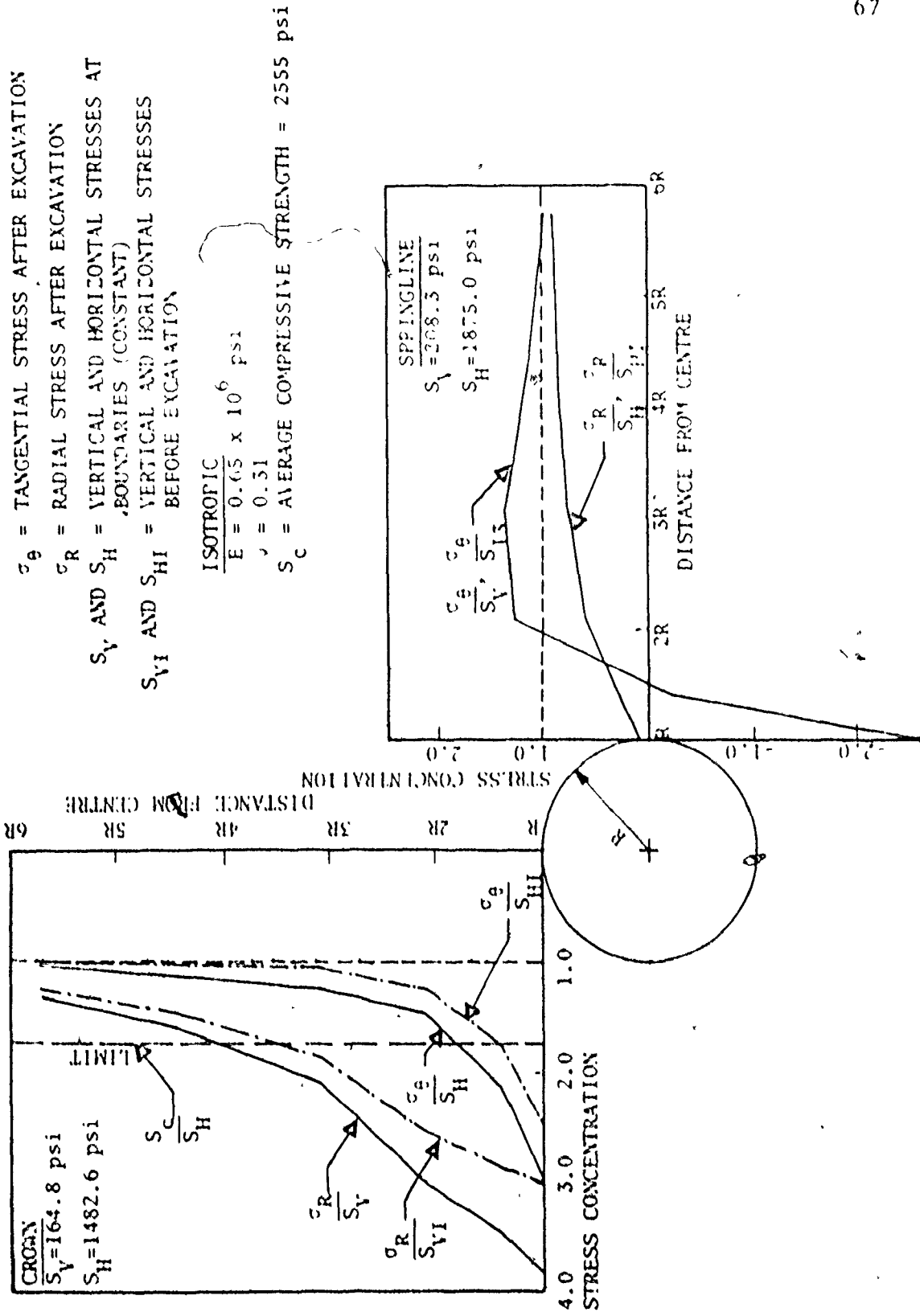


FIGURE 5.8 STRESS CONCENTRATION ALONG VERTICAL AND HORIZONTAL SECTIONS, ISOTROPIC, K = 9



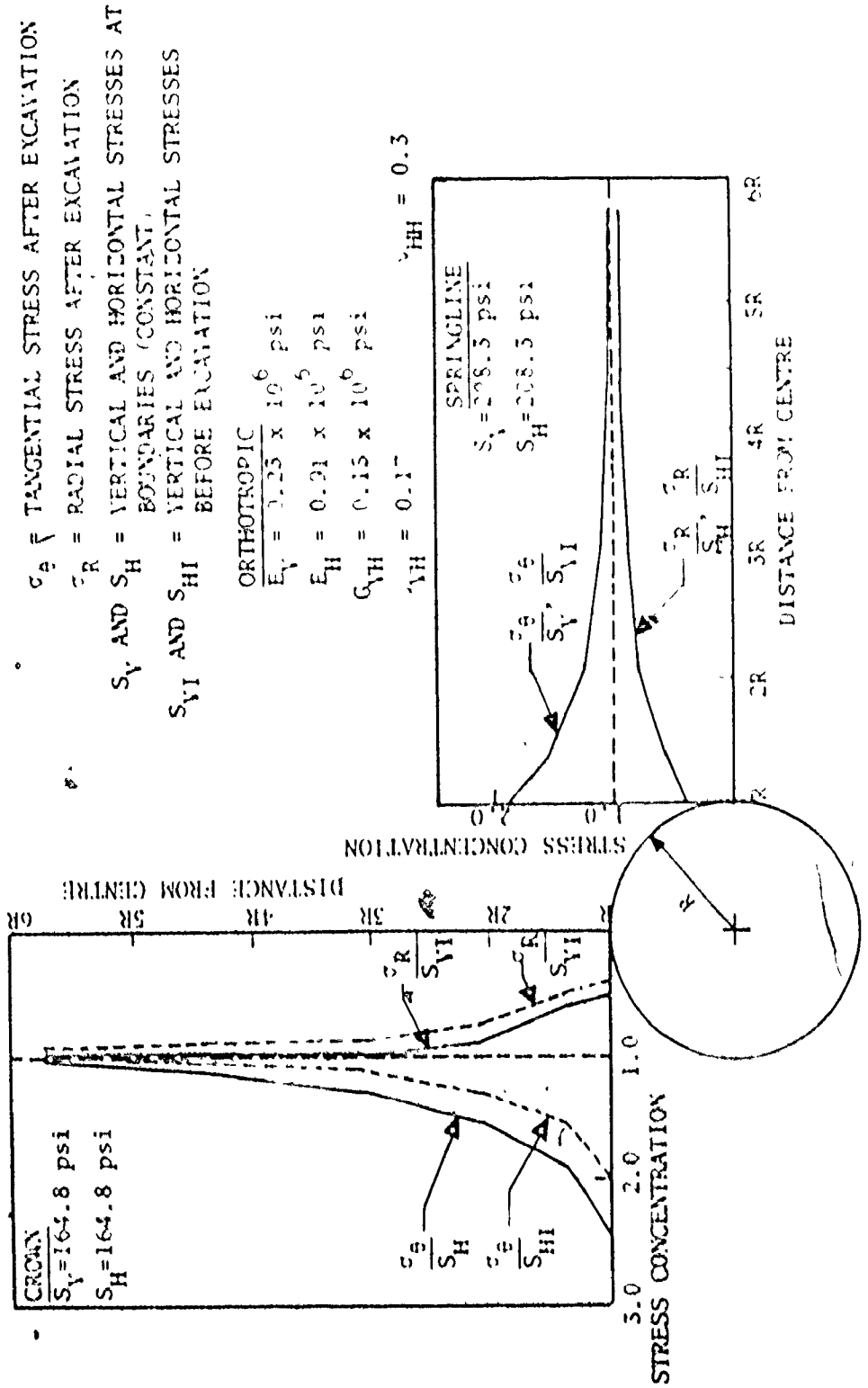


FIGURE 5.9. STRESS CONCENTRATION ALONG VERTICAL AND HORIZONTAL SECTIONS, ORTHOTROPIC A = 1.

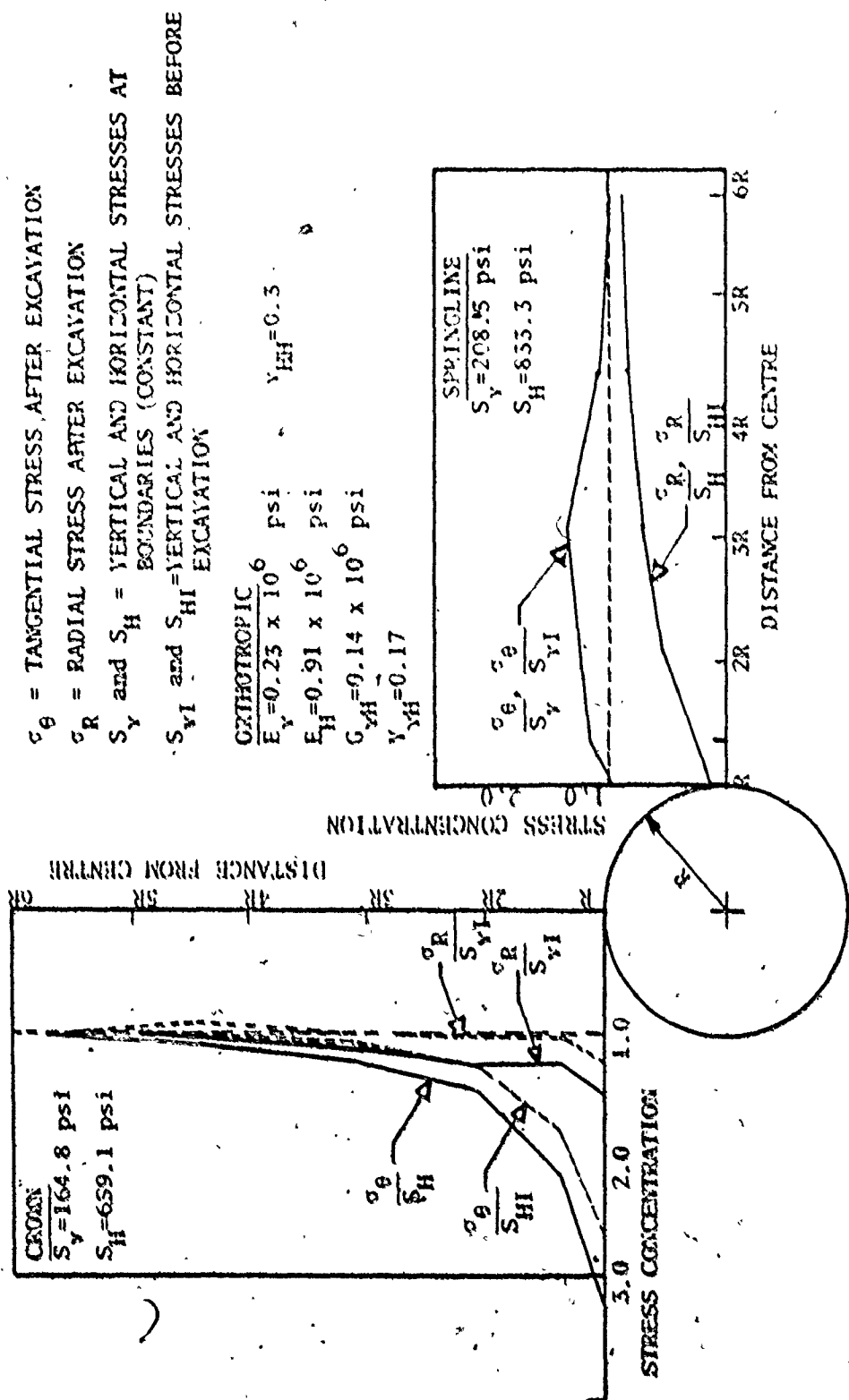


FIGURE 5.10 STRESS CONCENTRATION ALONG VERTICAL AND HORIZONTAL SECTIONS, ORTHOTROPIC, K = 4

stresses decreased and tension was developed for high values of  $K$  (7 and 9) as shown in Figures (5.7) and (5.8). At the crown, the radial and the tangential compressive stresses increased with increasing initial horizontal stresses, and some of these stresses ( $K$  equal to 7 and 9) exceeded the compressive strength for the rock as shown in Figures (5.7) and (5.8). This may cause cracks and failure of the rock at the crown. Such failures are often observed when tunnelling in rock with high lateral stresses.

The stress concentrations for isotropic and orthotropic elastic rock were almost the same for  $K$  equal to 1, but for the orthotropic case higher tangential compressive stresses at the crown and spring sections were developed for  $K$  equal to 4 and lower radial compressive stresses at the crown section as shown in Figures (5.9) and (5.10). Figure (5.11) gives a comparison between the horizontal stresses perpendicular to the tunnel axis measured in the field and the values computed by the finite element excavation method. Figure (5.12) gives a similar comparison between the calculated shear stresses from measurements. It can be seen that the computed values for  $K$  equal to 1 are in a reasonable agreement with the field measurements. It should be noted that field measurements in rock mechanics, particularly stress values, are subject to considerable scatter so that the agreement is considered to be very reasonable for this field study.

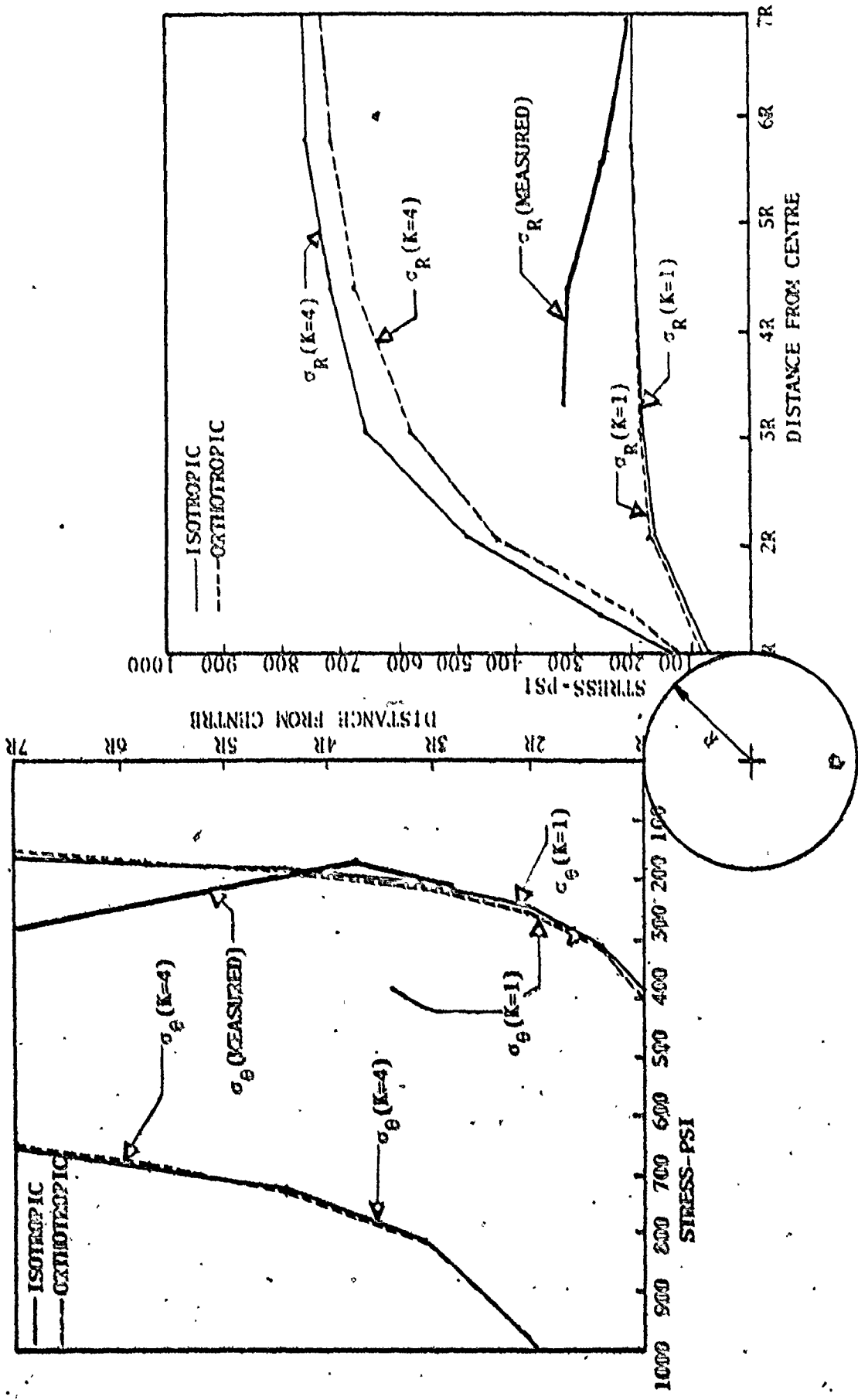


FIGURE 5.11 COMPUTED (FINITE ELEMENT) AND MEASURED HORIZONTAL NORMAL STRESSES PERPENDICULAR TO TUNNEL AXIS

\*CALCULATED FROM THE OVERCROING OBSERVATION ON THE ASSUPTION THAT THE ROCK IS ISOTROPIC (FTA, 1975)

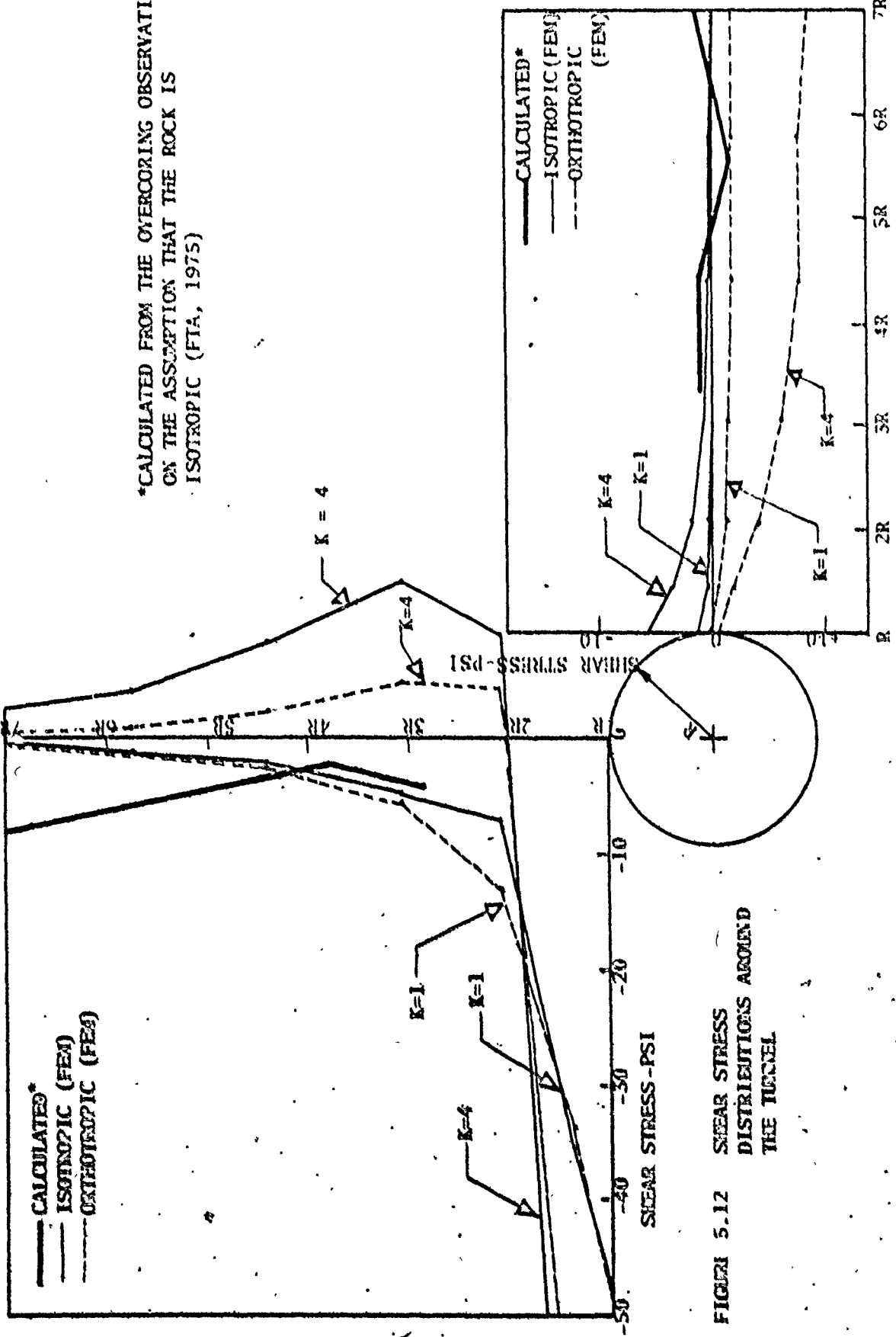


FIGURE 5.12 SHEAR STRESS DISTRIBUTIONS AROUND THE TUNNEL

#### 5.4 Creep

For the reasons discussed previously in Section (2.2.1), Equation (2.6) was adopted for the simulation of tunnel creep in rock. The constants for shale in this equation have been developed experimentally by Hobbs (1970). From these experimental results, he concluded that the slope of secondary creep for shale is independent of the stress level, and proposed the following creep equation:

$$\epsilon = \epsilon_0 + 1.98 \times 10^{-9} t + 7.56 \times 10^{-6} \sigma \log (t + 1) \quad (5.1)$$

where:  $\epsilon$  is the total strain (elastic and creep);  $\epsilon_0$  is the elastic strain immediately after excavation;  $t$  is the time in minutes; and  $\sigma$  is the stress in  $\text{MN/m}^2$ . Using the incremental, initial strain method discussed previously, Section (3.3), the creep analyses (approximately 4 1/2 months creep) for various representative  $K$  conditions (1, 4, 7 and 9) in isotropic elastic rock were started after the elastic solutions had been obtained.

#### 5.5 Discussion of Creep Solutions

##### a) Displacements

Figures (5.13) to (5.16) show the radial creep displacements of the tunnel (squeezing) with time for  $K$  equal to 1, 4, 7 and 9. It can be seen that the tunnel deforms at a constant creep rate for the various initial horizontal stress conditions after a brief primary period. For example, the creep deformation rate for  $K$  equal to 1 is 0.016 inches/month

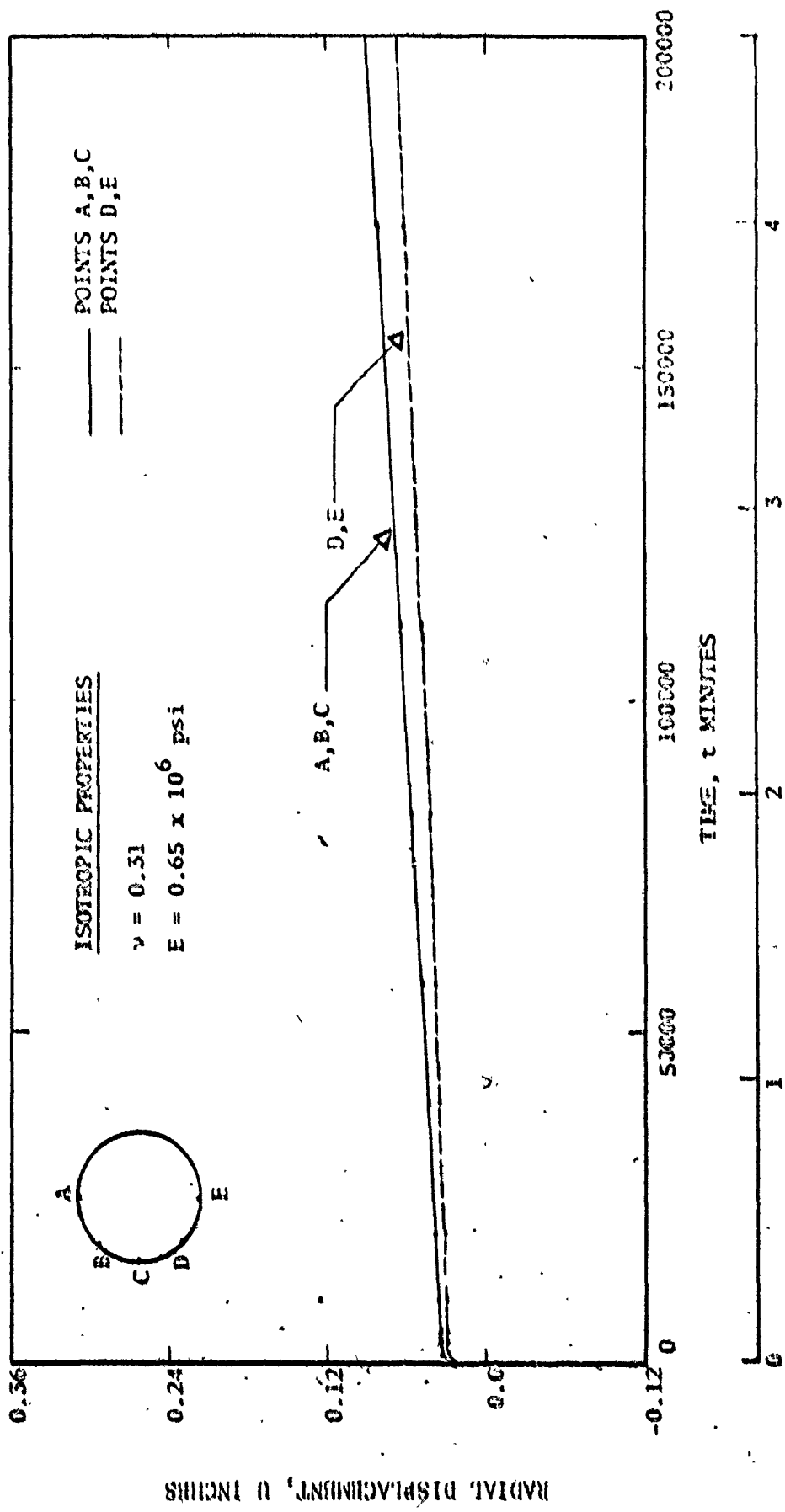


FIGURE 5.13 RADIAL DISPLACEMENT WITH TIME FOR  $K = 1$

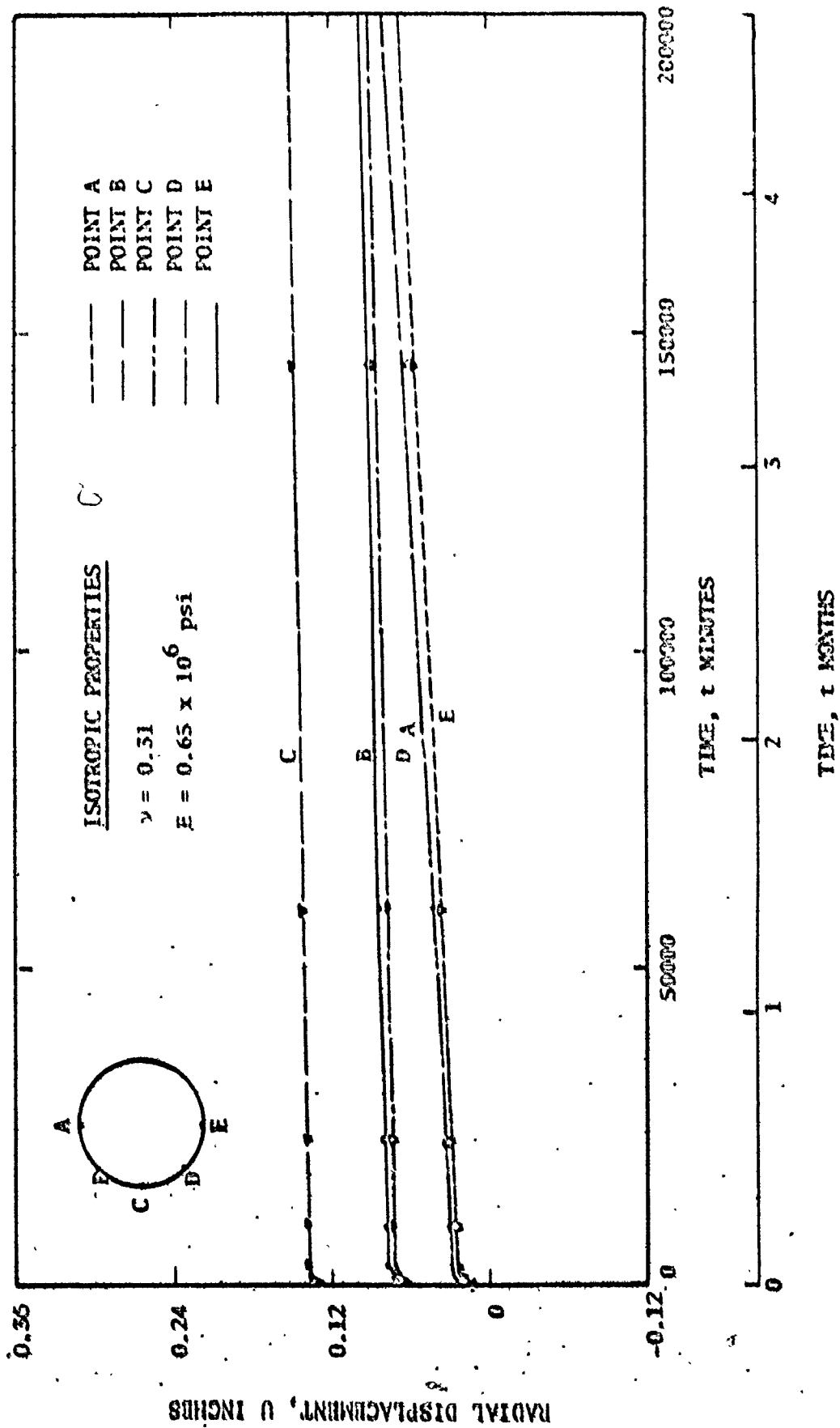


FIGURE 5.14 RADIAL DISPLACEMENT WITH TIME FOR  $K = 4$



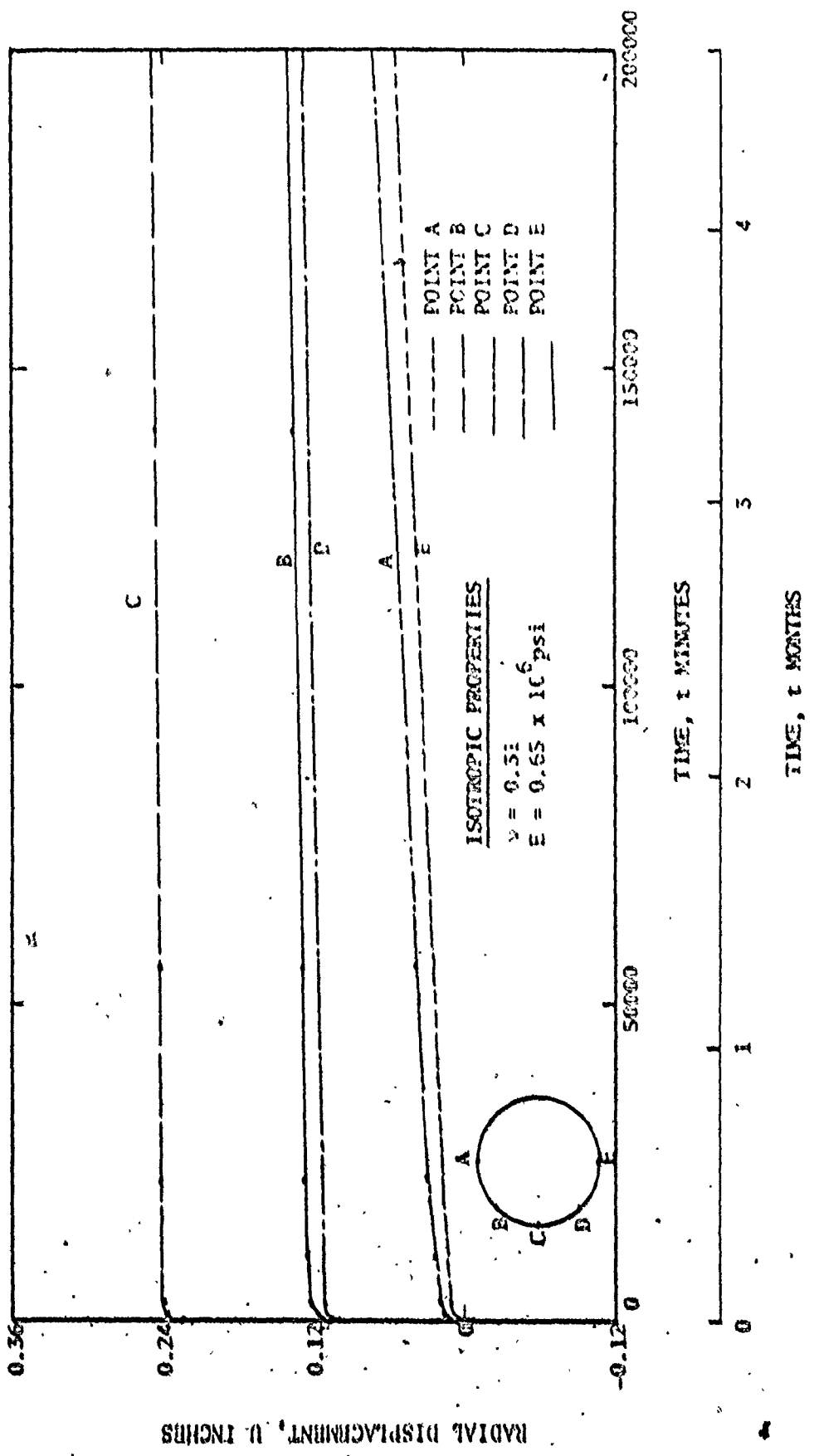


FIGURE 5.15 RADIAL DISPLACEMENT WITH TIME FOR  $K = 7$

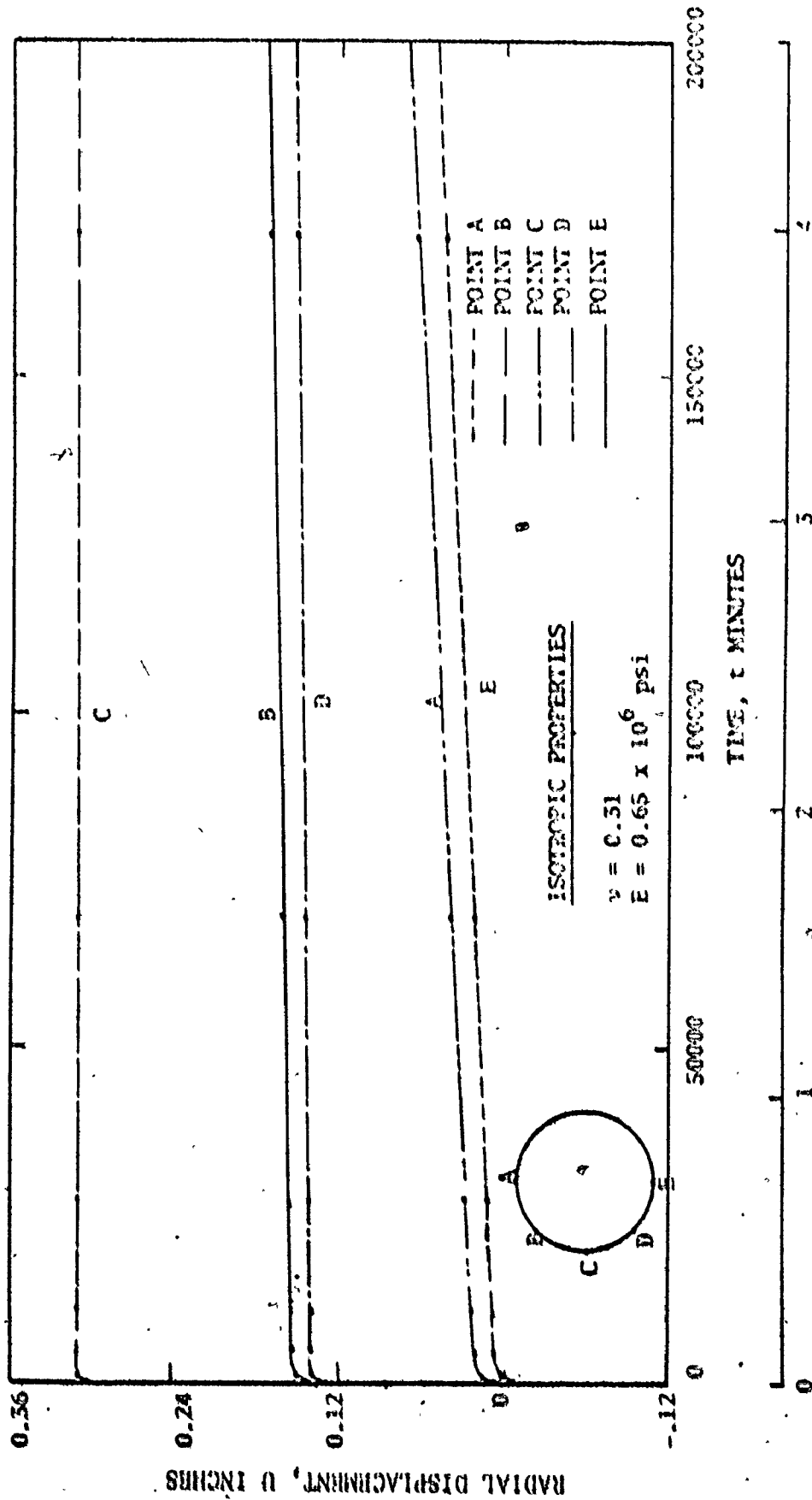


FIGURE 5.16 RADIAL DISPLACEMENT WITH TIME FOR  $K = 9$

(creep strain rate of 0.0002 inches/inch/month based on the radius of the opening). It can also be seen that the maximum creep deformation rate occurs at the crown point "A" for the various K conditions. Figures (5.17) and (5.18) show typical computed movements (magnitude and direction) around the tunnel for K equal to 1 and 4, respectively. Table (5.5) summarizes the computed convergence values (closure) and creep deformation rates for the various initial horizontal stress conditions. It can be seen that the vertical convergence rates are relatively independent of K while the horizontal convergence rates decrease with increasing K value.

Table (5.6) shows a comparison of the computed convergence rates with those measured in the field for the tunnel. These measured values were taken at 4 different locations (profiles) in the tunnel. Figure (5.19) shows a comparison between the measured creep displacements with those computed by the finite element excavation method. Generally, the computed values for the K equal to 1 condition are much closer to the measured values than those for K equal to 4. Thus, it would appear from the comparison of field measurements with the finite element simulation that the appropriate K value for this site is close to unity. This information, based on a simulation, is of great help when determining the lining stresses since direct determination of K is difficult in the field.

The computed inward horizontal displacements for

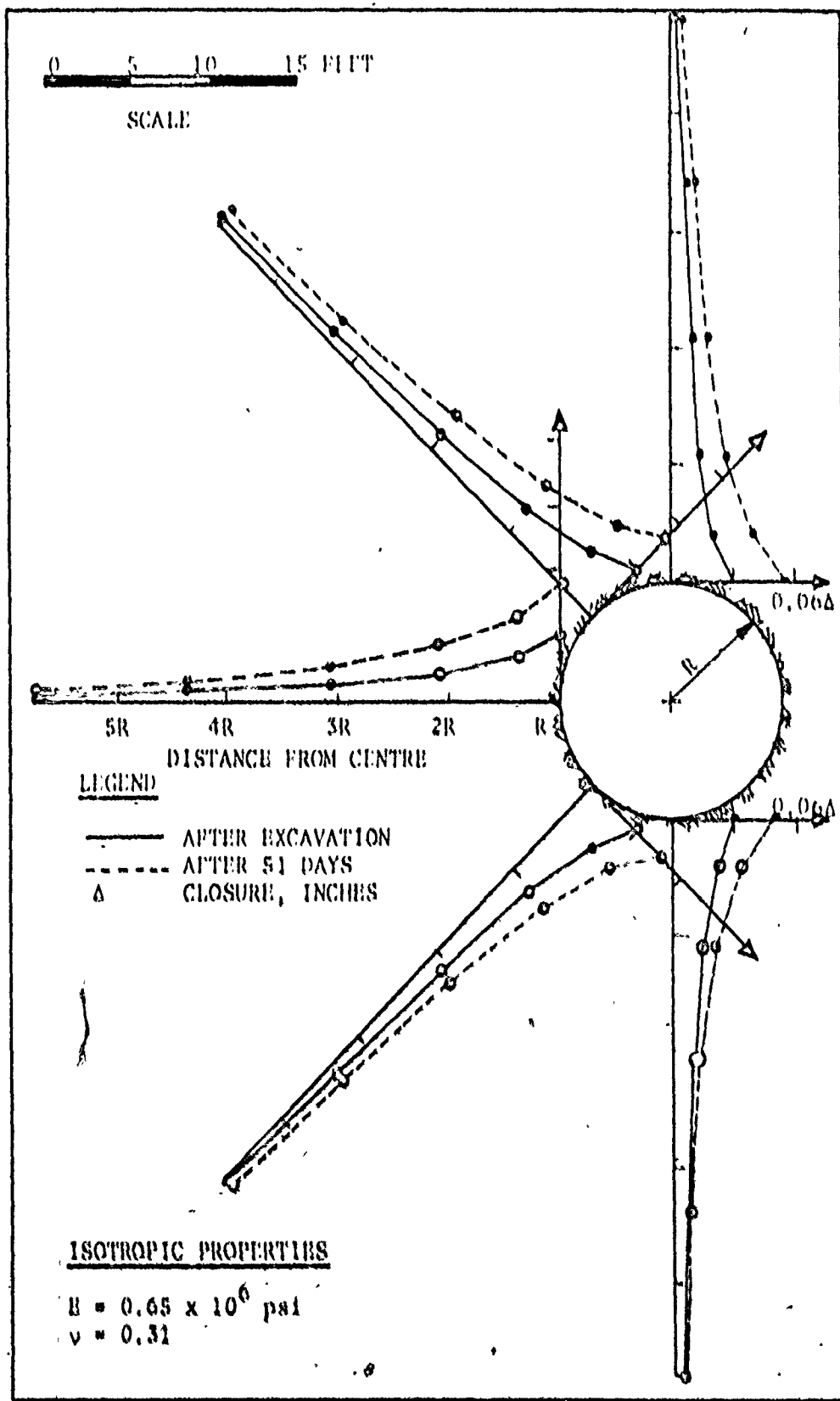


FIGURE 5.17 COMPUTED MOVEMENTS AROUND THE TUNNEL WITH TIME FOR  $K = 1$

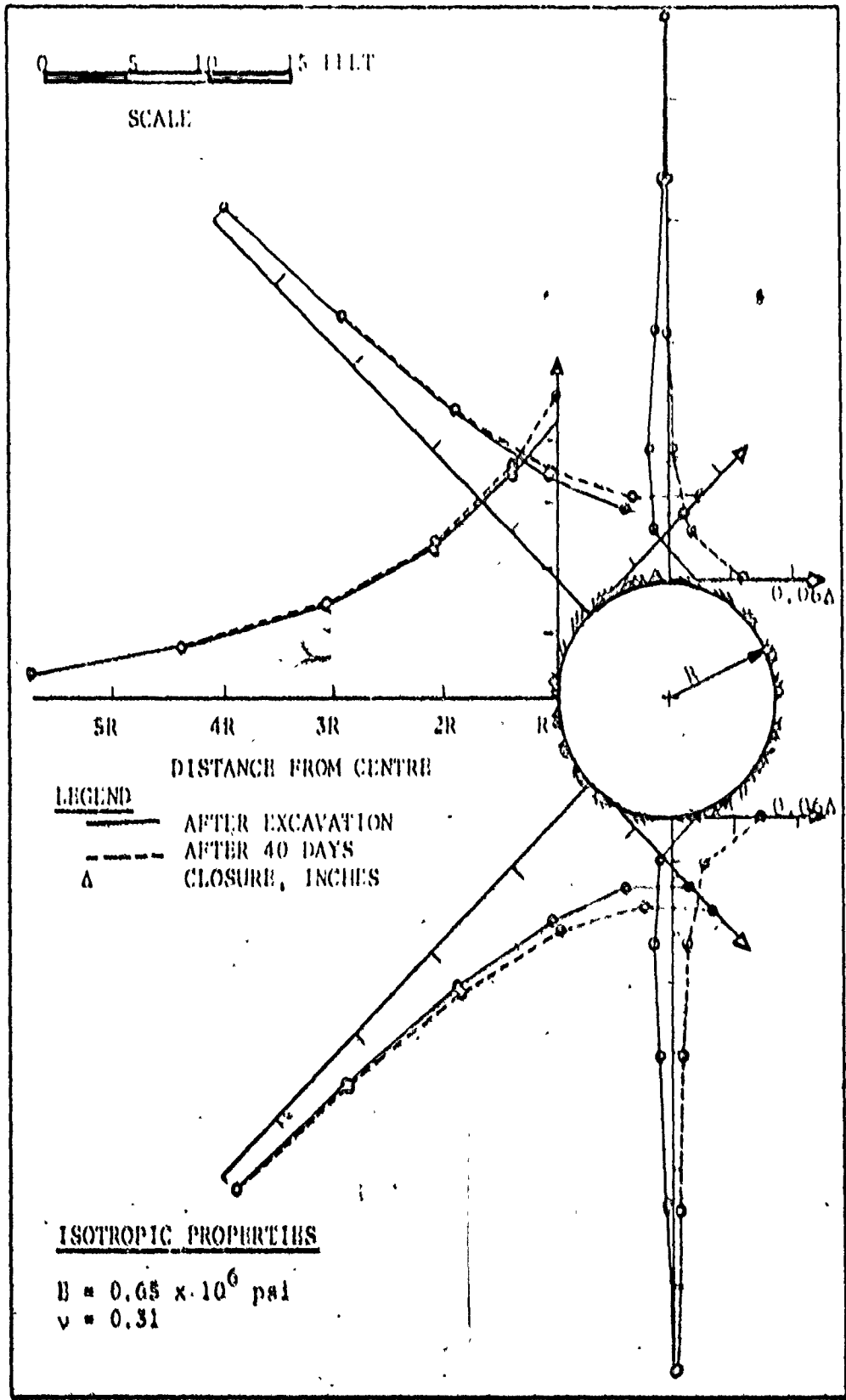
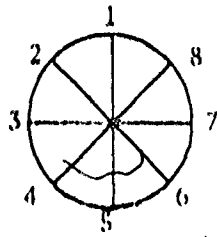


FIGURE 5.18 COMPUTED MOVEMENTS AROUND THE TUNNEL WITH TIME FOR  $K = 4$

TABLE 5.5 SUMMARY OF COMPUTED (FINITE ELEMENT) CONVERGENCE VALUES AND CREEP RATES

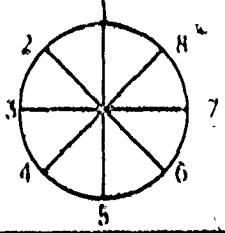


REFERENCE POINTS NUMBERING SYSTEM

INITIAL GROUND STRESS K	SPAN	CONVERGENCE (INCH)				RATE (IN. / MONTH)
		TIME SINCE EXCAVATION (DAYS)	MOVEMENT (INCH)	TIME SINCE EXCAVATION (DAYS)	MOVEMENT (INCH)	
1	1-5	21	0.079	127	0.152	0.021
	2-6*		0.075		0.137	0.017
	3-7		0.075		0.151	0.021
4	1-5	16	0.061	100	0.121	0.021
	2-6*		0.152		0.178	0.009
	3-7		0.275		0.295	0.007
7	1-5	16	0.047	97	0.101	0.020
	2-6*		0.240		0.260	0.007
	3-7		0.481		0.490	0.004
9	1-5	19	0.041	119	0.106	0.020
	2-6*		0.300		0.323	0.007
	3-7		0.619		0.626	0.002

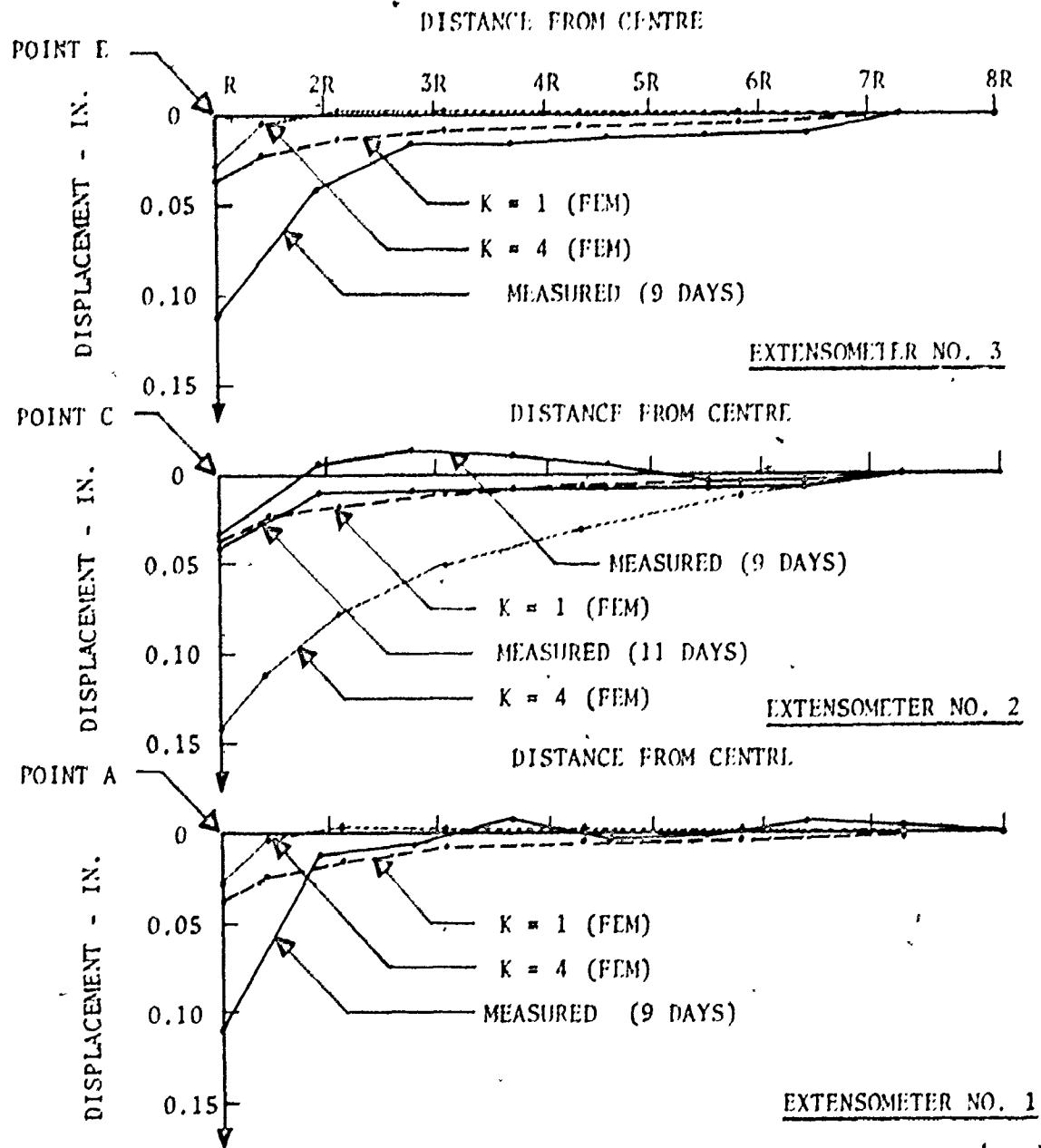
\* SPAN (4-8) IS SAME AS SPAN (2-6) FROM SYMMETRY

TABLE 5.6 COMPARISON OF MEASURED CONVERGENCE VALUES WITH THOSE COMPUTED BY FINITE ELEMENT METHOD



REFERENCE POINTS NUMBERING SYSTEM

MEASURED				COMPUTED (FEM)	
PROFILE NO.	SPAN	RATE (IN./ MONTH)	AVERAGE RATE	K	RATE (IN./ MONTH)
1	1-5	0.190	(AVERAGE OF 1, 2, 6, 4) 0.127	1	0.021
2	1-5	0.167		4	0.021
3	1-5	0.680		7	0.020
4	1-5	0.024		9	0.020
2	2-6	0.051	0.027	1	0.017
3	2-6	0.006		4	0.009
4	2-6	0.012		7	0.007
2	4-8	0.047	0.021	9	0.0069
4	4-8	0.017		1	0.021
2	3-7	0.058	0.027	4	0.007
3	3-7	0.010		7	0.004
4	3-7	0.014		9	0.002



- NOTES**
1. MEASURED VALUES BY FRANKLIN TROW ASSOCIATES LIMITED, AFTER 9 DAYS OF INSTALLATION THE EXTENSOMETERS.
  2. COMPUTED (FINITE ELEMENT) DISPLACEMENTS FOR  $K = 1$  AND  $4$  REPRESENTED 9 DAYS CREEP.
  3. POSITIVE (DOWNWARDS) DISPLACEMENT MAGNITUDES CORRESPOND TO INWARDS MOVEMENT.

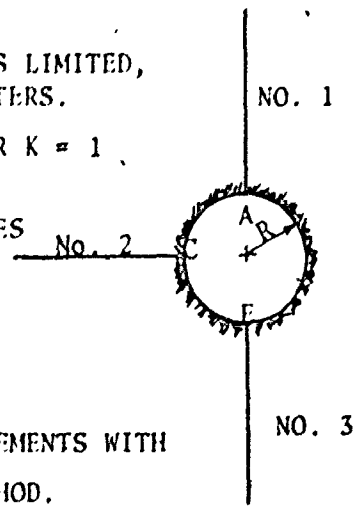


FIGURE 5.19 COMPARISON OF MEASURED CREEP DISPLACEMENTS WITH THOSE COMPUTED BY FINITE ELEMENT METHOD.

LOCATION OF EXTENSOMETERS



the spring point "C" for K equal to 1 are the same as the measured values (Extensometer No. 2, Figure (5.19)), but the computed inward vertical displacements at the crown point "A" and floor point "E" as shown in Figure (5.19) are less than the measured values. Also, the computed vertical convergence is less than the measured values as shown in Table (5.6). These differences are closely related to the influences of the bedding of the rock which was not considered in the creep analysis part of this study. Obviously, this must be the topic of future research where the anisotropic properties of rock are considered in the creep analysis. This will also require experimental information on the creep of bedded rock.

b) Stress Concentrations

Figures (5.20) and (5.21) show the stress concentrations for K equal to 1 and 4, respectively, after approximately 1 1/2 months of creep. The corresponding values after excavations are also shown for comparison purposes. Tables (5.7) and (5.8) show the radial and tangential creep stresses around the opening for K equal to 1 and 4, respectively, compared with the stresses before and after excavation. Generally, it can be seen that for K equal to 1, the radial and the tangential compressive stresses near the opening increase with time, while these stresses at some distance from the opening decrease with time. For K equal to 4, the creep behaviour of the tunnel is different from

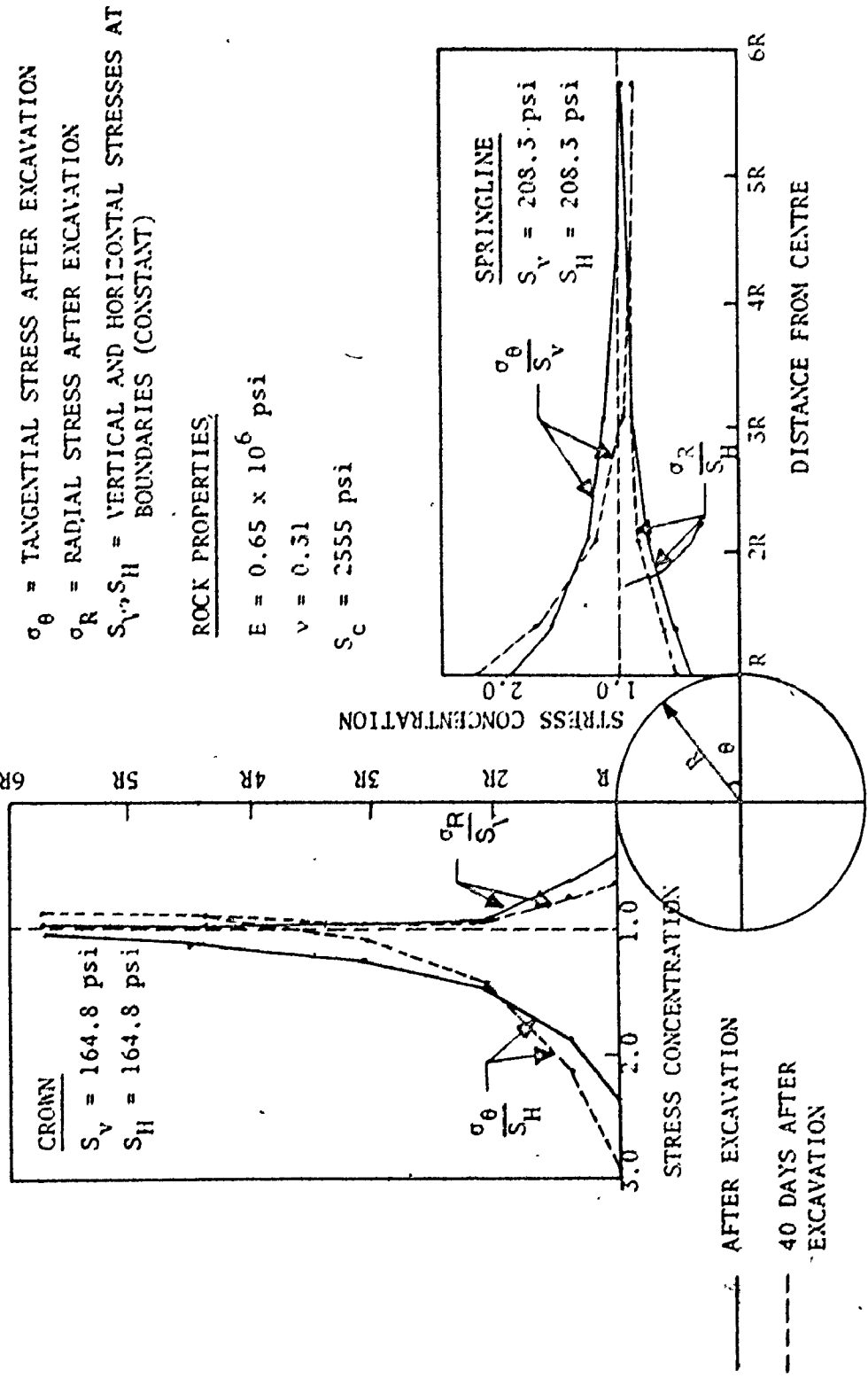


FIGURE 5.20 STRESS CONCENTRATION ALONG VERTICAL AND HORIZONTAL SECTIONS, CREEP,  $K = 1$

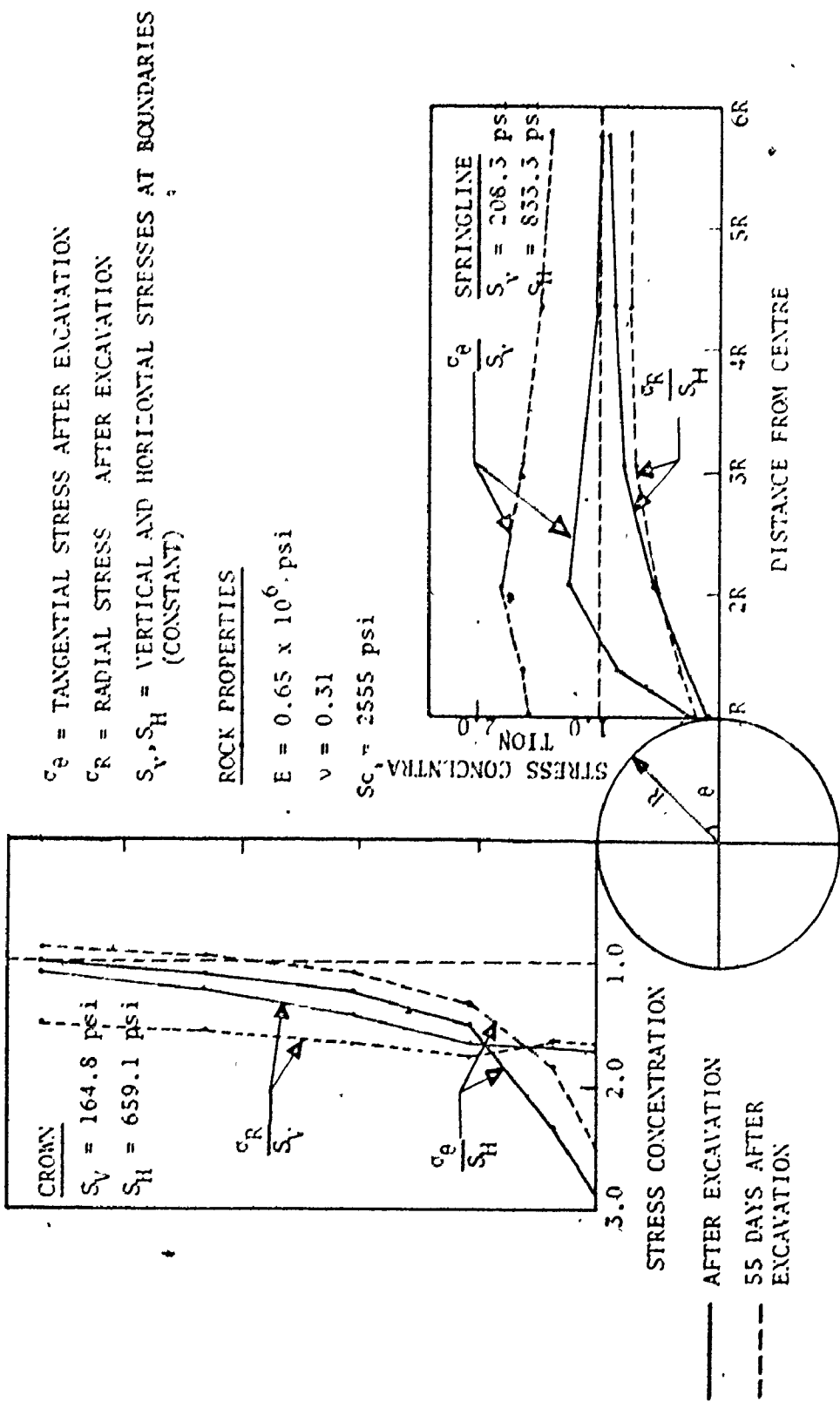


FIGURE 5.21 STRESS CONCENTRATION ALONG VERTICAL AND HORIZONTAL SECTIONS, CREEP,  $K = 4$

TABLE 5.7 RADIAL AND TANGENTIAL COMPRESSIVE STRESSES AROUND  
THE TUNNEL FOR  $K = 1$

STRESS CONDITION	CROWN POINT		SPRING POINT		FLOOR POINT	
	$\sigma_R$ psi	$\sigma_\theta$ psi	$\sigma_R$ psi	$\sigma_\theta$ psi	$\sigma_R$ psi	$\sigma_\theta$ psi
INITIAL STRESS	202	202	208	208	215	215
AFTER EXCAVATION	86	396	87	395	92	411
20 DAYS CREEP	97	426	97	410	103	433
58 DAYS CREEP	121	524	118	490	128	527
150 DAYS CREEP	158	637	153	591	169	638

TABLE 5.8 RADIAL AND TANGENTIAL COMPRESSIVE STRESSES AROUND THE TUNNEL FOR  $K = 4$

STRESS CONDITION	CROWN POINT		SPRING POINT		FLOOR POINT	
	$\sigma_R$ psi	$\sigma_\theta$ psi	$\sigma_R$ psi	$\sigma_\theta$ psi	$\sigma_R$ psi	$\sigma_\theta$ psi
INITIAL	202	808	833	208	215	859
AFTER EXCAVATION	289	1921	150	51	300	1995
22 DAYS CREEP	289	1743	162	238	300	1791
55 DAYS CREEP	283	1673	178	356	294	1706
137 DAYS CREEP	274	1554	236	567	284	1538

that for  $K$  equal to 1. At the crown, the radial stresses decrease slightly near the opening while at some distance from the opening these stresses increase due to creep effects as shown in Figure (5.21). The tangential stresses decrease with time at any point along this section. For the springline, the radial stresses increase near the opening and decrease with increasing distance from the opening. The tangential stresses increase with time at any point along this section since load is being transferred from above the opening to the tunnel sides. From Tables (5.7) and (5.8) it can also be seen that for  $K$  equal to 1, the stresses around the opening (radial and tangential stresses) increase (compared with the stresses after excavation) with time due to the effect of ground squeezing. For  $K$  equal to 4, the radial and the tangential stresses at the crown and the floor points decrease (compared with the stresses after excavation) with time due to stress relief, while the stresses at the spring point increase (compared with the stresses after excavation) with increasing time.

Finally, it can be concluded that, for  $K$  equal to 1 and 4, the stresses are compressive around the tunnel (squeezing the opening) and no tensile stresses were developed. This conclusion is of great help for constructing the plain concrete lining as discussed in the next section.

## 5.6 Concrete Lining

Figures (5.22) and (5.23) show the finite element idealization for modelling the rock, the concrete lining

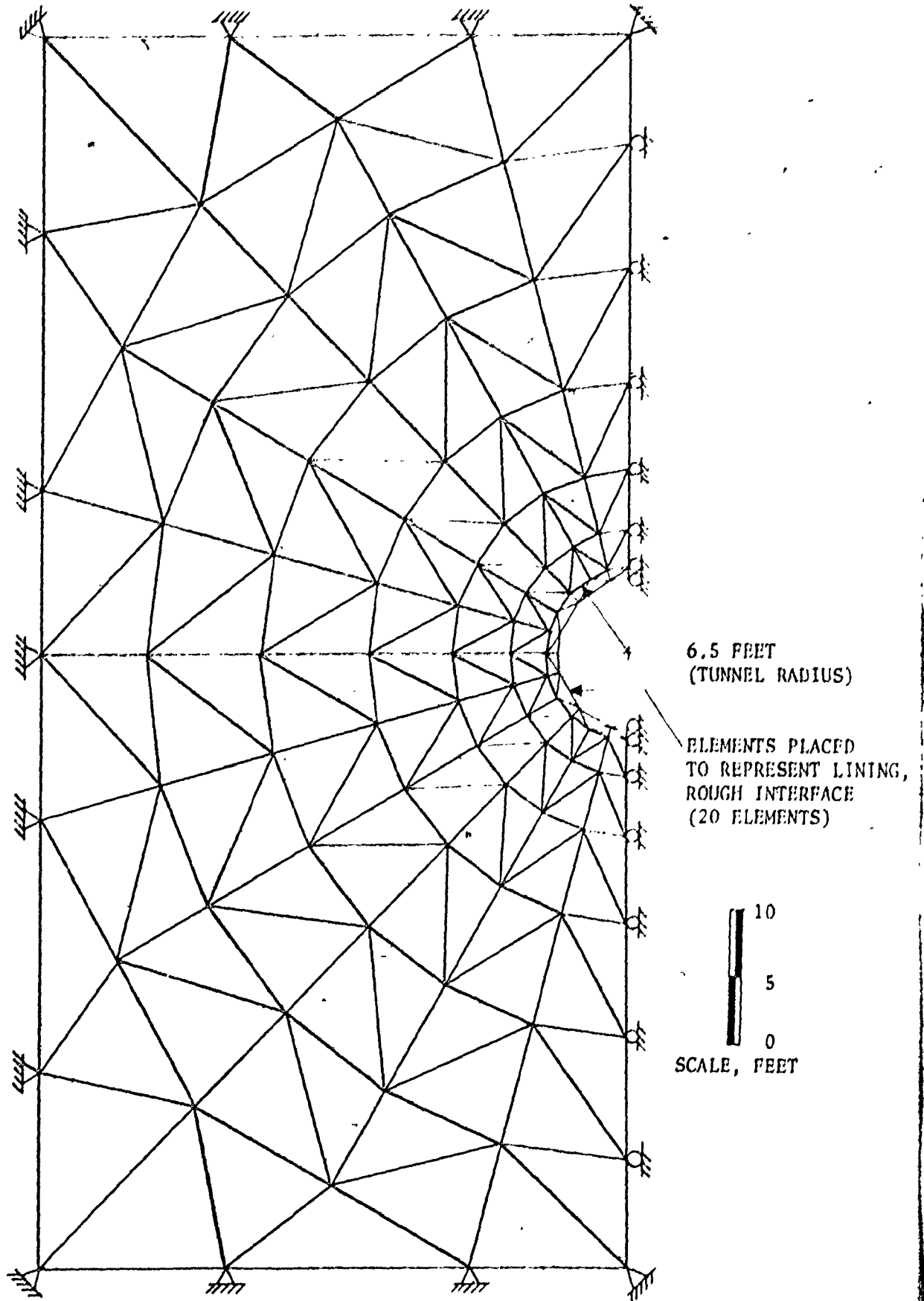


FIGURE 5.22 FINITE ELEMENT IDEALIZATION OF THE TUNNEL LINING, ROUGH

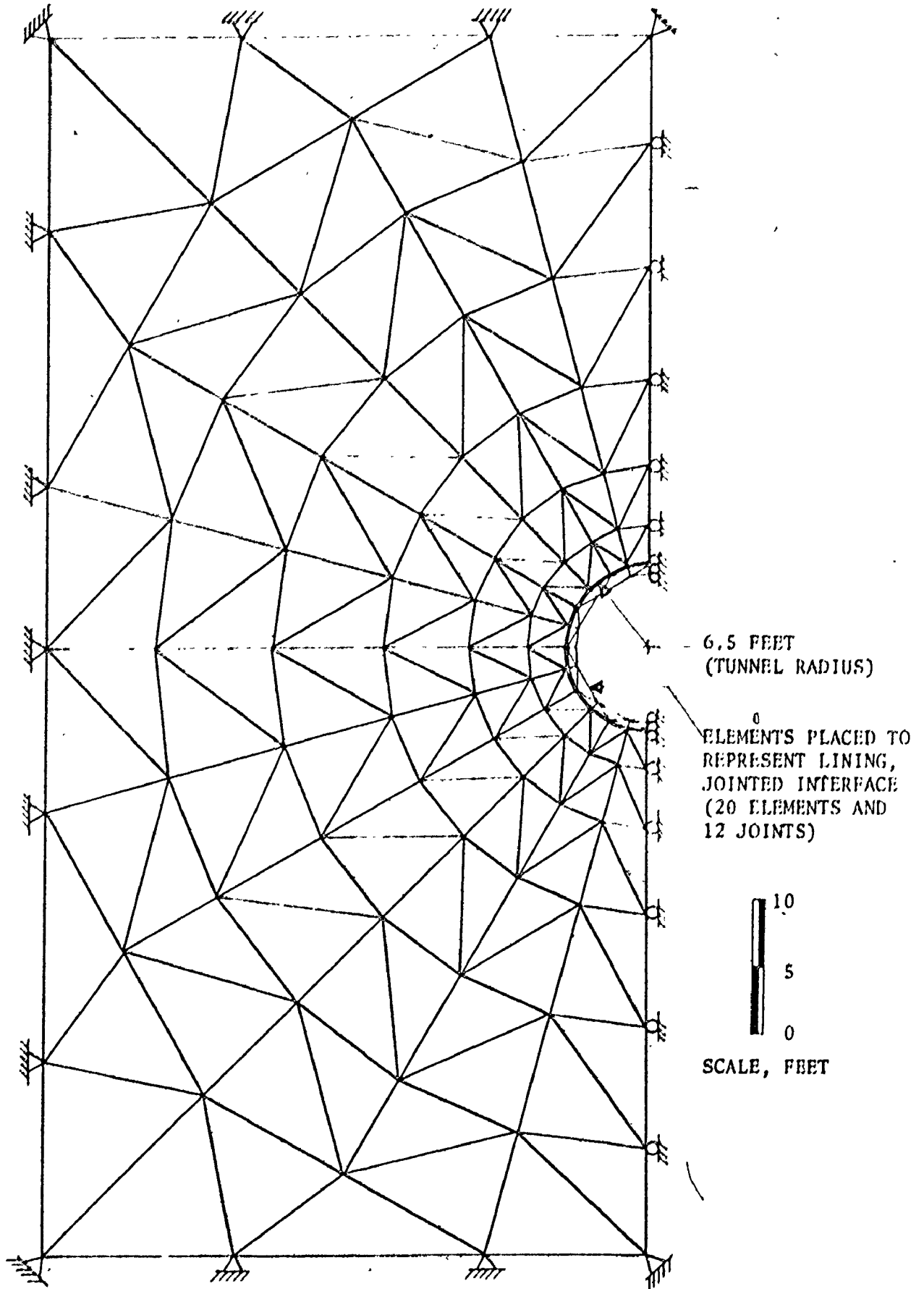


FIGURE 5.23 FINITE ELEMENT IDEALIZATION OF THE TUNNEL LINING,



and the interface between the concrete lining and the rock, as discussed previously in Section (4.3). A concrete lining 9.5 inches thick was used for this simulation as indicated for the initial design by FTA. The compressive strength specified for the concrete to be used is 4500 psi. A unit weight of 150 pcf is considered appropriate for the concrete, and the elastic modulus was obtained from (Neville, 1970):

$$E = 57000 \sqrt{f'_c} \quad (5.2)$$

where: E is the elastic modulus in psi; and  $f'_c$  is the compressive strength in psi. The properties assumed for the concrete lining are summarized in Table (5.9). Table (5.10) gives the properties assumed for the interface between the rock and the concrete lining as discussed previously in Section (4.3).

In this simulation, the concrete lining was considered for the worst possible operating conditions of the tunnel. First, the normal internal pressure of a 60 psi due to flow of water in the tunnel (140 feet depth of water above the tunnel axis) was not considered since this pressure would tend to reduce the stresses developed by the squeezing rock. Second, the total unit weight of the rock was utilized for the full height above the tunnel without any reduction for projected boundary effects due to water in the rock joints near the tunnel.

Two lining strategies were examined: a) the lining

TABLE 5.9 SUMMARY OF CONCRETE PROPERTIES FOR THE LINING

COMPRESSIVE STRENGTH psi	ELASTIC MODULUS psi	UNIT WEIGHT pcf	POISSON'S RATIO
4500	$3.8 \times 10^6$	150	0.15

TABLE 5.10 SUMMARY OF LINEAR ELEMENT (JOINT) PROPERTIES FOR THE INTERFACE BETWEEN THE ROCK AND THE CONCRETE LINING (FRICTION JOINT)

$K_h$ psf/ft	$K_s$ psf/ft	$K_{sr}$ psf/ft	C psf	$\phi$ degrees
$10 \times 10^6$	$5 \times 10^6$	$2/3 K_s$	0	25

was considered to be constructed immediately after excavation; and b) the lining was considered to be constructed approximately two months after excavation where some of the creep strains would already have been developed. From the previous analyses, Sections (5.3) and (5.4), it was concluded that the appropriate K value for this site is close to unity, thus for the lining strategies K was considered equal to 1. For comparison some cases were considered for K equal to 4. The creep period considered for the rock and the lining was generally two months which is considered a very high period for creep analysis. For more conservative design and to check the stress concentrations (maximum compressive and tensile stresses in the concrete lining), 5 1/2 months creep after lining construction was also considered for K equal to 1 and 4 as a long term analysis. The creep relationships adopted for rock and concrete were Equations (5.1) and (4.2), respectively.

a) Displacements

For K equal to 1, Figure (5.24) shows a comparison of the radial displacements with time for the concrete lining and the two placement strategies. It can be seen that the deformation rates (squeezing) for the concrete lining placed two months after excavation (rock has had time to creep) are less than those for the concrete lining placed immediately after excavation. (It should be noted that the scale is in terms of time from placement and there is actually a two months offset from the time of excavation

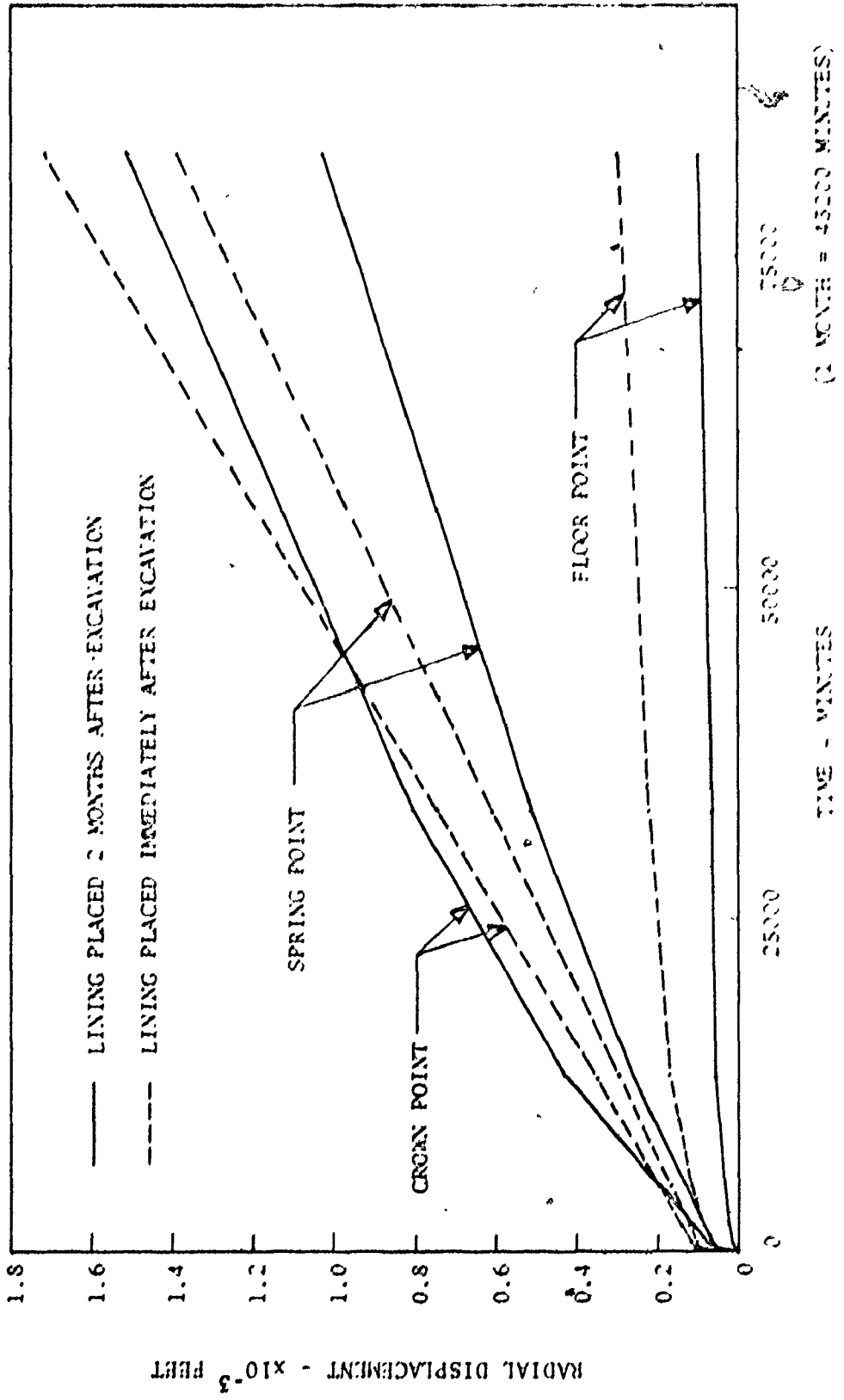


FIGURE SA.24 RADIAL DISPLACEMENTS FOR THE CONCRETE LINING WITH TIME FOR K = 1

for the delayed lining placement.) This is very important as it is clear evidence that delaying the lining installation will significantly reduce the induced stress levels in the lining. A delay of two months is also realistic from the viewpoint of field construction. Thus, as shown in Figure (5.25), two months creep for rock before lining construction was considered the base for all of the analyses of the deformations and stresses for the rock-lining creep simulation. This figure shows the influence of the concrete lining on the radial movements of the rock walls due to creep. The lining reduced the average deformation rates for the crown and spring points from 0.016 inches/month to 0.009 inches/month, and for the floor point from 0.008 inches/month to 0.002 inches/month.

Figure (5.26) shows the deformations for the two limiting conditions of rough and jointed interfaces used to model the interaction between the concrete lining and the rock. It can be seen that the creep deformations for the lining with joints are less than those for the rough interface. This is due to the characteristics of the linear elements that allow relative displacements between the two interfaces (i.e., slip). It is considered for blasted tunnels that the rough interface is probably the appropriate interface condition. However, for tunnels excavated with boring machines (moles) a smooth interface with potential slip is more appropriate. The tunnel being considered will be "moled" for most of its length, so the rough interface tends

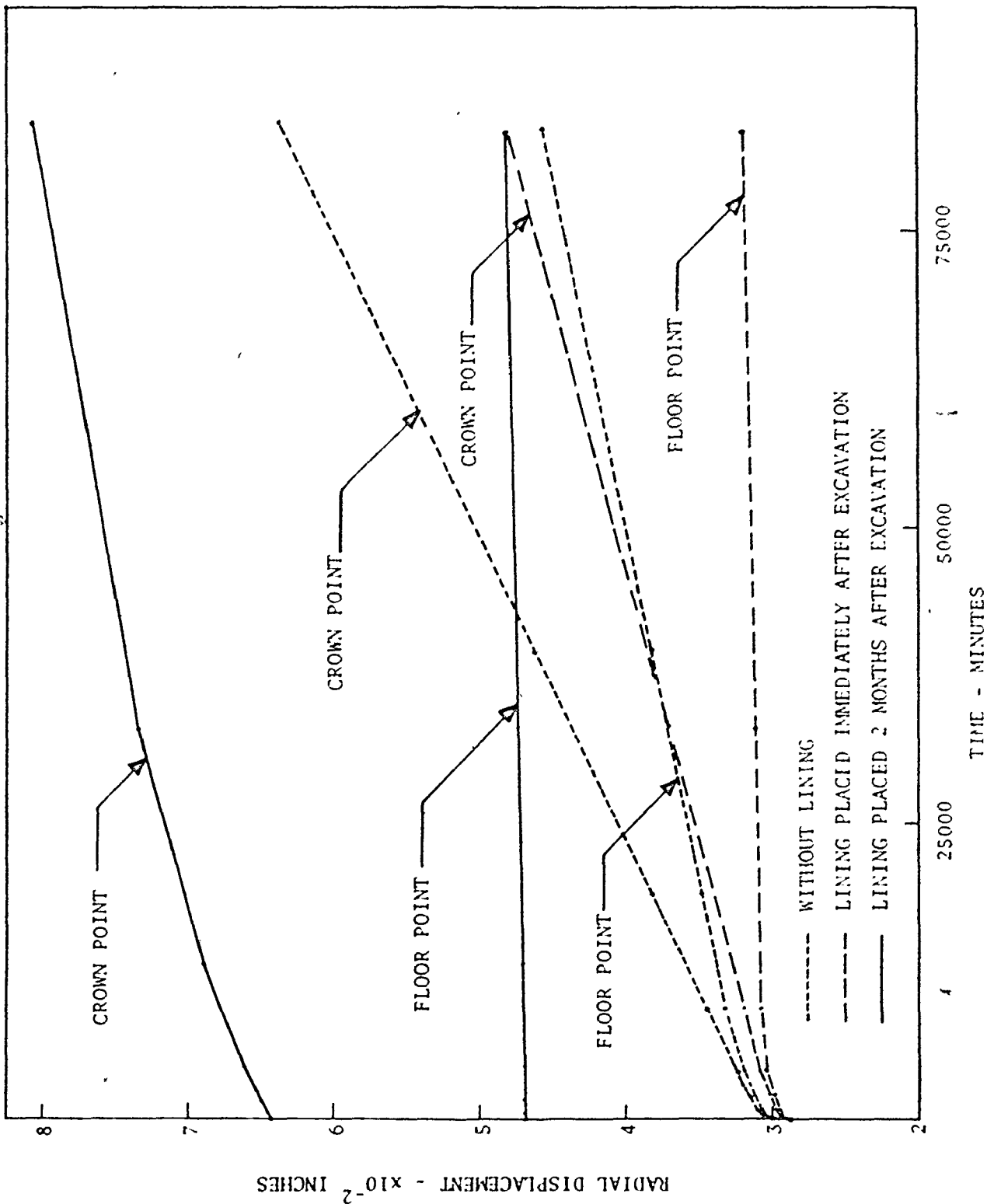


FIGURE 5.25 EFFECT OF THE LINING ON THE RADIAL DISPLACEMENTS FOR THE ROCK WITH TIME FOR  $\lambda = 1$

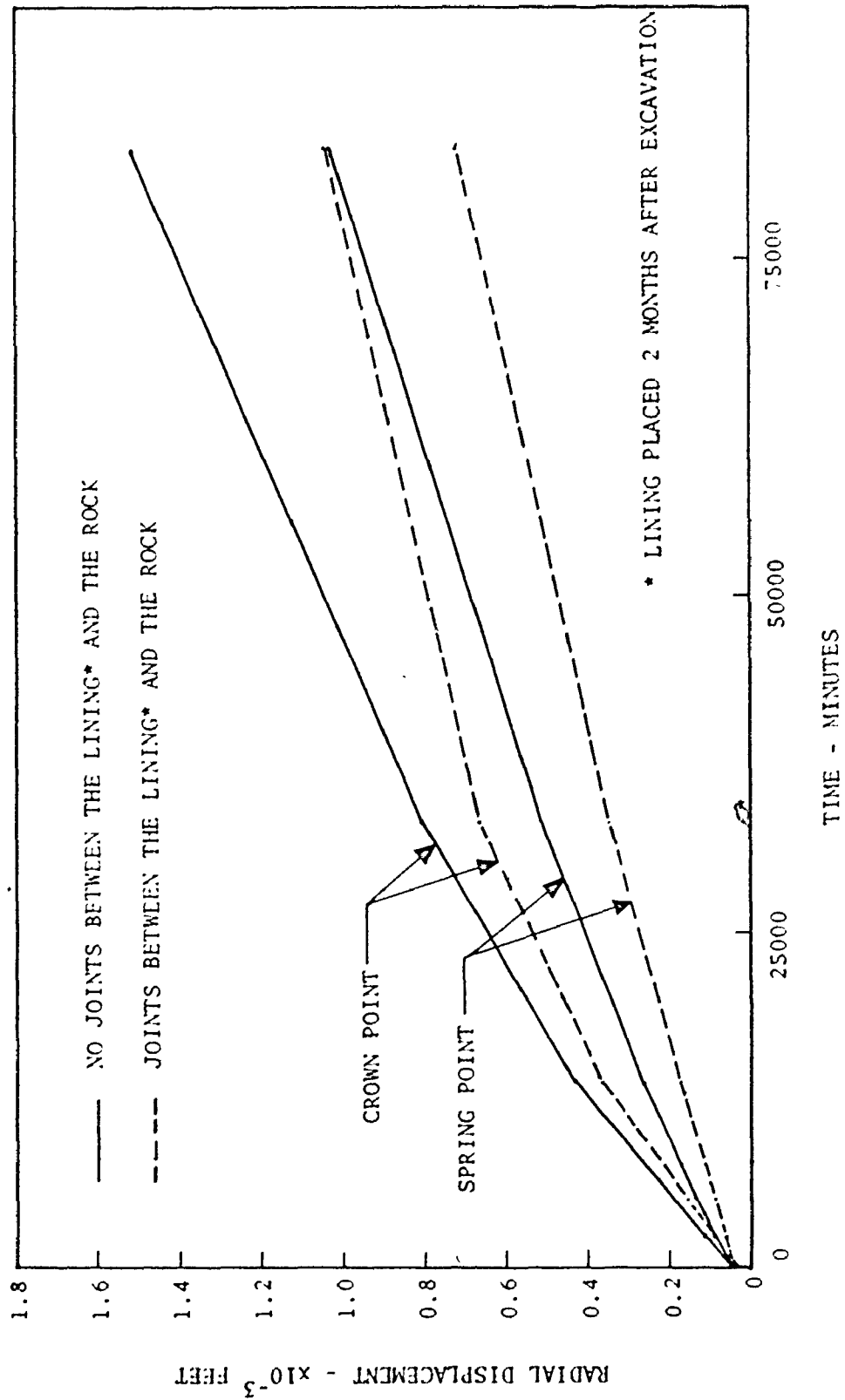


FIGURE 5.26 RADIAL DISPLACEMENTS FOR THE CONCRETE LINING WITH TIME, WITH AND WITHOUT JOINTS, FOR K = 1

to be a conservative assumption.

Figure (5.27) gives the radial displacements for the rock with time for  $K$  equal to 4 and the standard lining strategy of a two month delay. It can be seen that the crown point has a higher creep rate (0.008 inches/month) than the spring point (0.003 inches/month) and floor point (0.005 inches/month). These creep rates are very low, and while a steady-state condition is indicated, it is clear from laboratory and field studies for similar stress levels, that the creep rate would actually decrease and creep movement eventually stop. This of course would require modification of the adopted creep relationship with its steady-state secondary feature. Recent monitoring of the tunnel indicates that significant creep ends approximately three months after excavation if the face is some distance from the profile considered. However, small movements are probably still occurring that will of course accumulate over time. Thus, the analyses appear conservative.

b) Stress Concentrations

Figures (5.28) and (5.29) show for  $K$  equal to 1, the radial and tangential stresses for the rock and the concrete lining at the crown of the opening with time. Generally, it can be seen that the rock stresses increase after placing the lining. It can also be seen that if the concrete lining is placed immediately after excavation, the stresses in the concrete lining will be higher than if the placement of the lining is delayed for two months, while the



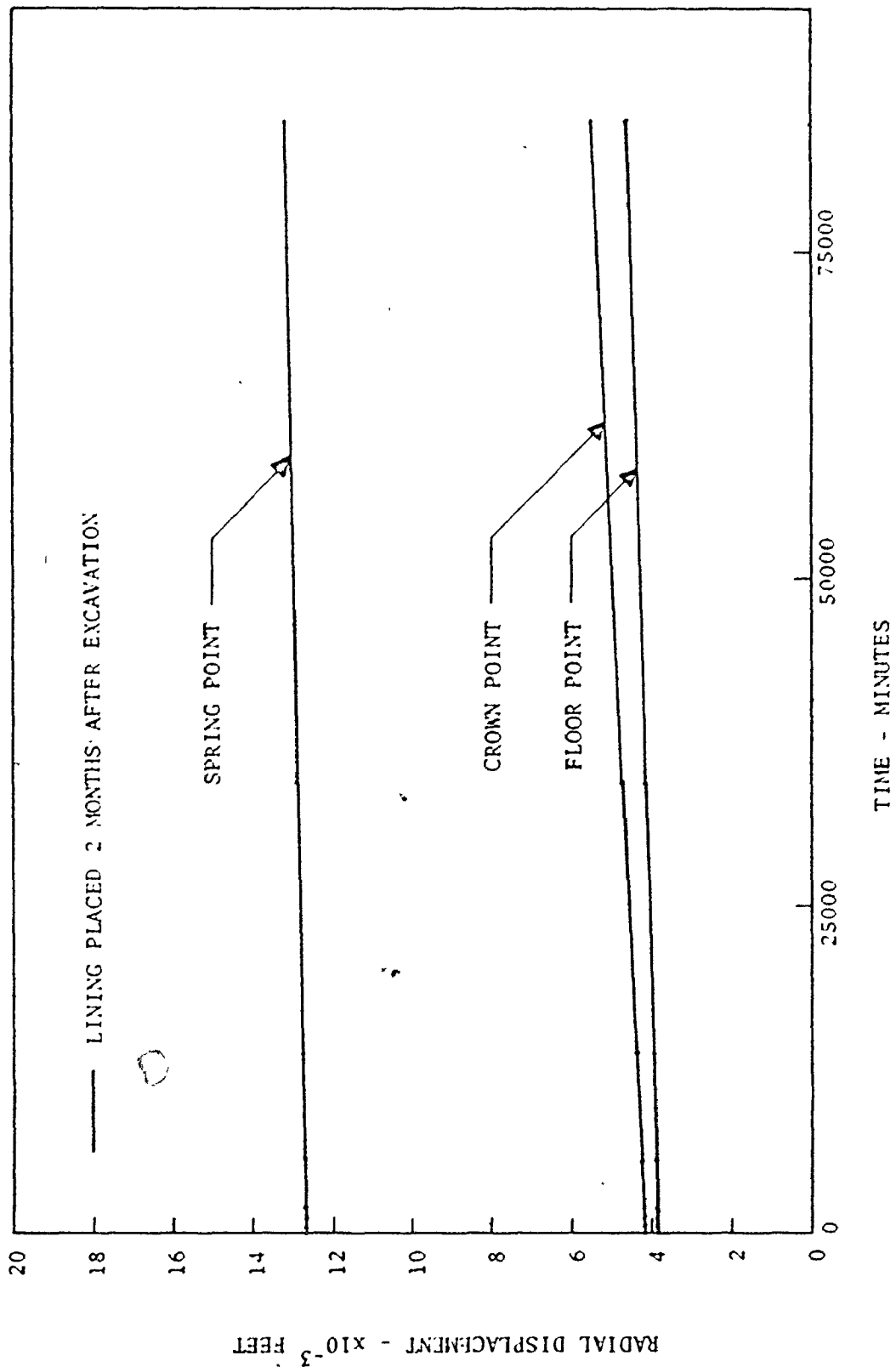


FIGURE 5.27 RADIAL DISPLACEMENTS FOR THE ROCK AFTER LINING WITH TIME FOR  $K = 4$

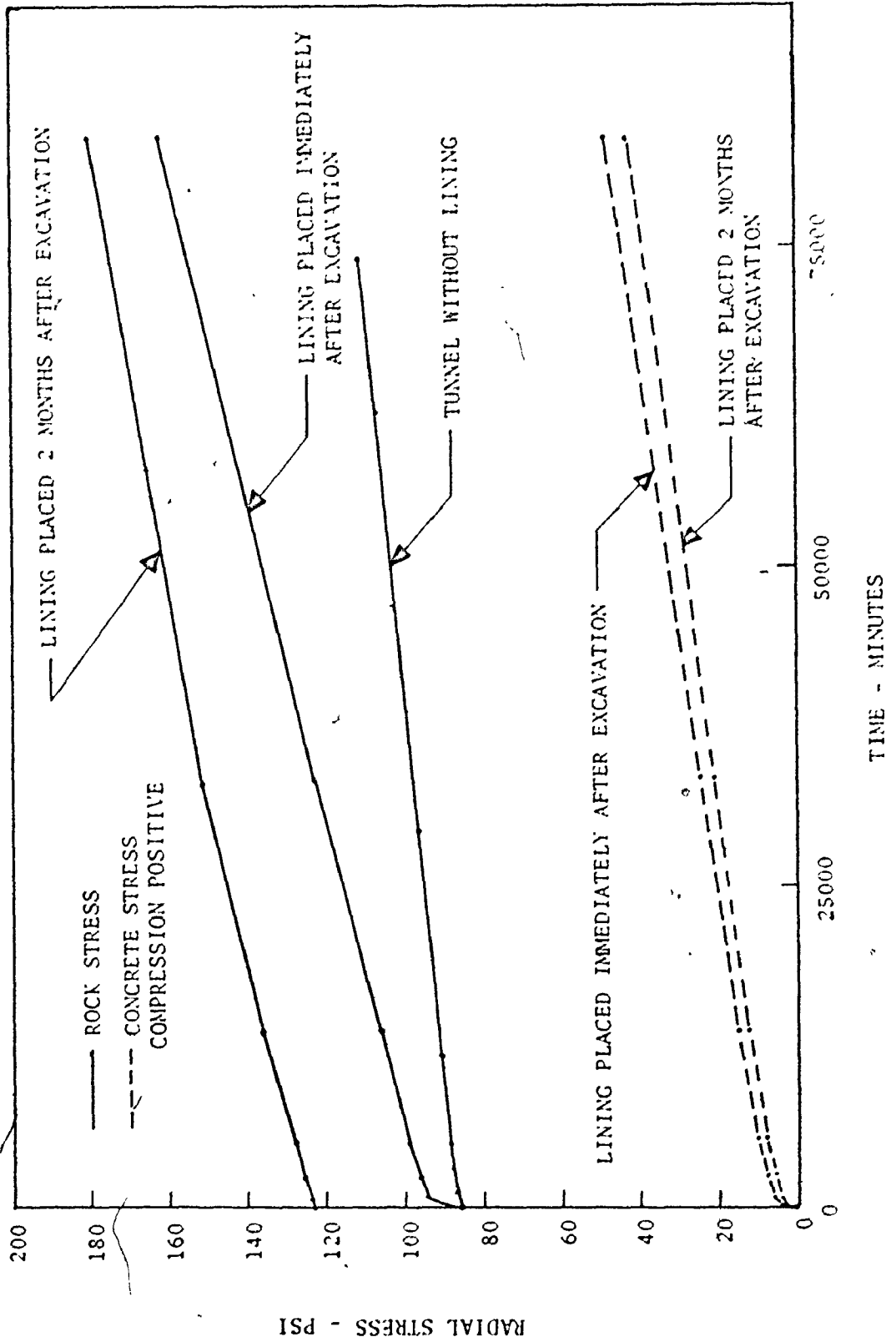


FIGURE 5.28 RADIAL STRESSES AT THE CROWN OF THE TUNNEL WITH TIME FOR  $k = 1$

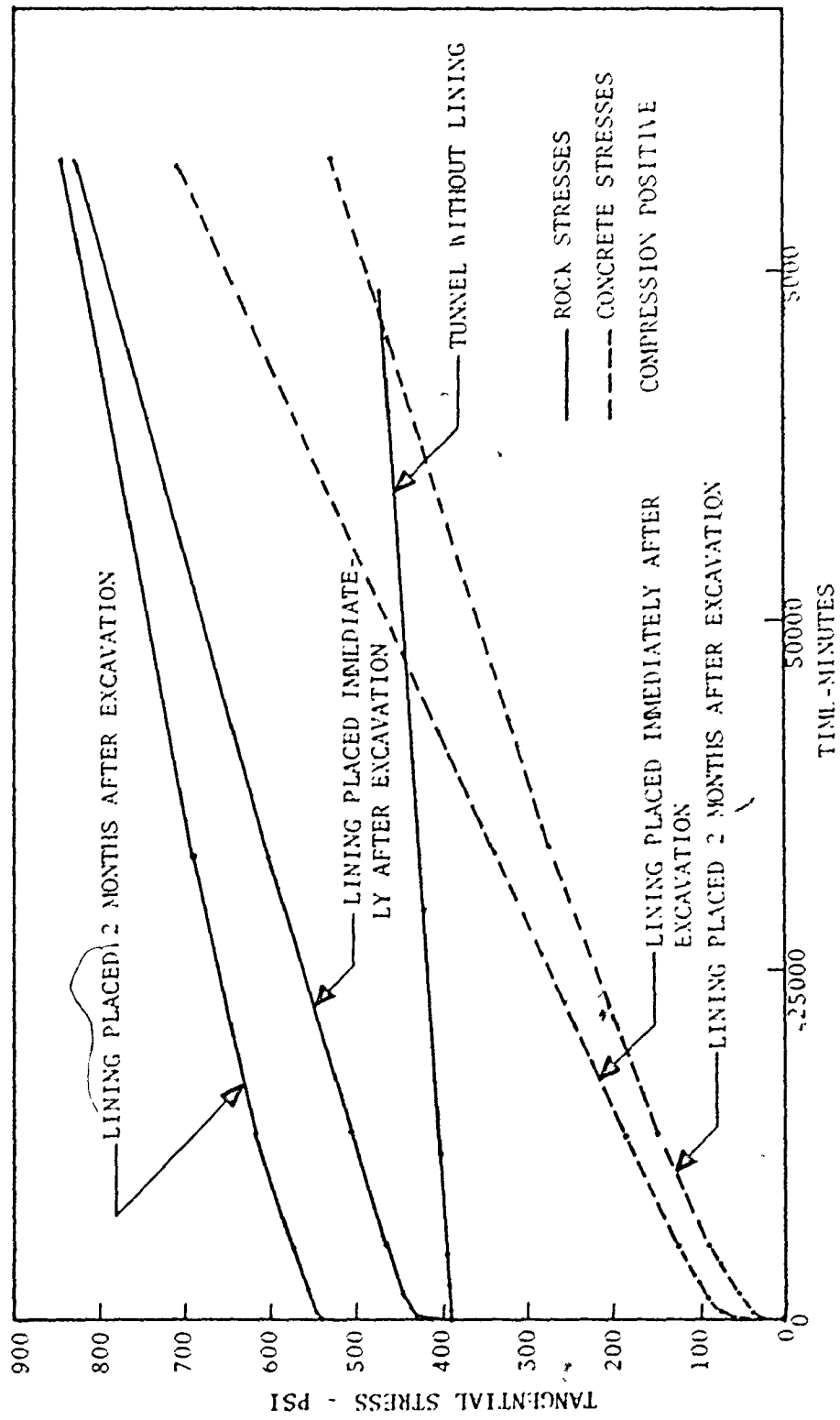


FIGURE 5.29 TANGENTIAL STRESSES AT THE CROWN OF THE TUNNEL WITH TIME FOR  $K = 1$

rock stresses will be less for placing the lining immediately after excavation, i.e., load sharing shows up clearly. Figures (5.30) and (5.31) show the radial and the tangential stresses for the rock and the concrete lining at the crown of the opening with time for the two cases of representing the lining placement using the rough and the jointed interfaces. Also, the normal stress for the joints with time is given in Figure (5.30). It can be seen that the concrete lining and the joints are subjected to compressive stresses due to ground squeezing. The compressive normal and shear stresses for the joints are very low as shown in Table (5.11) and no tensile stresses develop between the rock and the concrete.

Figures (5.32) and (5.33) give the radial and tangential stresses, respectively, at the crown and spring points for both the rock and the concrete for  $K$  equal to 4. It can be seen that the stresses are increasing at a constant rate, i.e., the steady state creep conditions have been reached.

Figure (5.34) gives the location of the points at which the rock and concrete stresses are summarized and these stresses are given in Tables (5.12) to (5.15). It can be seen that  $\sigma_x$  and  $\sigma_y$  remain in compression, for both the rock and concrete adjacent to the excavation ( $K$  equal to 1 and 4).

Since the single layer representation of the lining does not yield detailed stress distributions, the much refined

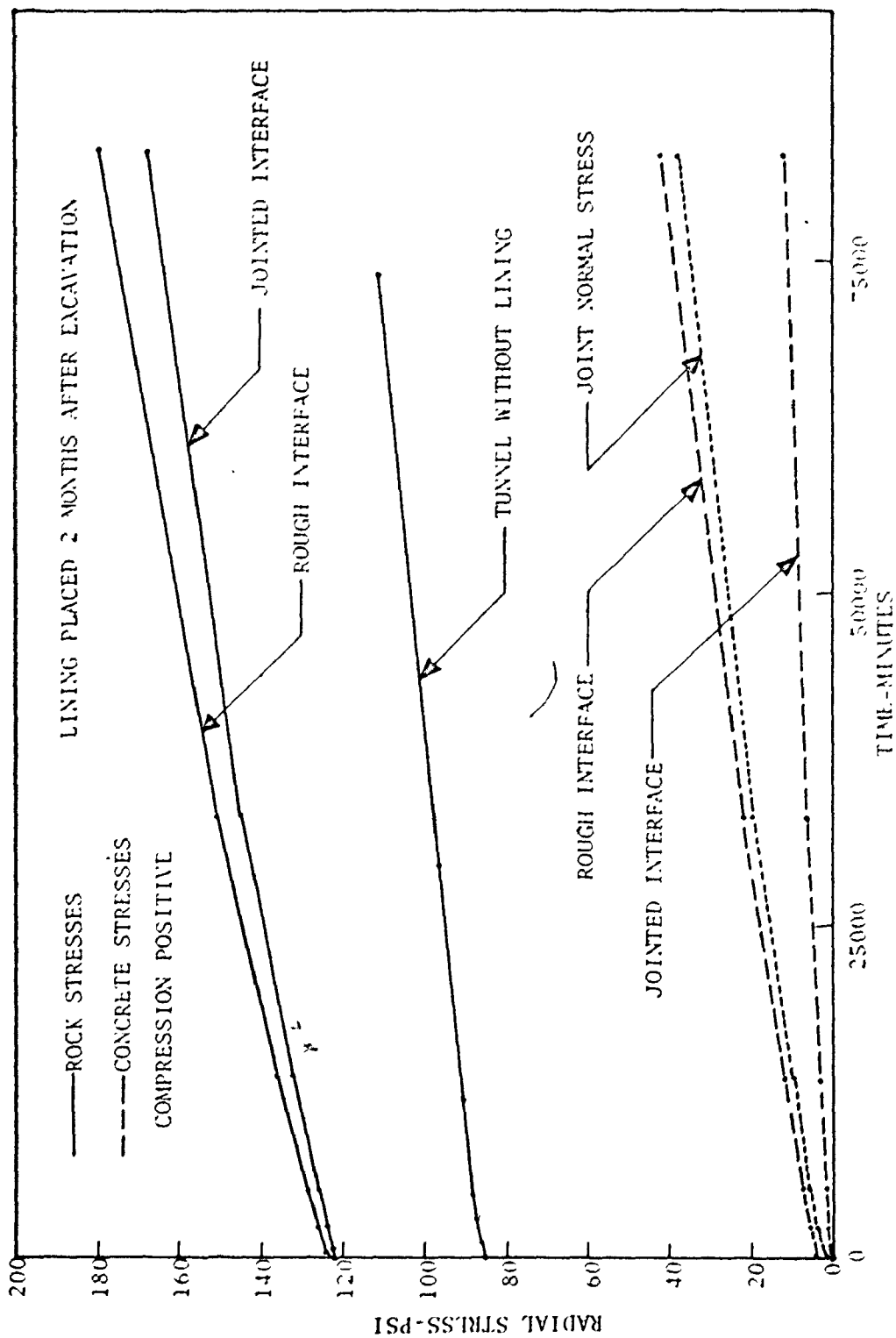


FIGURE 5.30 RADIAL STRESSES AT THE CROWN OF THE TUNNELL WITH TIME FOR THE ROUGH AND JOINTED INTERFACES, K = 1

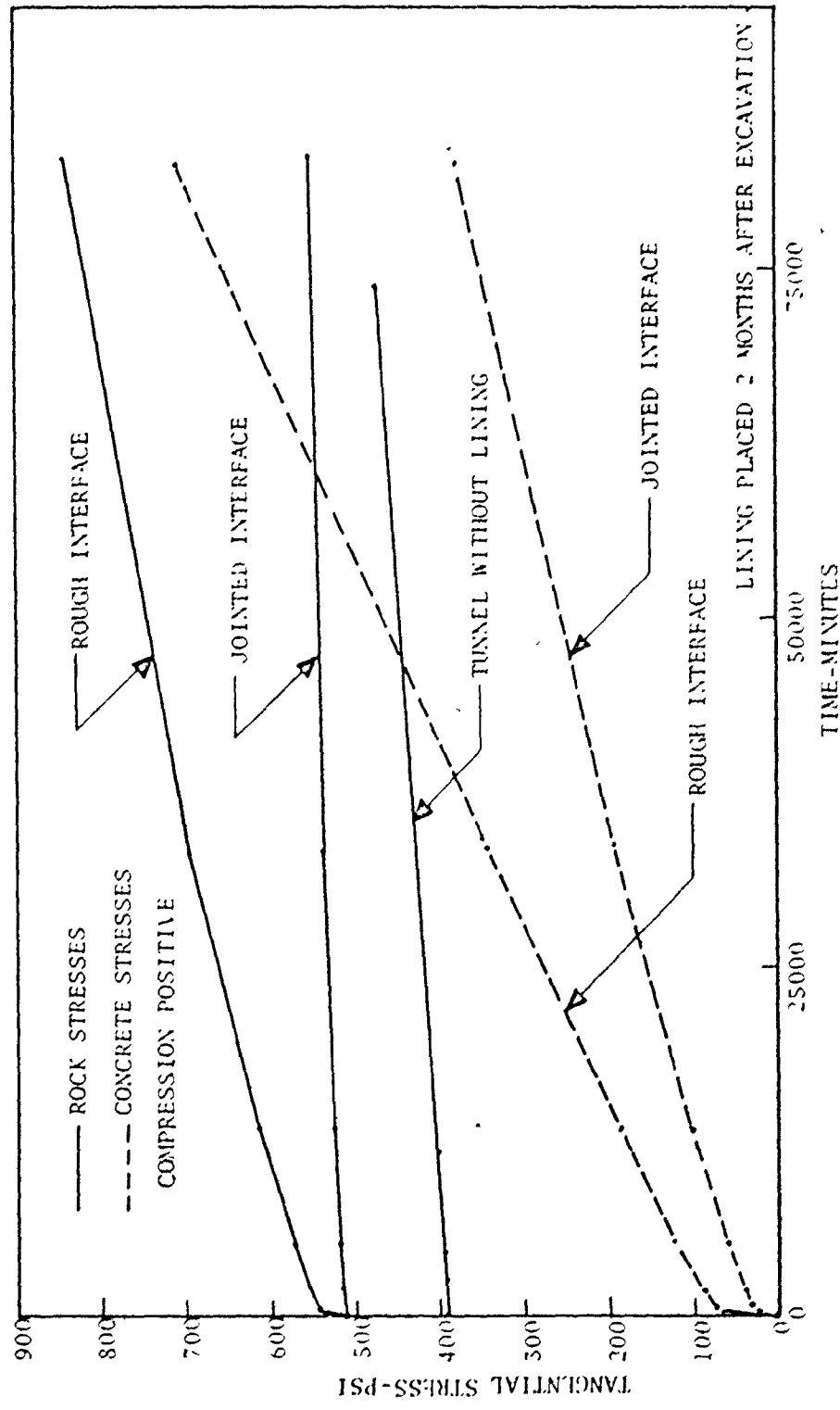


FIGURE 5.31 TANGENTIAL STRESSES AT THE CROWN OF THE TUNNEL WITH TIME FOR THE ROUGH AND JOINED INTERFACES,  $K = 1$

TABLE 5.11 STRESSES IN THE JOINTS BETWEEN THE ROCK AND THE CONCRETE LINING CONSTRUCTED 2 MONTHS AFTER EXCAVATION [SIGNS CORRESPONDING TO FIGURE (4.1)],  $K = 1$

STRESS CONDITION	CROWN POINT		SPRING POINT		FLOOR POINT	
	NORMAL STRESS psi	SHEAR STRESS psi	NORMAL STRESS psi	SHEAR STRESS psi	NORMAL STRESS psi	SHEAR STRESS psi
1 day creep	-3.6	-0.02	-3.7	-0.27	-3.8	0.08
23 days creep	-21.3	-0.13	-21.5	-0.78	-21.9	0.31
58 days creep	-39.9	-0.26	-40.4	-1.58	-41.0	5.80
171 days creep	-86.6	-1.35	-87.2	-3.82	-88.3	1.95

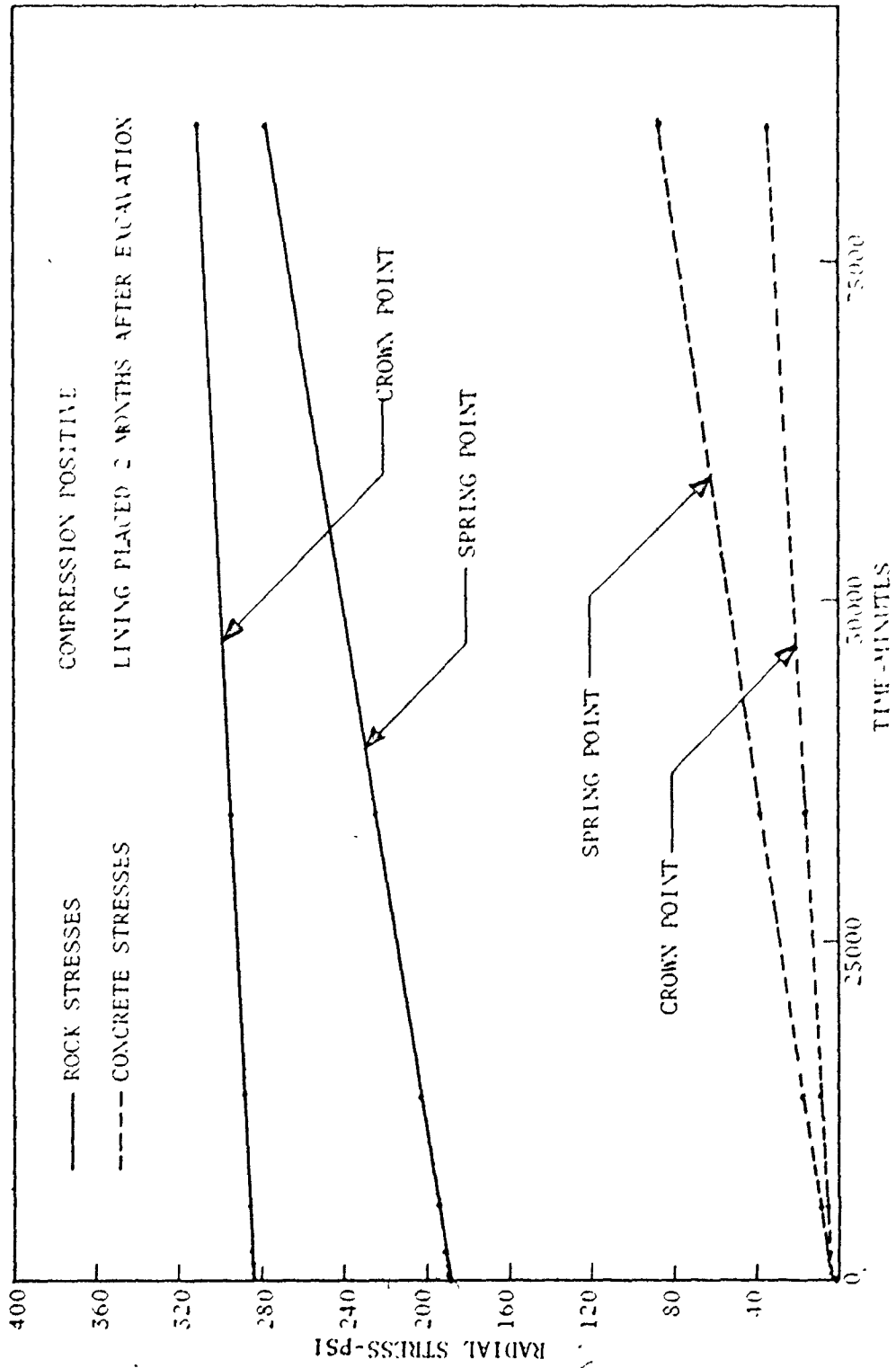


FIGURE 5.32 RADIAL STRESSES AT THE CROWN AND SPRING POINTS WITH TIME FOR  $k = 4$



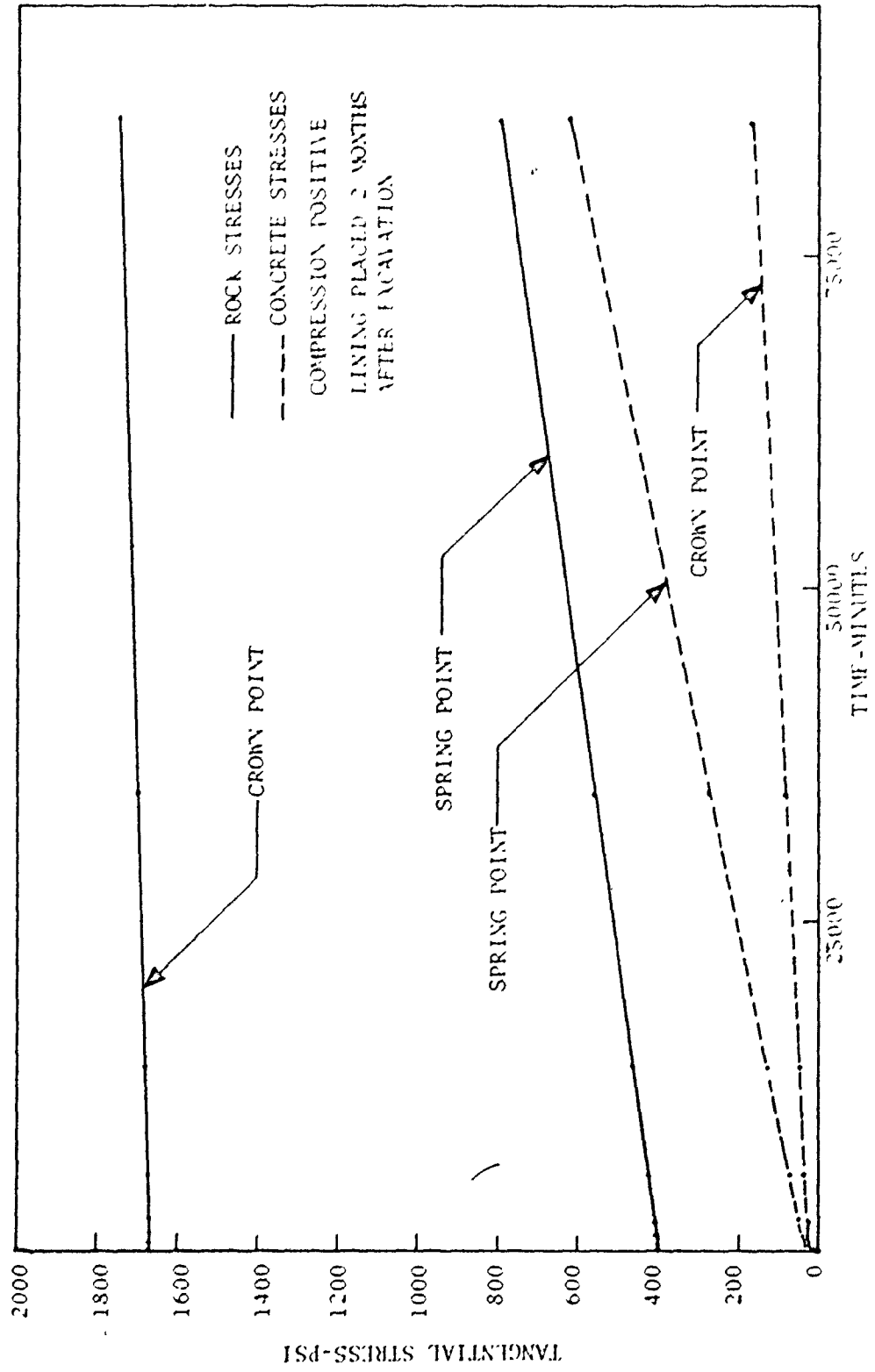


FIGURE 5.33 TANGENTIAL STRESSES AT THE CROWN AND SPRING POINTS WITH TIME FOR  $K = 4$ .

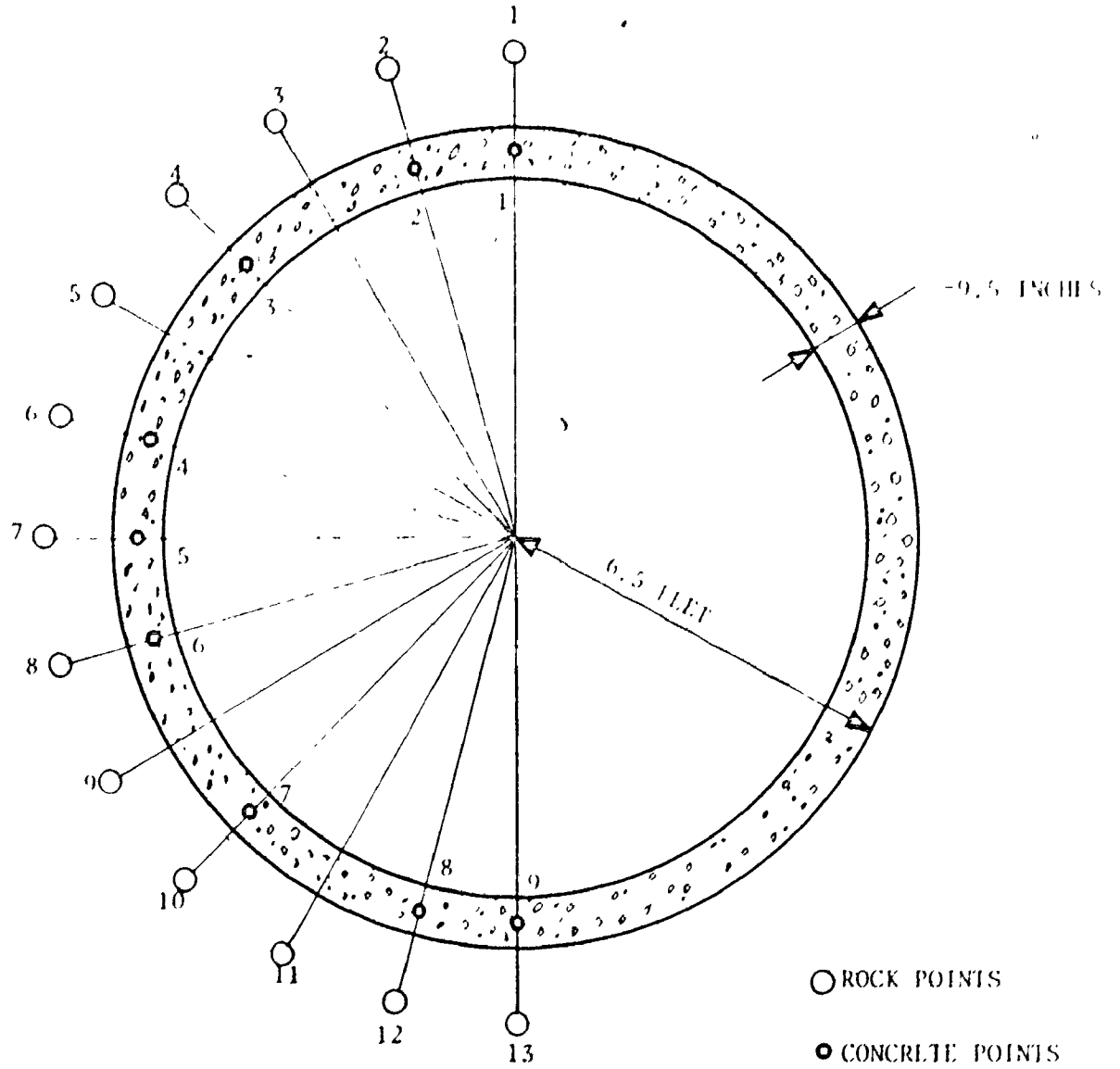


FIGURE 5.34 LOCATION OF ROCK AND CONCRETE POINTS

TABLE 5.12 LONG TERM STRESSES, ROCK, K = 1

ROCK STRESSES AFTER CONSTRUCTING THE LINING. LINING CONSIDERED TO BE  
 CONSTRUCTED 2 MONTHS AFTER EXCAVATION OF TUNNEL (COMPRESSIVE STRESS  
 POSITIVE).

POINT	APPROXIMATELY 3.5 MONTHS LINING CREEP			APPROXIMATELY 5.5 MONTHS LINING CREEP		
	$\sigma_x$ psi	$\sigma_y$ psi	$\tau_{xy}$ psi	$\sigma_x$ psi	$\sigma_y$ psi	$\tau_{xy}$ psi
1	998	219	-164	1130	254	-199
2	545	184	-117	571	199	-126
3	720	355	-285	797	395	314
4	347	328	-200	358	341	-206
5	382	663	-290	429	731	-324
6	194	521	-107	216	554	-116
7	205	951	23	235	1077	51
8	205	534	123	196	561	133
9	381	706	292	422	781	319
10	355	354	206	366	365	209
11	722	384	292	795	425	320
12	552	194	122	573	209	130
13	997	231	175	1120	266	210

TABLE 5.13 LONG TERM STRESSES, ROCK, K = 4

ROCK STRESSES AFTER CONSTRUCTING THE LINING. LINING CONSIDERED TO BE CONSTRUCTED 2 MONTHS AFTER EXCAVATION OF TUNNEL (COMPRESSIVE STRESS POSITIVE).

POINT	APPROXIMATELY 2 MONTHS LINING CREEP			APPROXIMATELY 5 MONTHS LINING CREEP		
	$\sigma_x$ psi	$\sigma_y$ psi	$\tau_{xy}$ psi	$\sigma_x$ psi	$\sigma_y$ psi	$\tau_{xy}$ psi
1	1749	310	-188	2085	378	-248
2	1231	267	-185	1336	351	-226
3	1299	435	-411	1520	588	-534
4	701	388	-329	773	542	-391
5	566	618	-371	717	962	-517
6	261	508	-153	353	787	-200
7	277	788	13	393	1360	35
8	264	526	171	343	813	234
9	571	663	387	702	1035	532
10	703	424	342	738	588	398
11	1287	466	424	1428	631	536
12	1228	282	191	1249	361	226
13	1716	320	194	1910	380	253

TABLE 5.14 LONG TERM STRESSES, CONCRETE,  $K = 1$   
 CONCRETE STRESSES AFTER CONSTRUCTING THE LINING. LINING CONSIDERED  
 TO BE CONSTRUCTED 2 MONTHS AFTER EXCAVATION OF TUNNEL (COMPRESSIVE  
 STRESS POSITIVE).

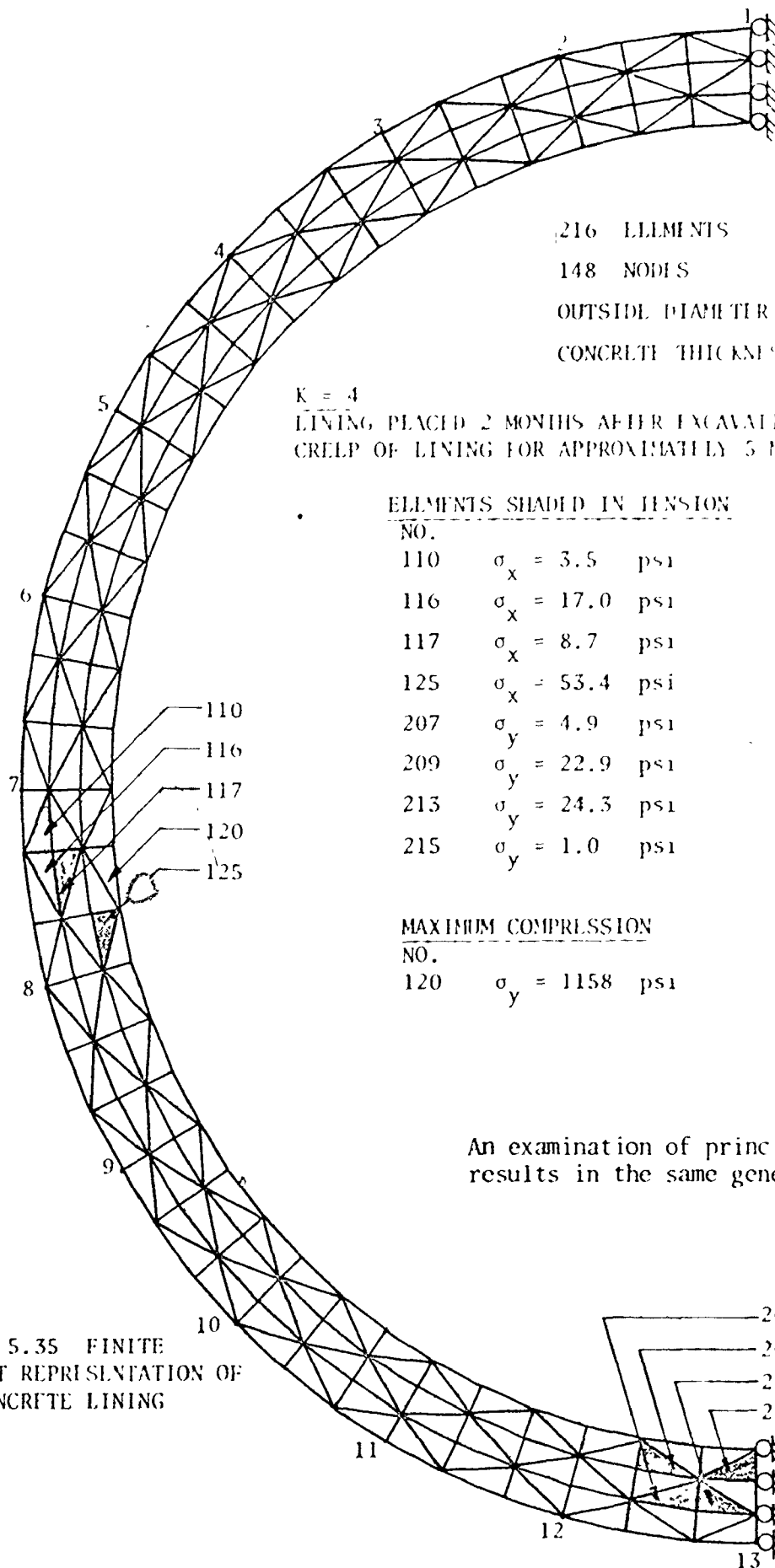
POINT	APPROXIMATELY 3.5 MONTHS LINING CREEP			APPROXIMATELY 5.5 MONTHS LINING CREEP		
	$\sigma_x$ psi	$\sigma_y$ psi	$\tau_{xy}$ psi	$\sigma_x$ psi	$\sigma_y$ psi	$\tau_{xy}$ psi
1	799	74	-110	1038	103	-155
2	631	129	-184	817	169	-242
3	363	343	-265	469	443	-342
4	130	590	-171	171	755	-224
5	77	740	16	105	950	24
6	133	621	190	174	799	249
7	361	361	270	466	466	345
8	622	128	188	796	173	248
9	772	86	128	990	119	178

TABLE 5.15 LONG TERM STRESSES, CONCRETE, K = 4  
 CONCRETE STRESSES AFTER CONSTRUCTING THE LINING. LINING CONSIDERED TO  
 BE CONSTRUCTED 2 MONTHS AFTER EXCAVATION OF TUNNEL (COMPRESSIVE STRESS  
 POSITIVE).

POINT	APPROXIMATELY 2 MONTHS LINING CREEP			APPROXIMATELY 5 MONTHS LINING CREEP		
	$\sigma_x$ psi	$\sigma_y$ psi	$\tau_{xy}$ psi	$\sigma_x$ psi	$\sigma_y$ psi	$\tau_{xy}$ psi
1	176	34	-51	758	72	-107
2	179	64	-77	649	179	-223
3	148	240	-148	458	597	-405
4	85	497	-144	223	1156	-340
5	85	616	8	187	1417	27
6	91	519	160	236	1222	384
7	133	257	153	399	639	407
8	113	64	75	432	174	207
9	67	42	63	417	91	136

mesh shown in Figure (5.35) was used in a more detailed stress analysis. The K equal to 4 condition which is considered the worst possible field situation for the concrete lining was examined. (As indicated previously, the site is probably closer to the condition of K equal to 1.) The stresses in the lining, due to five months squeezing (lining considered to be placed two months after excavation) were obtained by imposing the appropriate creep displacements as the external boundary conditions on the lining mesh.

Small tension zones were developed in the concrete, and these zones are shaded on Figure (5.35) and the values summarized in terms of  $\sigma_x$  and  $\sigma_y$  on this figure. The largest tension developed is a  $\sigma_x$  of 53.4 psi, while the largest compression developed is a  $\sigma_y$  of 1158 psi. This maximum compressive stress is in fair agreement with that obtained by the single layer analysis given in Table (5.13). The output also permits a consideration of principal stresses and maximum shear stresses, but it is clear that the low tensile stresses will cause no cracking problems. This method of studying the lining stresses allows the designer to select the critical lining thickness.



216 ELEMENTS  
 148 NODES  
 OUTSIDE DIAMETER 15 FT 11  
 CONCRETE THICKNESS 9.5 INCHES

$K = 4$   
 LINING PLACED 2 MONTHS AFTER EXCAVATION,  
 CREEP OF LINING FOR APPROXIMATELY 5 MONTHS

ELEMENTS SHADDED IN TENSION

NO.		
110	$\sigma_x = 3.5$	psi
116	$\sigma_x = 17.0$	psi
117	$\sigma_x = 8.7$	psi
125	$\sigma_x = 53.4$	psi
207	$\sigma_y = 4.9$	psi
209	$\sigma_y = 22.9$	psi
213	$\sigma_y = 24.3$	psi
215	$\sigma_y = 1.0$	psi

MAXIMUM COMPRESSION

NO.		
120	$\sigma_y = 1158$	psi

An examination of principal stresses results in the same general findings.

FIGURE 5.35 FINITE ELEMENT REPRESENTATION OF THE CONCRETE LINING



CHAPTER 6  
SUMMARY AND CONCLUSIONS

The major contribution of this study of tunnel excavations in creeping rock are:

1. A procedure based on the finite element method was developed for simulating the excavation of underground openings in rock for the actual initial state of stress in the field for various  $K$  conditions. This procedure can also incorporate orthotropic behaviour due to rock bedding, and other directional variations in the elastic properties of rock. Since high lateral stresses are often found in rock, it is important that they be considered in any stress analysis.

2. Coupling this excavation simulation into the time-dependent analysis of underground openings to study the influence of rock squeezing using the incremental initial strain method. Appropriate stress-strain-time relationships and strain accumulation methods are readily incorporated into this finite element program. (A survey of time-dependent constitutive relationships for rock is given to guide in the selection of appropriate creep laws).

3. Extension of the excavation and creep simulation aspects to model underground linings and lining placement strategies. This includes the ability to consider the lining

and the rock as two different materials with rough or jointed interfaces between them. Further, this simulation allows for creep of the rock before lining installation, and creep of the rock and concrete lining after its construction for appropriate rock and concrete constitutive relationships.

4. The full simulation procedure (excavation, creep and lining) was used to study an actual tunnel constructed in squeezing rock. There is reasonable agreement between the predicted performance and measured performance, to date, and this comparison with monitored field information is continuing.

Based on this study, the following topics appear to require further study or extension:

1. The stress-strain-time relationships for a variety of rock types and for various loadings, particularly multi-axial, should be obtained in order to develop guidelines for the selection of rock creep laws. Such laws must ultimately take multi-axial behaviour into account and this may require an extensive creep testing program.

2. The anisotropic properties of rock should be incorporated into the creep analysis to more accurately represent field conditions.

3. The representation of jointed interfaces between the rock and the concrete appears adequate to simulate the field conditions, but there is little information available on the actual mechanical properties of joints between rock

and concrete. The development of "creep" joints appears essential and will most probably require experimental studies.

4. For low or moderate stress levels there is no need to extend this work to include elasto-plastic behaviour. However, for high stress levels simulation of this behaviour would be essential.

An extension of this work to consider cracked elements and low tensile strength of brittle materials appears to be a logical complementary step to the above items. Further, with the heavy use of the computer in creep analyses, solution efficiency must always be considered. It is anticipated that most of these aspects will be considered in the continuing program to study the creep of geotechnical materials.

BIBLIOGRAPHY

Afrouz, A. and Harvey, J. M., "Rheology of Rocks Within the Soft to Medium Strength Range", International Journal of Rock Mechanics and Mining Sciences, Vol. 11, 1974, pp. 281-290.

Bollinger, G. A., "Blast Vibration Analysis", Southern Illinois University Press, Feffer and Simons Inc., New York, 1974.

Boresi, A. P. and Deere, D. U., "Creep Closure of a Spherical Cavity in an Infinite Medium (with Special Application to Project Dribble, Tatum Salt Dome, Mississippi)", for Holmes Narver, Inc., Las Vegas Division, 1963.

Cruden, D. M., "Single-Increment Creep Experiments on Rock Under Uniaxial Compression", International Journal of Rock Mechanics, and Mining Sciences, Vol. 8, 1971, pp. 127-142.

Desai, C. S. and Abel, J. F., "Introduction to the Finite Element Method", Van Nostrand Reinhold Company, New York, 1972.

Desai, C. S., "Applications of the Finite Element Method in Geotechnical Engineering", Proceedings of the Symposium held at Vicksburg, Mississippi, 1971.

Dhir, R. K. and Sangha, C. M., "A Study of the Relationships between Time, Strength, Deformation, and Fracture of Plain Concrete", Magazine of Concrete Research, Vol. 24, No. 81, December 1972, pp. 197-208.

Emery, J. J., "Finite Element Analysis of Creep Problems in Soil Mechanics", Ph.D. Thesis, University of British Columbia, June 1971.

Farmer, I. W., "Engineering Properties of Rocks", Spon, London, 1968.

Feld, J., "Rock as an Engineering Material", Soiltest, Inc., Evanston, Ill., 1966.

Franklin Trow Associates Ltd., Rock Engineering Consultants, "Supplementary Study, Easterly Filtration Plant Intake Tunnel, Scarborough, Ontario", personal communication, November 1975, Rexdale, Ontario.

Goodman, R. E., Taylor, R. L. and Brekke, T. L., "A Model for the Mechanics of Jointed Rock", Journal of the Soil Mechanics, and Foundation Division, ASCE, Vol. 94, No. SM3, Proc. Paper 5937, May 1968, pp. 637-659.

Greenbaum, G. A., "Creep Analysis of Axisymmetric Bodies", Ph.D. Thesis, University of California, 1966.

Hobbs, D. W., "Stress-Strain-Time Behaviour of a Number of Coal Measure Rocks", International Journal of Rock Mechanics and Mining Sciences, Vol. 7, 1970, pp. 149-170.

Illston, J. M., and Jordaan, I. J., "Creep Prediction for Concrete Under Multiaxial Stress", Journal of the American Concrete Institute, Vol. 69, March 1972, pp. 158-164.

Jaeger, C., "Rock Mechanics and Engineering", Cambridge University Press, London, 1972.

Kulhawy, F. H., "Finite Element Modelling Criteria for Underground Openings in Rock", International Journal of Rock Mechanics, and Mining Sciences, Vol. 11, 1974, pp. 465-472.

Kulhawy, F. H., "Stress and Displacements around Openings in Homogeneous Rock", International Journal of Rock Mechanics, and Mining Sciences, Vol. 12, 1975, pp. 43-57.

Lane, K. S., "Field Test Sections Save Cost in Tunnel Support", Report from Underground Construction Research Council, ASCE, October 1975.

Lo and Morton, "Tunnels in Bedded Rock with High Horizontal Stresses", Twenty-eighth Canadian Geotechnical Conference, Montreal, October 1975.

Lubahn, J. D. and Felgar, R. P., "Plasticity and Creep of Metals", John Wiley and Sons Inc., New York, 1961.

Meek, J. L., "Excavation in Rock; An Application of the Finite Element Method of Analysis", Proceedings of the 1973 Tokyo Seminar on Finite Element Analysis, University of Tokyo Press.

Murrell, S. A. F. and Misra, A. K., "Time-Dependent Strain or Creep in Rocks and Similar Non-Metallic Materials", Bull. Inst. Mining Met., Vol. 71, Pt. 7, 1962, pp. 353-378.

Nair, K., Chang, C. Y., Singh, R. D., and Abdullah, A. M., "Time-Dependent Analysis to Predict Closure in Salt Cavity", Fourth Symposium on Salt, Ohio, Vol. 2, 1973, pp. 129-139.

Neville, A. M., "Creep of Concrete: Plain, Reinforced, and Prestressed", North-Holland Publishing Company, Amsterdam, 1970.

Nguyen, T. Q., "Simulation of Ice Flow Using the Finite Element Method", M.Eng. Thesis, McMaster University, Hamilton, Ontario, March, 1976.

Obert, L. and Duvall, W. I., "Rock Mechanics and the Design of Structures in Rocks", John Wiley and Sons Inc., New York, 1967.

Penny, R. K. and Marriott, D. L., "Design for Creep", McGraw-Hill, New York, 1971.

Robertson, E. C., "Viscoelasticity of Rocks", International Conference on the State of Stress in the Earth's Crust, Santa Monica, California, May 1963, pp. 181-220.

Semple, R. M. Hendron, A. J., and Mersi, G., "The Effect of Time-Dependent Properties of Altered Rock on Tunnel Supported Requirement", Federal Railway Administration, Department of Transportation, Washington, D.C., December 1973.

Singh, A. and Mitchell, J. K., "A General Stress-Strain Time Function for Soils", Journal of the Soil Mechanics and Foundation Division, ASCE, Vol. 94, No. SM1, 1968, pp. 21-46.

Spooner, D. C., "Stress-Strain-Time Relationships for Concrete", Magazine of Concrete Research, Vol. 23, No. 75-76, June 1971, pp. 127-131.

Straub, L. G., "Plastic Flow in Concrete Arches", Journal of the Structural Division, ASCE, Vol. 56, January 1930, pp. 49-114.

Terzaghi, K., "Rock Defects and Loads on Tunnel Supports", in Rock Tunnelling with Steel Supports, Commercial Shearing and Stamping (1946).

United States Army Corps of Engineers, "Project Dribble - Petrographic Examination and Physical Tests of Cores, Tatum Salt Dome, Mississippi", Tech. Report No. 6-614, January 1963, Vicksburg, Mississippi.

Winkle, B. V., "Time-Dependent Analysis of Rock Mechanics Problems", Ph.D. Thesis, University of Colorado, 1970.

Zienkiewicz, O. C., "The Finite Element Method in Engineering Science", McGraw-Hill, New York, 1971.

Zienkiewicz, O. C. and Holister, G. S., "Stress Analysis", John Wiley and Sons Inc., New York, 1965.

APPENDIX A  
FINITE ELEMENT METHOD

The basic concept of the finite element method is the representation of the actual structure by a set of simple elements of finite size. These elements are assumed to be connected to adjacent elements at a finite number of points called the nodal points of the elements. The behaviour of each element is described by the relationship between the generalized forces  $\{q\}$  and the displacements  $\{U\}$  at the nodal points of the element. The coefficient matrix of the force-displacement relationship is called the stiffness matrix  $[k]$  for the element (the displacement method is used throughout).

The displacement (stiffness) method is based on the minimization of the potential energy of the body. For static equilibrium, the principle of minimum potential energy states that: of all the compatible displacement fields that satisfy the specified boundary displacements, the displacement field that also satisfies the conditions of equilibrium minimizes the potential energy. This is given by:

$$\delta \left( \int_V W \, dV - \int_{S_T} T_i U_i \, dS - \int_V F_i U_i \, dV \right) = 0 \quad (\text{A.1})$$

where: the terms in brackets represent the potential energy of the body;  $W$  is the strain energy density;  $V$  is the volume of

the body;  $S_T$  is that part of the surface,  $S$ , where tractions  $T$  are prescribed;  $F_i$  are the body forces; and  $U_i$  are the displacement fields.

From Equation (A.1), the stiffness matrix  $[K]$  is given by:

$$[k] = \int_V [A^{-1}]^T [B]^T [D] [B] [A^{-1}] dV \quad (A.2)$$

where:  $[A^{-1}]$  is the displacement transformation matrix relating the vector of generalized coordinates to the vector of nodal displacement;  $[B]$  is the strain-displacement matrix; and  $[D]$  is the stress-strain matrix (Desai et al., 1972).

Once the stiffness relationships for all elements of the structure are obtained, the governing system of equations for the body is formulated by superposition of the element stiffness relationships to satisfy the following conditions:

- a) the displacement at any node must be the same for all elements attached to that node; and,
- b) the generalized forces acting on each element must be in equilibrium with adjacent element forces, and the applied loads.

From the relationship between the force vector  $\{Q\}$  and the total stiffness matrix  $[K]$ :

$$[K] \{U\} = \{Q\} \quad (A.3)$$

the nodal displacement vector  $\{U\}$  can be calculated. The strain  $\{\epsilon\}$  within any element can then be calculated from



the appropriate strain-displacement relationships (Zienkiewicz, 1971; Desai et al., 1972). Finally, the stress  $\{\sigma\}$  can then be obtained from the appropriate stress-strain relationships (Zienkiewicz, 1971; Desai et al., 1972).

## APPENDIX B

### GENERAL INCREMENTAL APPROACH FOR NONLINEAR ELASTIC CREEP PROBLEMS (Taken from Emery, 1971)

a) Formulation for the Incremental Approach

To handle the nonlinear elastic problem by the incremental approach, it is necessary to expand the Principle of Minimum Potential Energy to permit the determination of an incremental state superimposed upon a body with an existing equilibrium stress state. For this case, the potential energy,  $V$ , of the body from Equation (A.1) becomes:

$$\begin{aligned}
 V = V^{(I)} + \Delta V = & \int_V (W^{(I)} + \Delta W) dV - \int_{S_T} (T_i^{(I)} + \Delta T_i)(U_i^{(I)} + \Delta U_i) dS \\
 & - \int_V (F_i^{(I)} + \Delta F_i)(U_i^{(I)} + \Delta U_i) dV \quad (B.1)
 \end{aligned}$$

where the superscript (I) and prefix  $\Delta$  indicate the initial equilibrium values of the variables and the incremental change in these variables, respectively. Expanding this equation and truncating the Taylor series expression for the change in strain energy after two terms gives:

$$\begin{aligned}
 V = V^{(I)} + \Delta V = & V^{(I)} + \int_V \left( \frac{\partial W}{\partial \epsilon_{ij}^E} \bigg|_{\epsilon_{ij}^{E(I)}} \Delta \epsilon_{ij}^E + \frac{\partial^2 W}{\partial \epsilon_{ij}^E \partial \epsilon_{kl}^E} \bigg|_{\epsilon_{ij}^{E(I)}} \frac{\Delta \epsilon_{ij}^E \Delta \epsilon_{kl}^E}{2} \right) dV \\
 & - \int_{S_T} (T_i^{(I)} \Delta U_i + \Delta T_i U_i^{(I)} + \Delta T_i \Delta U_i) dS
 \end{aligned}$$

$$- \int_V (F_i^{(I)} \Delta U_i + \Delta F_i U_i^{(I)} + \Delta F_i \Delta U_i) dV \quad (B.2)$$

where:  $\epsilon$  is the strain; and the superscript E denotes elastic behaviour. The incremental state must be such that the strain increment is small enough to truncate the Taylor series expansion after the second term. From the principle of virtual displacements:

$$\int_V \sigma_{ij}^{(I)} \Delta \epsilon_{ij}^E dV - \int_{S_T} T_i^{(I)} \Delta U_i dS - \int_V F_i^{(I)} \Delta U_i dV = 0 \quad (B.3)$$

and, noting that:  $W = \frac{1}{2} D_{ijkl} \epsilon_{ij}^E \epsilon_{kl}^E$  ;

$$\left. \frac{\partial W}{\partial \epsilon_{ij}^E} \right|_{\epsilon_{ij}^E(I)} = \sigma_{ij}^{(I)}; \quad \text{and} \quad \left. \frac{\partial^2 W}{\partial \epsilon_{ij}^E \partial \epsilon_{kl}^E} \right|_{\epsilon_{ij}^E(I)} \Delta \epsilon_{kl}^E = \Delta \sigma_{ij} \quad (B.4)$$

where  $D_{ijkl}$  is the material tensor, Equation (B.2) reduces to:

$$\mathcal{V} = \mathcal{V}^{(I)} + \int_V \frac{1}{2} \Delta \sigma_{ij} \Delta \epsilon_{ij}^E dV - \int_{S_T} \Delta T_i (U_i^{(I)} + \Delta U_i) dS - \int_V \Delta F_i (U_i^{(I)} + \Delta U_i) dV \quad (B.5)$$

Substituting the linear incremental stress-strain law for  $\Delta \sigma_{ij}$ ,

$$\Delta \sigma_{ij} = D_{ijkl} \Delta \epsilon_{kl}^E \quad (B.6)$$

into Equation (B.5) and taking variations with respect to all admissible incremental displacement fields yields the desired variational principle:

$$\delta = \delta \left\{ \int_V \frac{1}{2} D_{ijkl} \Delta \epsilon_{ij}^E \Delta \epsilon_{kl}^E dV - \int_{S_T} \Delta T_i \Delta U_i dS - \int_V \Delta F_i \Delta U_i dV \right\} = 0 \quad (B.7)$$

Comparing this equation to Equation (A.1), it can be seen that the previous formulation for the linear elastic case may be used where the variables  $\epsilon_{ij}^E$ ,  $\sigma_{ij}$ ,  $T_i$ ,  $F_i$ ,  $U_i$  are now replaced by increments of the variables  $\Delta \epsilon_{ij}^E$ ,  $\Delta \sigma_{ij}$ ,  $\Delta T_i$ ,  $\Delta F_i$ ,  $\Delta U_i$ .

#### b) Introduction of Creep Strain

The increment of total strain  $\Delta \epsilon_{ij}^E$ , and an increment of non-recoverable creep strain,  $\Delta \epsilon_{ij}^C$ . The increment of creep strain is assumed to be an initial strain for any time interval  $\Delta t$  and to be constant during the interval.

$$\Delta \epsilon_{ij} = \Delta \epsilon_{ij}^E + \Delta \epsilon_{ij}^C \quad (B.8)$$

or

$$\Delta \epsilon_{ij}^E = \Delta \epsilon_{ij} - \Delta \epsilon_{ij}^C \quad (B.9)$$

Substituting Equation (B.9) into Equation (B.7) yields:

$$\delta \left\{ \int_V \frac{1}{2} D_{ijkl} (\Delta \epsilon_{ij} \Delta \epsilon_{kl} - \Delta \epsilon_{ij} \Delta \epsilon_{kl}^C - \Delta \epsilon_{ij}^C \Delta \epsilon_{kl} + \Delta \epsilon_{ij}^C \Delta \epsilon_{kl}^C) dV - \int_{S_T} \Delta T_i \Delta U_i dS - \int_V \Delta F_i \Delta U_i dV \right\} = 0 \quad (B.10)$$

Then, using the incremental forms and the symmetry condition (Desai and Abel, 1972), Equation (B.10) gives:

$$\delta \left[ \sum_N \left[ \int_{V_N} \left[ \frac{1}{2} \{\Delta Q\}_N^T [A^{-1}]_N^T [B]_N^T [D]_N [B]_N [A^{-1}]_N \{\Delta Q\}_N - \{\Delta Q\}_N^T [A^{-1}]_N^T [B]_N^T [D]_N \{\Delta \epsilon^C\}_N + \frac{1}{2} [D]_N [\Delta \epsilon^C] [\Delta \epsilon^C] \right] dV - \int_{S_{T_N}} \{\Delta Q\}_N^T [A^{-1}]_N^T [\phi_s]_N^T \{\Delta T\}_N dS - \int_{V_N} \{\Delta Q\}_N^T [A^{-1}]_N^T [\phi]_N^T \{\Delta F\}_N dV \right] \right] = 0 \quad (B.11)$$

where the summation is carried out for all the elements and  $[\phi_s]$  represents the spatial functions specialized to surface positions. Taking variations of Equation (B.11) with respect to the increment of nodal displacements and assuming that the creep strains are constant during the time increment yields the desired stiffness relationship:

$$\sum_N \left[ \int_{V_N} \left\{ [A^{-1}]_N^T [B]_N^T [D]_N [B]_N [A^{-1}]_N (\Delta Q)_N - [A^{-1}]_N^T [B]_N^T [D]_N [\Delta \epsilon^C] \right\} dV \right. \\ \left. - \int_{S_{TN}} [A^{-1}]_N^T [\phi_S]_N^T (\Delta T)_N dS - \int_{V_N} [A^{-1}]_N^T [\phi]_N^T (\Delta F)_N dV \right] = 0 \quad (B.12)$$

$$\text{or} \quad \sum_N \left\{ [K]_N (\Delta Q)_N = \{\Delta P\}_N + \{\Delta L\}_N \right\} \quad (B.13)$$

where the element stiffness matrix  $[K]_N$  is given by,

$$[K]_N = \int_{V_N} [A^{-1}]_N^T [B]_N^T [D]_N [B]_N [A^{-1}]_N dV \quad (B.14)$$

the element nodal load vector  $\{\Delta P\}_N$  is given by,

$$\{\Delta P\}_N = \int_{S_{TN}} [A^{-1}]_N^T [\phi_S]_N^T (\Delta T)_N dS + \int_{V_N} [A^{-1}]_N^T [\phi]_N^T (\Delta F)_N dV \quad (B.15)$$

and the creep strain nodal 'load' vector is given by,

$$\{\Delta L\}_N = \int_{V_N} [A^{-1}]_N^T [B]_N^T [D]_N [\Delta \epsilon^C] dV \quad (B.16)$$

The value of the coefficients of the material matrix  $[D]_N$  for each element depends on the stresses and elastic strains for the increment.

## APPENDIX C

### EQUATIONS REQUIRED FOR THE DETERMINATION OF THE TIME INCREMENTS AND THE COMPONENTS OF THE CREEP STRAIN INCREMENT

The strain hardening constitutive relationship (mechanical equation of state) for the creep rate at constant temperature is given by:

$$\dot{\epsilon}_c = f(\sigma_e, \epsilon_e^c) \quad (C.1)$$

where:  $\dot{\epsilon}_c$  is the creep strain rate,  $\epsilon_e^c$  is the equivalent accumulative creep strain; and  $\sigma_e$  is the equivalent stress which is usually given for plane strain by (Desai, et al., 1972):

$$\sigma_e = \frac{1}{\sqrt{2}} [(\sigma_x - \sigma_y)^2 + (\sigma_y - \sigma_z)^2 + (\sigma_z - \sigma_x)^2 + 6\tau_{xy}^2]^{1/2} \quad (C.2)$$

This strain hardening assumption is widely adopted in rock mechanics and appears most appropriate for this study. However, the solution method can incorporate other creep strain accumulative rules such as time hardening or combinations of strain and time hardening.

In the incremental procedure for nonlinear creep problems, the time intervals selected must be small enough to ensure the stability of the solution process (Greenbaum, 1966; Emery, 1971). This stability is ensured by the following

limits:

$$\frac{\Delta \epsilon_e^C}{\epsilon_e^E} \leq \frac{1}{25} \quad (C.3)$$

where:  $\Delta \epsilon_e^C$  is the equivalent creep strain increment; and  $\epsilon_e^E$  is the equivalent elastic strain, and

$$\Delta t_{j+1} \leq 1.2 \Delta t_j \quad (C.4)$$

where:  $\Delta t$  is a time increment.

The components of the creep strain increment for plane strain problems are then obtained from:

$$\Delta \epsilon_x^C = \frac{\Delta \epsilon_e^C}{2\sigma_e} (2\sigma_x - \sigma_y - \sigma_z) \quad (C.5)$$

$$\Delta \epsilon_y^C = \frac{\Delta \epsilon_e^C}{2\sigma_e} (2\sigma_y - \sigma_z - \sigma_x) \quad (C.6)$$

$$\Delta \gamma_{xy}^C = 3 \frac{\Delta \epsilon_e^C}{\sigma_e} \tau_{xy} \quad (C.7)$$

These creep strain increment expressions are developed from the Prandtl-Reuss incremental plastic flow equation (strain increment directions coincide with the deviatoric stress directions and no volume change due to creep strains).

Complete details on the above are given by Emery (1971).